# SEMMELWEIS EGYETEM DOKTORI ISKOLA

Ph.D. értekezések

3356.

# **MOLDVAI DOROTTYA**

Molekuláris és experimentális onkológia című program

Programvezető: Dr. Bödör Csaba, egyetemi tanár

Témavezetők: Dr. Sebestyén Anna, kutatóprofesszor

# MTOR-DRIVEN METABOLIC SHIFTS IN CANCERS AND IN 3D BIOPRINTED TISSUE-MIMETIC STRUCTURES

# PhD thesis

# Dorottya Moldvai

# Semmelweis University Doctoral School Pathological and Oncological Division





Supervisor: Anna Sebestyén, D.Sc

Official reviewers: Erna Nyitrayné Pap, Ph.D

Edina Gyukity-Sebestyén, Ph.D

Head of the Complex Examination Committee: József Tímár, MD, D.Sc

Members of the Complex Examination Committee: Hargita Hegyesi, Ph.D Krisztina Takács-Vellai, Ph.D

Budapest 2025

# **Table of contents**

List of	abbreviations	4
1.	Introduction	8
1.1.	Role of metabolic adaptation in malignant tumors	8
1.2.	The central regulator of metabolism: the PI3K/Akt/mTOR pathway	9
1.3.	Preclinical models play a crucial role in the success of clinical trials	11
1.4.	3D bioprinting in preclinical modeling of cancer	14
1.4.1	. Bioprinter types	15
1.4.2	Bioinks for 3D bioprinting	15
1.4.3	3D bioprinting parameters	17
1.5.	Advances in 3D bioprinting for biomedical applications in cancer research	18
1.5.1	. 3D bioprinted breast cancer models	18
1.5.2	2. 3D bioprinted renal cell carcinoma models	19
1.6.	Issues concerning the comprehensiveness of 3D bioprinting literature	19
1.7.	Molecular characteristics of renal cell carcinoma subtypes	21
1.8.	Targeting the PI3K/Akt/mTOR pathway in renal cell carcinoma	22
1.9.	Immunosuppressive therapy and cancer risk after kidney transplantation	22
2.	Objectives	26
2.1.	Establishment and characterization of 3D bioprinted cancer models	26
2.2.	Tumorigenic role of tacrolimus in post-transplant renal cell carcinoma	27
3.	Methods	28
3.1.	Cell cultures and in vitro reagents	28
3.2.	In vitro proliferation assays (Alamar Blue and Sulforhodamine B)	29
3.3.	Preparing hydrogels for 3D bioprinting	29
3.4.	3D bioprinting of tissue-mimetic structures	30
3.5.	Renal cell carcinoma cohort and tissue microarray construction	31
3.6.	Immunohistochemistry and hematoxylin-eosin staining	31
3.7.	Western Blot and WES <sup>TM</sup> Simple analysis	33
3.8.	Renal ischemia reperfusion mouse model	34
3.9.	Human xenograft and syngeneic mouse model	34
3.10.	Isolating cells from <i>in vivo</i> tumor	35

3.	11.	Statistical analysis
4.		Results
4.	1.	Establishment of 3D bioprinted cancer models via Gesim BioScaffolder 36
	4.1.1.	Validation of growth and cellular dynamics in 3D bioprinted tissue-mimetic
	struct	ures
	4.1.2.	Increase and redistribution of cell-cell and cell-matrix adhesion proteins
	withi	n 3D bioprinted tissue-mimetic structures
	4.1.3.	Reduced activation and increased heterogeneity of mTOR-pathway
	comp	onents in 3D bioprinted tissue-mimetic structures
	4.1.4.	Quantitative analysis of mTOR signaling in 3D-bioprinted tissue-mimetic
	struct	ures
	4.1.5.	Altered response to mTOR-targeted therapies in 3D bioprinted tissue-
	mime	etic structures
	4.1.6.	3D bioprinted "patient-derived" breast cancer model for drug testing 45
4.	2.	Metabolic characterization of post-transplant renal cell carcinomas
	4.2.1.	Clinicopathological features of the renal cell carcinoma cohort
	4.2.2.	Elevated mTOR signaling is detected in end-stage renal disease following
	immu	nosuppression compared to healthy kidney tissue
	4.2.3.	Tacrolimus enhances the mTOR activity in the ischemic kidney of mice . 49
	4.2.4.	Pronounced activation of the mTORC2 signaling axis in post-transplant renal
	cell c	arcinomas compared to non-transplant, de novo renal cell carcinomas 50
	4.2.5.	mTOR signal activating effects of tacrolimus on normal tubular epithelial
	cell li	ne in vitro
	4.2.6.	In vitro effects of tacrolimus on renal cell carcinoma cell lines: activation of
	mTO	R signaling and increasing proliferation
	4.2.7.	3D effects of tacrolimus on renal cell carcinoma cell lines: increasing
	prolif	Peration and tumor growth
	4.2.8.	Tacrolimus-mediated activation of mTOR signaling in 3D bioprinted renal
	cell c	arcinoma model and in tumors of xenograft mice
5.		Discussion
5.	1.	Establishment and investigation of 3D bioprinted cancer models
5.	2.	Tumorigenic role of tacrolimus in post-transplant renal cell carcinoma 63

<b>6.</b>	Conclusions	65
7.	Summary	67
8.	References	68
9.	Bibliography of the candidate's publications	91
10.	Acknowledgements	95

#### List of abbreviations

2D two-dimensional

3D three-dimensional

4EBP1 4E-binding protein 1

AB Alamar Blue
AM antimetabolite

ATCC American Type Culture Collection

BC breast cancer

BDB BD Biosciences

ccRCC clear cell renal cell carcinoma

Cis cisplatin

CLM cross-linking method
CNI calcineurin inhibitor

CS corticosteroid
CS Cell Signaling
CsA cyclosporine A

DAB 3,3'-diaminobenzidine

DMEM Dulbecco's Modified Eagle Medium

DNA deoxyribonucleic acid

Doxo doxorubicin

ECM extracellular matrix

EGF epidermal growth factor

EMA European Medicines Agency

EMT epithelial—mesenchymal transition

ESRD end-stage renal disease

EU European Union

FBKBP-12 FK506-binding protein

FBS fetal bovine serum

FDA U.S. Food and Drug Administration FFPE formalin-fixed, paraffin-embedded

FH fumarate hydratase

Gen. mod. genetic modification

GTX GeneTex

H human

HE hematoxylin-eosin

HG high glucose

HIF hypoxia-inducible factor IHC immunohistochemistry

IP intraperitoneal Ipa ipatasertib

IR ischemia-reperfusion
IS immunosuppressive

JNK c-Jun N-terminal kinase
KTR kidney transplant recipient

LBB laser-based bioprinting

LKB1 liver kinase B1

lum. luminal M mouse

MAPK mitogen-activated protein kinase

MEM Minimum Essential Medium

MMF mycophenolate mofetil

mTOR mammalian target of rapamycin

mTORC1 mTOR complex 1
mTORC2 mTOR complex 2
mTORI mTOR inhibitor
neg.reg. negative regulator

NFAT nuclear factor of activated T-cells

non-tx non-transplant not significant

OXPHOS oxidative phosphorylation

p-HEMA poly-(2-hydroxyethyl methacrylate)

PBS phosphate-buffered saline

PCL polycaprolactone

PDGF platelet-derived growth factor

PI3K phosphoinositide 3-kinase

PKCα protein kinase C alpha

post-tx post-transplant

PPP pentose phosphate pathway

pRCC papillary renal cell carcinoma

prot. protein

PTC proximal tubular cell

PVDF polyvinylidene fluoride

Rapa rapamycin

RCC renal cell carcinoma

Rheb Ras homolog enriched in brain

Rictor rapamycin-insensitive companion of mTOR

RPMI Roswell Park Memorial Institute (origin)

RT room temperature

S6K1 S6 kinase 1

SA Sigma-Aldrich
SB SinoBiological

SDH succinate dehydrogenase

SGK1 serum and glucocorticoid-regulated kinase 1

SHAM placebo surgery

SRB Sulforhodamine B

TAC tacrolimus

TCA tricarboxylic acid

TF Thermo Fischer Scientific

TGFβ transforming growth factor-β

TMA tissue microarray

TME tumor-microenvironment
TMS tissue-mimetic structure

TMZ temozolomide

TNBC triple negative breast cancer

transcr. transcription

TSC tuberous sclerosis protein complex

UV ultra-violet light

VEGF vascular endothelial growth factor

VHL von Hippel-Lindau

WB western blot

#### 1. Introduction

# 1.1. Role of metabolic adaptation in malignant tumors

Changes in metabolism and energy use are important parts of how cancer cells survive and grow. *Warburg and Minami* were the first to describe these changes in 1923 (1). The role of tumor metabolism was overshadowed by advances in molecular genetics, but it is now gaining renewed interest.

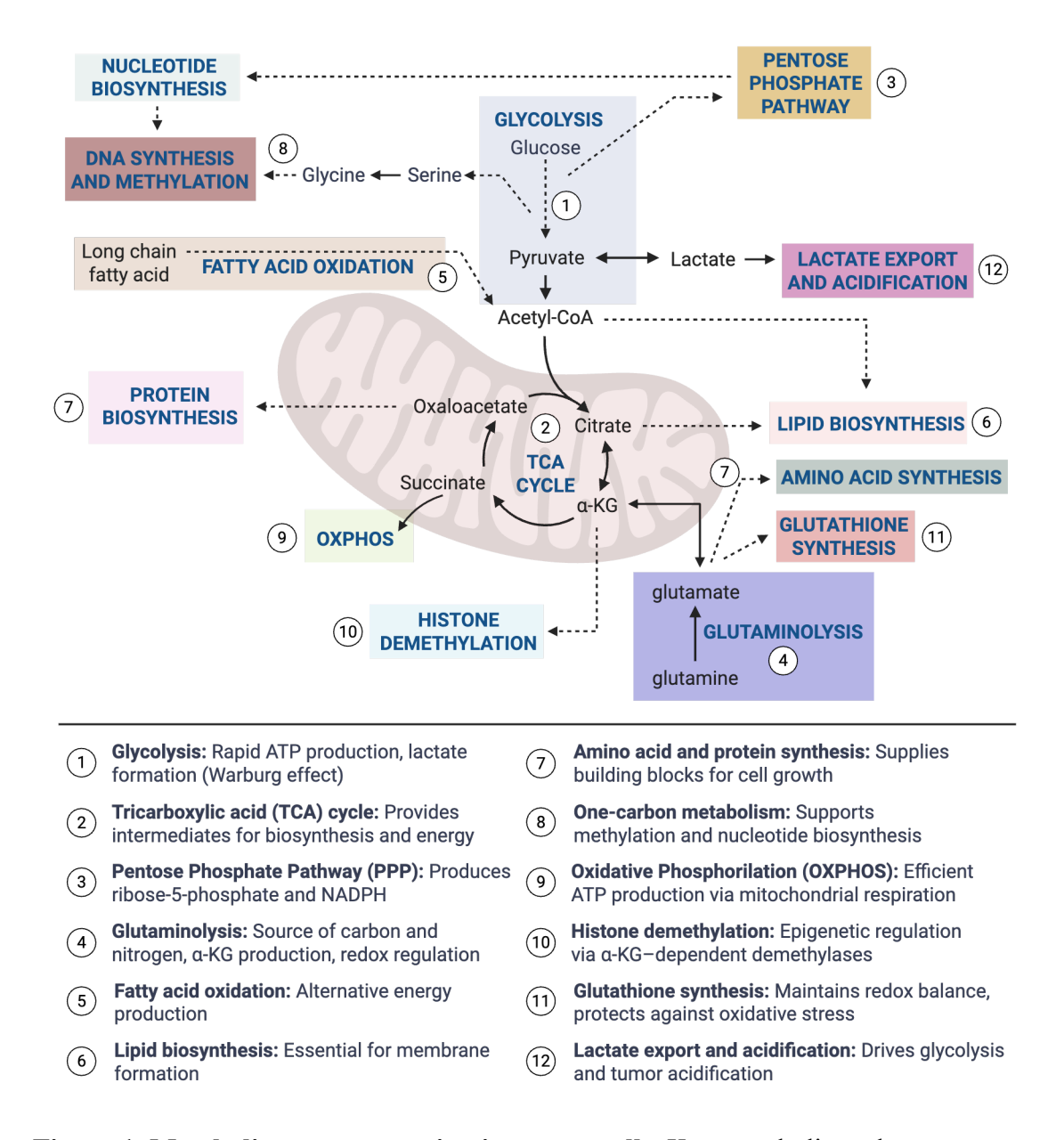


**Figure 1. Metabolic reprogramming in cancer cells**. Key metabolic pathways support rapid growth, survival, and adaptation. Through glycolysis, glutaminolysis, and biosynthetic pathways, tumors convert nutrients into energy and biomass and alter TME.

Cancer cells accumulate metabolic changes that help them utilize different nutrient sources to build new cellular components for uncontrolled growth. Moreover, tumors produce certain metabolites to influence their own behavior and that of nearby cells in the tumor microenvironment (TME) (2). Cancer metabolism is complex and flexible, enabling growth under diverse and often unfavorable conditions. Tumors use multiple metabolic routes to fulfill their needs (3, 4). Glucose is rapidly metabolized through glycolysis, not only to produce ATP but also to generate intermediates for biosynthetic pathways. Unlike normal cells that primarily rely on oxidative phosphorylation (OXPHOS) for efficient energy production, cancer cells often favor aerobic glycolysis even in the presence of oxygen (5, 6). This leads to lactate accumulation and acidification of the TME, which promotes invasion and supports angiogenesis (7, 8). Glutaminolysis supports energy production, redox balance, and the synthesis of macromolecules (9, 10). Metabolites from the tricarboxylic acid (TCA) cycle are used to produce lipids, amino acids, and nucleotides (11). Additionally, pathways such as the pentose phosphate pathway (PPP) and one-carbon metabolism provide building blocks for nucleotide synthesis and cofactors for redox homeostasis and methylation reactions (12, 13). Fatty acid oxidation and acetate metabolism offer alternative sources of acetyl-CoA and energy in nutrient-poor or hypoxic environments (14, 15). Altogether, this metabolic rewiring supports rapid proliferation, survival, and adaptation, making it a hallmark of malignant transformation (16, 17) (**Figure 1**).

## 1.2. The central regulator of metabolism: the PI3K/Akt/mTOR pathway

The phosphoinositide 3-kinase (PI3K)/Akt/mammalian target of rapamycin (mTOR) axis is a central regulator of cellular homeostasis, growth, and proliferation through the response of nutrients, stress, growth factors and other external stimuli (18). Dysregulation of the pathway is among the most frequent alterations in human malignancies, occurring in approximately 50% of all cancers (19-21). Beyond oncogenesis, aberrant mTOR signaling is implicated in the pathogenesis of various non-malignant conditions (e.g. metabolic syndrome, aging, neurodegenerative and cardiovascular diseases) (22) (**Figure 2**).

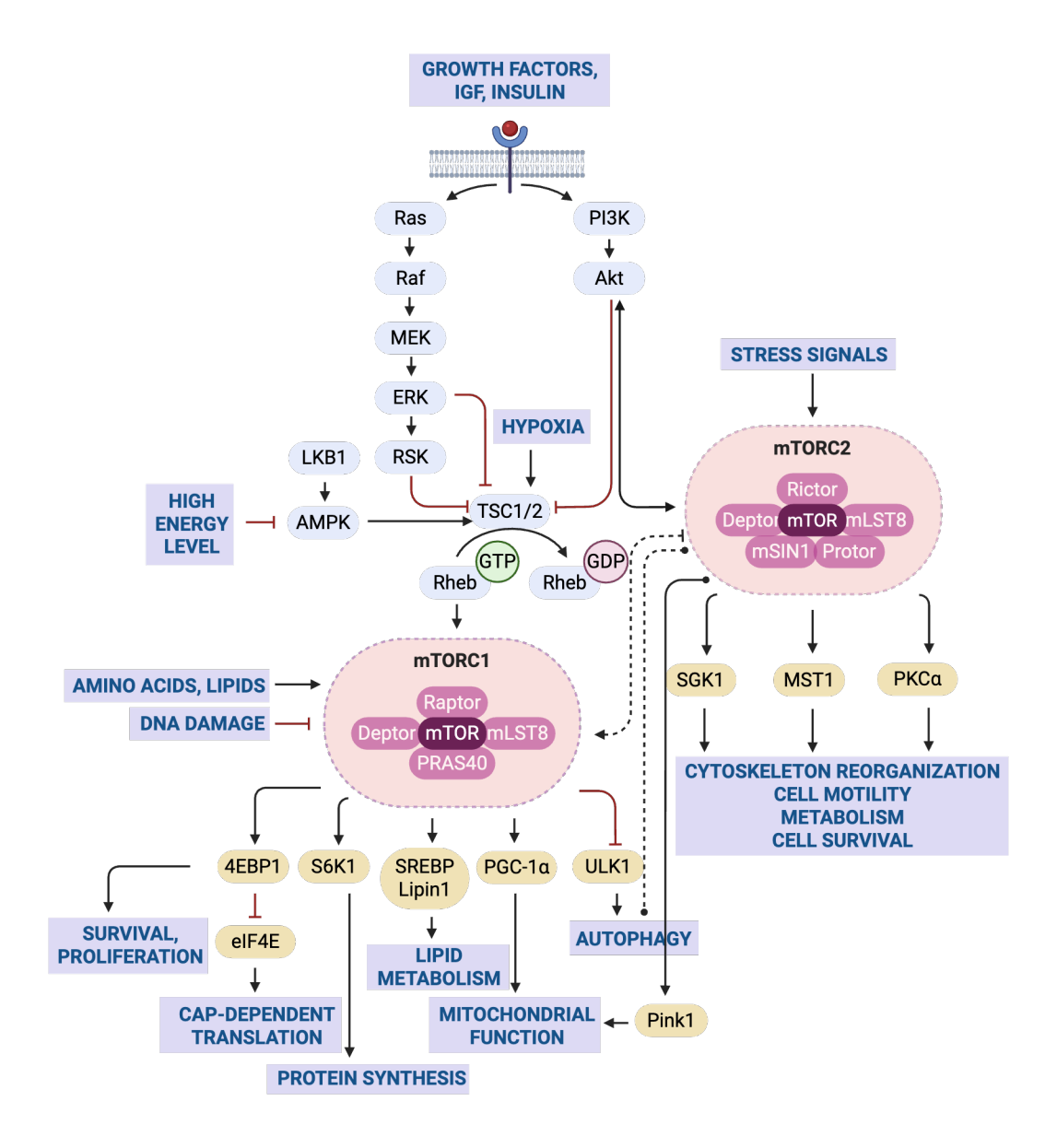


**Figure 2. mTORC1 and mTORC2 complexes** are the central regulator of metabolism (23), integrating signals from growth factors, nutrients, energy status, and stress to control processes such as protein synthesis, lipid metabolism, autophagy, and cell survival.

Inappropriate activation of membrane receptors (receptor tyrosine kinases or G-protein coupled receptors), upregulation of upstream oncogenes of PI3K, altered kinase activities, lower expression/loss-of-function of PTEN and amplification/overexpression of Akt can initiate the hyperactivation of the downstream metabolic pathways. Hyperactivation of the PI3K/Akt/mTOR axis facilitates tumor growth (24) and enhances metastatic potential by promoting increased cell motility and epithelial–mesenchymal

transition (EMT) (25). Furthermore, mutations or altered regulation of the tuberous sclerosis protein complex (TSC complex) (26), Ras homolog enriched in brain (Rheb) (27, 28), liver kinase B1 (LKB1) (29), and rapamycin-insensitive companion of mTOR (Rictor) (30) have also been involved in tumors, underscoring that multiple nodes within the PI3K/Akt/mTOR axis are vulnerable to several oncogenic alterations.

mTOR functions as the catalytic subunit in two multiprotein complexes – mTOR complex 1 (mTORC1) and mTOR complex 2 (mTORC2) – each is characterized by unique components, upstream regulators, and downstream targets. mTORC1 (the rapamycin-sensitive complex) includes Raptor and is primarily involved in regulating cell growth, protein, lipid, and nucleotide biosynthesis, as well as autophagy in response to nutrient availability and growth factors. Its key downstream effectors are S6 kinase 1 (S6K1) and 4E-binding protein 1 (4EBP1) (24). In contrast, the other complex, mTORC2 contains Rictor and is rapamycin insensitive. mTORC2 is activated mainly by growth factor signaling and is involved in cytoskeletal organization, cell survival, and metabolism through phosphorylation of Akt at Ser473, serum and glucocorticoid-regulated kinase 1 (SGK1), and protein kinase C alpha (PKCα).

mTORC1 and mTORC2 integrate environmental and intracellular signals to coordinate anabolic and catabolic processes; their dysregulation is implicated in tumorigenesis across multiple cancer types (e.g. breast cancer and kidney cancer) (31).

## 1.3. Preclinical models play a crucial role in the success of clinical trials

Aggressive cancers behave like "aberrant organs" using the patient's resources to grow and survive. Although tumors within the same (sub)type may share certain characteristics, each tumor is unique. This inter-patient and intra-tumoral heterogeneity – detectable at both cellular and molecular levels – presents a major challenge for experimental cancer modeling (32).

High-quality, biologically relevant experimental models are essential for imitating the complexity of tumors and their microenvironment. Accurate modeling is critical for understanding cancer biology and improving the predictive value of preclinical studies. The use of robust and physiologically relevant cancer models could increase the success rate in clinical trials and enhance the probability of regulatory approval. Accordingly,

drug development could become more cost-effective and sustainable, significantly lowering the price of new therapies.

In 2020, global pharmaceutical research and development expenses were estimated at 53.83 billion USD and are projected to rise to 66.66 billion USD by 2026, with nearly 30% of this spending allocated to oncology drug development (33). The development of a new drug averages 1.3 billion USD and 12 years (34). Despite these investments, the success rate is low, with only about 16% of drugs entering phase I clinical trials – lowest in oncology (8.3%) and highest in ophthalmology (29.5%) (35). In addition, safety issues that go undetected during preclinical development can lead to post-market withdrawals (1990-2009, 22/528 of newly approved active substances were withdrawn) (36, 37).

The outcome of clinical trials is influenced by multiple factors (38), one of the most critical being the selection of a suitable drug candidate (39). While preclinical studies are essential for this selection, even well-constructed models often fail to predict human responses, leading to wasted resources, time, and animal lives. Furthermore, many potentially effective compounds may be discarded during preclinical testing, despite their possible therapeutic benefit in humans.

The use of conventional two-dimensional (2D) cell monocultures in preclinical cancer research can contribute to the high failure rate in clinical trials. These simplified *in vitro* cultures fail to replicate biological mechanisms such as cell–cell and cell–extracellular matrix (ECM) interactions, tissue organization, cellular morphology, and polarity (40). While *in vivo* animal models offer higher complexity and allow the examination of systemic effects, their usability is limited by interspecies differences, poor reproducibility, limited clinical predictability and growing ethical concerns (41-44).

The drive to develop more advanced model systems is urged not only by the limitations of current models but also from regulatory shifts aimed at reducing animal testing (45). From April 2023, the European Union (EU) not only bans the animal testing of newly introduced cosmetic products but also prohibits the marketing of cosmetic products that contain newly tested ingredients on animals, even if the final product has not been tested on animals or if the tests were conducted outside the EU and the United States (46). Although pharmaceutical testing has not yet introduced the same strict rules, both the European Medicines Agency (EMA) and the U.S. Food and Drug Administration

(FDA) have publicly committed to modernizing drug development. This includes reducing reliance on animal testing by adhering to the 3R principles (Replacement, Reduction, Refinement) and promoting the development of novel *in vitro* human disease models as soon as possible (47-49). In 2025, the FDA announced plans to gradually phase out the requirement for animal testing in the approval process for monoclonal antibodies and other drugs (50).

Therefore, there is a growing need for preclinical disease models that more accurately replicate the biological behavior of human tumor tissues (51, 52). Over the past 15 years, a major paradigm shift has taken place in cancer modeling, moving away from traditional 2D cell cultures towards more sophisticated three-dimensional (3D) approaches, which are now gaining an increasing role in basic research and preclinical drug testing. Techniques such as organoid and spheroid cultures (e.g., using low-attachment plates or hanging drop methods), matrix-embedded cell cultures, magnetic levitation, and the relatively novel technology of 3D bioprinting are now being widely studied (33, 53, 54). While 2D cultures have greatly contributed to our understanding of basic cancer biology and signaling pathways, they fail to mimic the complex behavior of tumors due to the absence of variable networks within living structures (55-57), as well as proper cell-cell interactions among cancer cells and various non-cancerous cells, ECM components, and immune elements (58, 59). However, researchers must also acknowledge the different limitations of every model and carefully select the ones that best suit their specific biological question (**Figure 3**).

Advanced cancer models allow temporal and spatial analysis of treatment responses – something that is not possible in human patients. However, this complexity requires more refined analyses, as traditional biochemical assays are often inadequate for complex 3D or co-culture models.

As George E. P. Box famously said, "All models are wrong, but some are useful" (60). Testing adequate models for different research goals can help researchers find new treatments. A strategic combination of in silico, in vitro, ex vivo, and in vivo approaches will be a key to understanding the complexity of cancer biology and optimizing the development of new therapies.

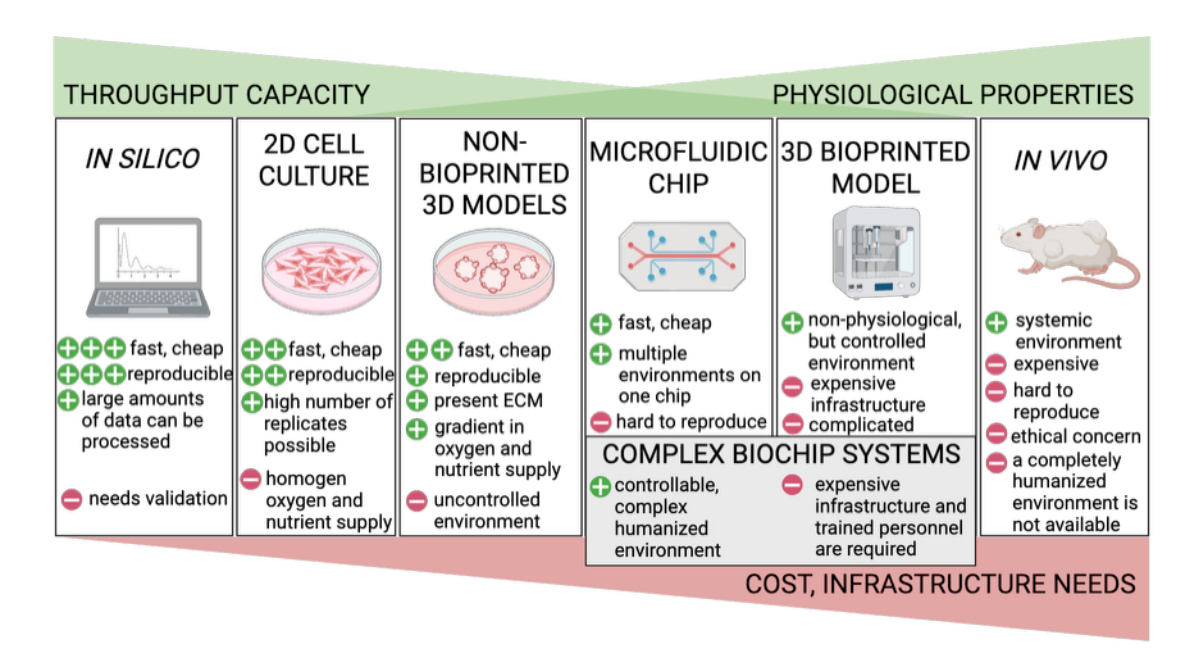


**Figure 3.** Advantages and limitations of preclinical model systems used in drug development. A wide range of models is available depending on permeability, physiological relevance, or cost-efficiency, including *in silico* simulations, *in vitro* models (2D cell cultures, spheroids, organoids, biochips, 3D bioprinted cultures), and *in vivo* models (ECM = extracellular matrix) (61).

#### 1.4. 3D bioprinting in preclinical modeling of cancer

Live-cell 3D bioprinting was first demonstrated using regular inkjet printer, which places tiny drops of material onto a surface (62). Bioprinting has its roots in the early 1980s, when *Hewlett-Packard* introduced "Cytoscribing" – the use of inkjet printers to deposit living cells in hydrogels (63). In 2003, *Thomas Boland* advanced this approach with modified inkjet printers, while *Gábor Forgács* contributed by positioning living cells in gels to enable functional tissue formation (64). The technique has redefined tissue engineering by enabling the precise fabrication of biologically functional 3D bioprinted tissue-mimetic structures (TMSs) (65).

An optimal 3D bioprinted cancer model should accurately replicate the biological behavior, mechanical structure, and dynamics of the tumor (66, 67). Therefore, the selection of the appropriate bioprinting technique, bioink, and crosslinking strategy is critical for the successful modeling of different tumor types.

# 1.4.1. Bioprinter types

The most widely used 3D bioprinting techniques are extrusion-based, droplet-based, laser-assisted, and vat polymerization-based bioprinting (68, 69). Each bioprinting technique presents distinct advantages and limitations. In the following, the most commonly used extrusion-based bioprinters, including those used in our own work, will be exclusively presented.

Extrusion-based bioprinters (introduced in 2002 at the Freiburg Research Center (70)) are also called direct ink writing and represent the most widely used bioprinting technique due to their versatility, cost-effectiveness, and capacity to produce large-scale 3D bioprinted TMSs (71, 72). In extrusion-based bioprinting, bioink is extruded through a nozzle from a syringe using either mechanical or pneumatic force to create filaments. These filaments are deposited onto a receiving substrate and layered to form the desired 3D structure, while the movement of the nozzle is guided by software. Several parameters – including temperature, nozzle diameter, extrusion pressure, print speed, extrusion rate, and spacing between filaments – influence the quality and properties of the final 3D bioprinted TMS. This method allows the use of a wide range of bioinks and supports high cell density. However, its limitations are the lower resolution, hydrogel deformation, and potential nozzle clogging or cell death due to pressure. Despite these limitations, extrusion-based systems dominate the commercial bioprinting market (57%) (73).

## 1.4.2. Bioinks for 3D bioprinting

The term bioink refers to printable formulations containing living cells or cell aggregates, typically embedded within biomaterials. In 3D bioprinting, it is important to distinguish cell-laden bioinks from cell-free biomaterial inks. While bioinks deliver cells during printing, biomaterial inks are often seeded with cells post-printing (74).

Hydrogels are the most common base for bioinks due to their biocompatibility and adjustable gelation. These include synthetic (e.g., acrylamide), protein-based (e.g., gelatin), and polysaccharide-based (e.g., alginate) hydrogels. Bioinks may also incorporate nanoparticles for drug delivery (75), nanofibers to enhance mechanical properties (76), or microgels or microspheres for added functionality (77, 78) (**Table 1**).

To ensure successful bioprinting, bioinks must exhibit appropriate viscoelasticity, gelation, resolution, and maturation properties. Rheological characteristics – such as

viscosity, shear stress, and flow behavior – define print accuracy and cell viability (79). Most hydrogel-based bioinks exhibit non-Newtonian shear-thinning behavior, facilitating extrusion while preserving shape fidelity (80, 81). However, viscosity must be balanced: higher values enhance stability but risk clogging and cell damage, while lower values improve viability but reduce printability (82). Shear stress should remain low to preserve cell integrity (83), while biocompatibility must be high to avoid harmful degradation byproducts that may reduce cell viability (84, 85).

Table 1. Bioinks used in extrusion-based 3D bioprinting related to cancer research (86).

Base		Advantages	Disadvantages	CLM
	alginate	low cost good printability rapid gelation	poor cell adhesion immunogenicity non-biomimetic ECM	ionic
	gelatine	excellent biocompatibility low cost high cellular adhesion thermally reversible	needs temperature control low mechanical strength low viscosity at RT	chemical thermal UV
SOURCES	cellulose	low cost good printability various CLM	low cell viability needs other biomaterials	chemical thermal UV
NATURAL 3	Matrigel	most used material biocompatibility well characterized	complex rheology low mechanical properties expensive high batch variability	thermal
DERIVED FROM NATURAL SOURCES	collagen-I	biocompatibility high cellular adhesion low immunogenicity enzymatically degradable close to native tissue	low shape fidelity low mechanical properties	pH thermal
DE	hyaluronic acid	excellent biocompatibility variety of modifications interacts with cell receptors fast gelation promotes proliferation	poor mechanical strength mainly used as mixture	physical covalent
	agaro se	good biocompatibility high ECM similarity	poor cell viability poor printability	thermal ionic

		thermo reversible high stability	poor cell adhesion not degradable			
	fibrin	high shape fidelity biocompatibility enzymatically degradation rapid gelation	medium cell adhesion low mechanical properties limited printability	enzymatic		
	peptides	good biocompatibility self-assembly soft-tissue applications	low pH	-		
	dECM	renders natural ECM tissue specific high biological relevance high cell survival	low stability poor printability long procedure undefined and inconsistent loss of native ECM	enzymatic UV chemical		
NTHETIC	acrylamide	elastic, flexible most standardized protocol	needs other supportive material for proliferation	UV		
OM SY	PCL	good mechanical strength controllable degradation	not compatible with live cell 3D bioprinting	chemical thermal		
DERIVED FROM SYNTHETIC SOURCE	pluronic	high shape fidelity good printability	lack of cell-binding domains low cell viability poor mechanical strength	thermal UV		

CLM = cross-linking method, dECM = decellularized extracellular matrix, ECM = extracellular matrix, PCL = polycaprolactone, RT = room temperature, UV = ultraviolet light

## 1.4.3. 3D bioprinting parameters

The properties of the created 3D bioprinted TMSs depend on the printing precision and construct integrity (e.g., resolution, size, shape, stability), as well as cell functionality (e.g., viability, proliferation, differentiation, tissue formation), which are influenced by printing parameters.

Nozzle size and applied pressure impact resolution, layer thickness, as well as overall print quality, and play a critical role in cell viability. Smaller nozzle diameters and higher pressures increase shear stress, leading to greater cell damage during printing (87-90). High printing speeds can decrease cell viability during the fabrication of the structures. Speed affects not only total print time but also the final shape and dimensions

of the printed structures. Additionally, nozzle or extrusion temperature plays a significant role, especially in inkjet-based printing, as it influences layer uniformity, printing accuracy, and cell survival (91, 92).

Viscoelasticity is a material property where a substance exhibits both elastic (solid-like) and viscous (fluid-like) behavior. In bioprinting, this refers to the ability of the bioink to flow under pressure but also retain its shape after printing, which is essential for printing stability and cell protection. A balanced viscoelasticity is recommended to optimize filament formation and shape retention, while avoiding clogging or collapse of the structure (93, 94).

# 1.5. Advances in 3D bioprinting for biomedical applications in cancer research

3D bioprinting enables tumor modeling with greater complexity than traditional *in vitro* methods. By using multiple bioinks and cell types (e.g., cancer cells, fibroblasts, immune cells, and endothelial cells), 3D bioprinting enables the modeling of complex and heterogeneous TME. Advances in bioink formulation also allow the replication of key mechanical and biochemical features of the ECM. This technology supports the study of progression, drug resistance, and therapeutic response in a more physiologically relevant context. While diverse tumor models have been developed, this dissertation focuses on breast and renal cancers.

#### 1.5.1. 3D bioprinted breast cancer models

A variety of 3D bioprinted breast cancer models has been established to mimic the TME. In these models, cell proliferation and tissue integrity could be successfully demonstrated by incorporating co-cultured cells and maintaining physiological structures (95). Chimeric organoids were generated by co-printing breast cancer and mammary epithelial cells, resulting in increased 5-hydroxymethylcytosine levels in tumor cells (96). Bone metastasis of breast cancer was modeled using osteoblast- and mesenchymal stem cell co-cultures, where cancer-driven vascular endothelial growth factor (VEGF) upregulation and stromal suppression was observed, alongside the growth stimulation of breast cancer cells (97). For modeling adipogenic functions, adipose-derived stromal cell spheroids were bioprinted, where tumor-induced matrix alterations could be detected, which highlight the tumor-adipose tissue interactions (98). Adipose-derived

mesenchymal stem cells were shown to enhance doxorubicin resistance by decreasing apoptosis and stiffening the matrix (99). A vascularized tumor model was constructed from metastatic cells, endothelial cells, and fibroblasts, enabling the study of stromal density effects on angiogenesis and invasion (100). Acidic conditions were shown to increase chemotherapeutic uptake (101, 102) and the efficacy of photothermal therapy (103, 104) in 3D environment. Immune-tumor co-cultures revealed cytokine-mediated immune cell activation and complete tumor clearance by T-cells within three days (105).

#### 1.5.2. 3D bioprinted renal cell carcinoma models

3D bioprinted living kidney tissues are mainly used in regenerative medicine, disease modeling, and toxicity testing, while renal cancer models are rarely developed (106-111). A 3D bioprinted renal cell carcinoma (RCC) model was developed using collagen—alginate—gelatin hydrogel to form tunneling nanotube-like structures, where mitochondrial transfer and tumor communication was studied (112). A patient-specific vascular model of clear cell renal cell carcinoma (ccRCC) was generated in a microfluidic system using tumor and normal endothelial cells to observe differences in angiogenesis and drug response between 2D and 3D models – sirolimus was effective only in 2D (113). A 3D spheroid model of papillary renal cell carcinoma (pRCC) was built by layering tumor cells over fibroblasts, restoring MET-dependent growth and drug sensitivity, highlighting the role of fibroblasts in progression (114). A bioprinted neuroblastoma renal metastasis model was also developed, and drug responses were shown to be dependent on both cell-type and model system (115).

## 1.6. Issues concerning the comprehensiveness of 3D bioprinting literature

Although there are abundant review articles on the topic of 3D bioprinting, review articles comprise approximately 40% of the publications, overshadowing original research (**Figure 4**). This imbalance may suggest that the scientific community is more focused on summarizing existing knowledge rather than generating new findings (116), highlighting the need for a stronger influx of original research to drive the field forward.

Several factors may explain this pattern. The Coronavirus disease 2019 (COVID-19) pandemic shifted research priorities, leading to a rise in the publication of literature reviews. Furthermore, pressures within the academic ecosystem (peer-review, research funding, and academic degrees) have also influenced research output.

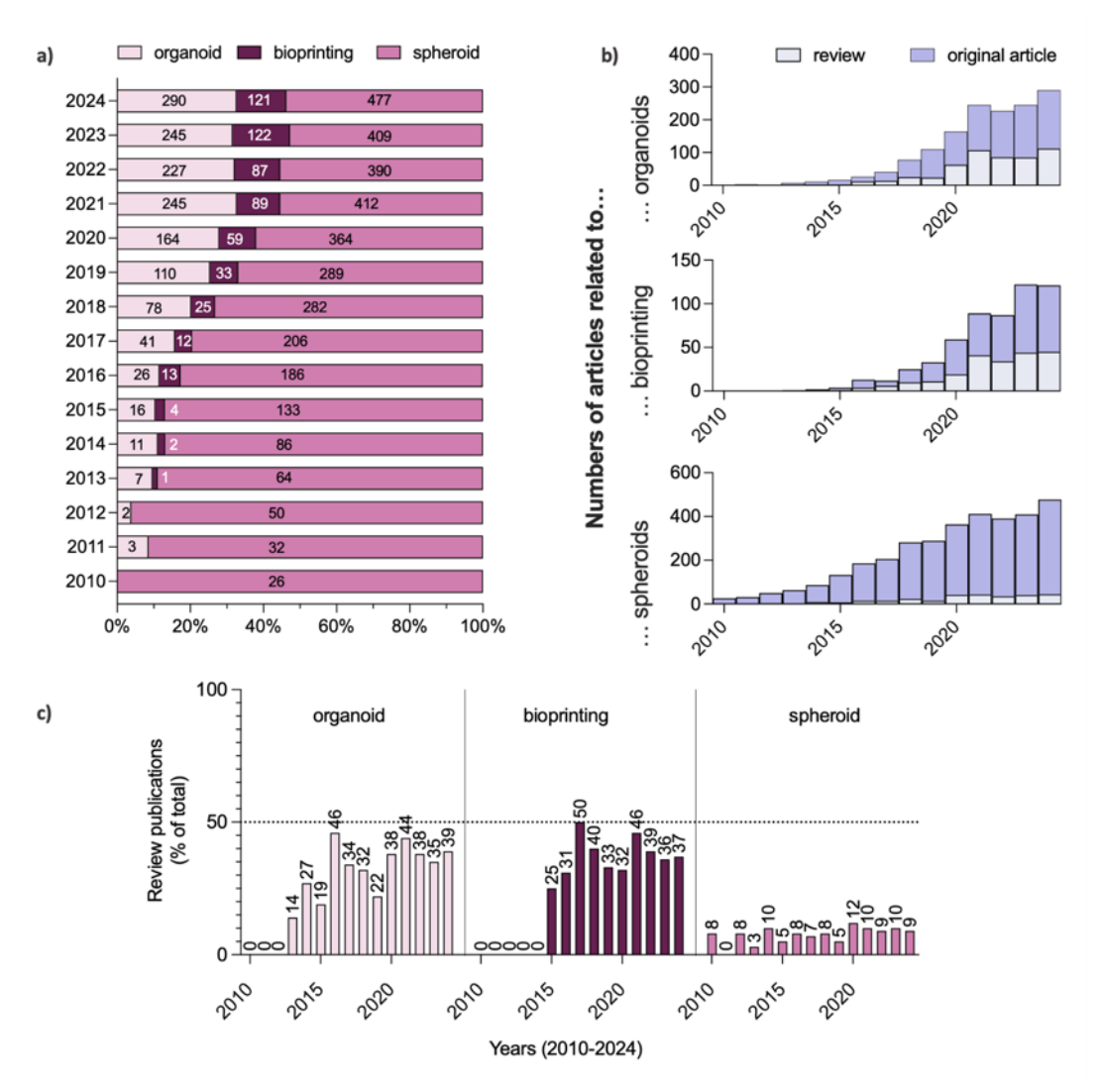


**Figure 4. Evolution of scientific publications on 3D** *in vitro* models based on a **PubMed data search** (2010–2024; data retrieved on February 5, 2025). *(a)* Proportional distribution (%) and absolute number of publications using different 3D model systems in cancer research – organoids, spheroids, and 3D bioprinting (100% stacked column chart). *(b)* Comparative ratio of review articles to original research articles across the different 3D model platforms (stacked column chart). *(c)* Yearly percentage of review articles relative to the total number of publications within the field.

# 1.7. Molecular characteristics of renal cell carcinoma subtypes

RCC originates from the renal tubular epithelial cells, with distinct histological and molecular subtypes (117). The most common subtypes are ccRCC (75–80%), and pRCC (10–15%), which differ in morphology, clinical behavior, molecular alterations and metabolic profiles. RCC is considered a metabolic disease driven by dysregulated pathways involved in oxygen, energy, and nutrient utilization (118).

ccRCC is characterized by frequent loss of function of the von Hippel-Lindau (VHL) tumor suppressor gene (119). The inactivation of VHL leads to the stabilization of hypoxia-inducible factors (HIF-1 $\alpha$  and HIF-2 $\alpha$ ) even under normoxic conditions. HIF-mediated transcriptional activity promotes the expression of genes involved in angiogenesis (e.g., VEGF, platelet-derived growth factor -PDGF), glucose metabolism (e.g., GLUT1, GLUT4), and proliferation (e.g., epidermal growth factor -EGF). Consistent with these characteristics, ccRCC is characterized mainly by the Warburg phenotype; it exhibits increased aerobic glycolysis, reduced OXPHOS, and high levels of lactate production (120).

In contrast, pRCC exhibits greater molecular heterogeneity (121). Type 1 pRCC is often associated with activating mutations in the MET proto-oncogene, which is involved in cell growth, motility, and survival. Type 2 pRCC can be divided into even more heterogeneous subgroups, which often involve alterations in TCA cycle enzymes: fumarate hydratase (FH) or succinate dehydrogenase (SDH) (122). Loss of function in these enzymes leads to the accumulation of TCA intermediates that function as oncometabolites and promote tumorigenesis through epigenetic dysregulation (122-124). Additionally, our research group highlighted that ccRCC primarily relies on aerobic glycolysis ("Warburg" phenotype), whereas pRCCs exhibit a less glycolytic, predominantly OXPHOS-driven metabolism, relying on glutamine and other TCA cycle substrates (125).

The glycolytic dependence of ccRCC makes it vulnerable to agents targeting glucose metabolism or HIF activity, while the oxidative and glutamine-driven profile of pRCC suggests different vulnerabilities, such as inhibition of glutaminolysis or mitochondrial function. These differences may be particularly important in the context of post-transplant (post-tx) RCC, where immunosuppressive (IS) regimens may influence the TME, metabolism and progression across subtypes (126).

The distribution of post-tx RCC subtypes after transplantation changes compared to the general population. The predominance of pRCC (51%) among post-tx RCCs – significantly higher than the 10-15% typically observed in the *de novo* population – has been reported in previous studies (127). This shift in subtype distribution suggests that the altered metabolism may play an important role in the development of post-tx RCC (128, 129).

# 1.8. Targeting the PI3K/Akt/mTOR pathway in renal cell carcinoma

The PI3K/Akt/mTOR pathway plays an important role in the development and progression of RCC by promoting protein synthesis, angiogenesis, metabolic reprogramming, and resistance to apoptosis (130). Genetic alterations affecting the mTOR signaling cascade have been detected in 28% of RCC cases, especially in ccRCC (120). Activation can occur through multiple mechanisms, including growth factor receptor overexpression (e.g., VEGF, EGF), mutations in PI3K/Akt/mTOR components themselves or in regulatory components (e.g., TSC1, TSC2, PTEN), or loss of VHL function. In pRCC, mTOR pathway alterations are less frequent, especially in type 2 pRCC (131-133).

Therefore, the mTOR pathway has become a therapeutic target for managing RCC, particularly in patients with poor prognosis or those who have progressed after VEGF-targeted therapy (134, 135). Temsirolimus showed survival benefits in poorprognosis metastatic RCC patients, with FDA approval in 2007 following a successful phase III trial (136). However, later clinical trials have shown mixed results: temsirolimus was less effective in non-clear-cell RCC when compared to axitinib (137).

Clinical responses to mTOR inhibitors are often modest; therefore, they are used typically as second-line or later options, or in specific settings such as post-tx malignancies where both IS and antiproliferative effects are required. Their dual role in immunomodulation and tumor suppression makes them particularly relevant in transplant recipients (138).

## 1.9. Immunosuppressive therapy and cancer risk after kidney transplantation

Kidney transplantation remains the treatment of choice for patients with end-stage renal disease (ESRD), offering improved quality of life and long-term survival compared

to dialysis (139). The success of transplantation depends on lifelong IS therapy to prevent graft rejection, which necessitates a balanced IS regimen to suppress immune responses and minimize adverse effects (**Table 2**).

It is well-known that there is an elevated risk of malignancies among kidney transplant recipients (KTRs) (140-147). According to a recent study, about 25% of KTRs will develop a tumor (excluding non-melanoma skin cancer, which occurs in 50% of recipients). Post-tx tumors occur in approximately 7–33% of cases, with RCC being the most frequent (14%) (148, 149). In addition to the higher occurrence of cancer, cancerspecific mortality – where tumor or comorbidity is the cause of death (150) – is also higher in KTRs. This can be due to the immunocompromised status caused by maintenance IS therapy (151). The connection between IS regimen and cancer risk is not completely clear, since transplant patients usually receive combination treatments, so it is complicated to examine the role of individual substances.

Life-long maintenance IS therapy includes various combinations, and most of them have already been linked to elevated tumor risk. These include calcineurin inhibitors (CNIs) such as tacrolimus (TAC) or cyclosporine A (CsA). The tumorigenic effect of CsA has been confirmed in many studies (152-157). TAC tends to be superior to CsA in improving graft survival, although it has also shown neoplastic effects: topical use of TAC can induce squamous cell carcinoma (158, 159) and in also associated with an increased risk of lymphoma (160). TAC is associated with higher risk of cancer in KTRs, with similar or even higher carcinogenicity as CsA (161, 162), as it has been linked to earlier RCC onset compared to CsA (163). Nonetheless, some studies do not find an association between TAC and skin cancer development (164-166); however, these studies evaluated topical use, where minimal systemic absorption occurs (167). TAC can drive tumorigenesis by inducing TGF- $\beta$  via ERK, promoting EMT, ECM remodeling/buildup, and immune evasion (168, 169). CNIs can also activate the mTOR pathway through Ras activation, potentially increasing mTORC1 activity cell-type specifically (170).

Other commonly used IS drugs have also been associated with carcinogenic effects. Most KTRs receive high-dose corticosteroids to prevent acute rejection in early period after transplantation and then taken at a lower dose as maintenance therapy. Based on numerous studies, the carcinogenesis-inducing effect of corticosteroids is still unclear: they tend to increase the risk of malignancies (171, 172), but there are contradictions in

the experimental data, as well (173-175). Azathioprine was also associated with increased risk of carcinogenesis (176-179), but some studies claim no increased risk of malignancies (180, 181). Mycophenolate mofetil (MMF) and mycophenolic acid demonstrated a correlation with lower risk of malignancies (182-184), however, it might be related to Kaposi sarcoma (185).

Rapamycin (Rapa, sirolimus) was first registered by the FDA as an immunosuppressant in 1999 for using in combination with CsA. In November 2000, the drug was registered by the EMA as an alternative to CNI for maintenance IS therapy. Increasing evidence suggests a connection between the use of mTOR inhibitors and a lower risk of overall malignancies among recipients (186-192). For this reason, conversion to Rapa in patients with a history of cancer is recommended and safe regarding renal function and graft survival (193, 194). Early conversion to an mTOR inhibitor-based IS regimen was noninferior to other IS regimens (195); however, other studies suggest that early mTOR inhibitor initiation is preferred, as later conversion may be limited by existing CNI-induced nephrotoxicity (196, 197).

CNIs prevent acute rejection but are associated with nephrotoxicity, graft dysfunction, and possible malignancies. mTOR inhibitors are nephroprotective and antiproliferative, potentially lowering post-tx cancer risk, though they have adverse effects. Overall, early CNI minimization might support both short- and long-term kidney function (198).

**Table 2. Overview of common maintenance immunosuppressive drugs used in solid-organ transplantation.** It includes representative agents, brand names, molecular targets, mechanisms of action, and typical side effects.

Class	Agent	Brand name	Target	Effect	Side effects
CS	Methyl- prednisolone	Medrol	Cytosolic glucocorticoid receptor	Modulates gene expression	Hypertension, glucose intolerance, dyslipidemia, osteoporosis, thin skin, muscle loss, gastric ulcers, infections, psychosis
CNI	CsA	Sandimmune Neoral; Ciclosporin IDL	Binds cyclophilin; inhibits nuclear translocation of NFAT; inhibits calcineurin	Inhibits T-cell activation	Nephrotoxicity, hypertension, dyslipidemia, neurotoxicity, glucose intolerance, vomiting, diarrhea, gingival hyperplasia, infections
CINI	TAC	Adport; Prograf; Envarsus; Advagraf; Modigraf; Tacforius	Binds FKBP-12; inhibits nuclear translocation of NFAT; inhibits calcineurin	Inhibits T-cell activation	Hypertension, dyslipidemia, glucose intolerance
AM	Azathioprine	Imuran	Purine nucleotides are released	Inhibits <i>de novo</i> and salvage purine synthesis	Anemia, neutropenia, thrombocytopenia, hepatotoxicity, pancreatitis
	MMF	Cellcept; Myclausen; Myfenax	Inhibits IMPDH; inhibitis cGMP synthesis	Inhibits <i>de novo</i> purine synthesis	Diarrhea, nausea, vomiting, leukopenia, thrombocytopenia, anemia
mTORI	Sirolimus (Rapa); Everolimus	Rapamune; Certican	Binds FKBP-12; blocks p70S6K	Inhibits T-cell activation; blocks cell cycle	Dyslipidemia, thrombocytopenia, hepatotoxicity, pneumonitis, infections, hypokalemia, hyperglycemia, hypertension, acne

AM = antimetabolite, CNI = calcineurin inhibitor, CS = corticosteroid, CsA = cyclosporin A, NFAT = nuclear factor of activated T-cells, TAC = tacrolimus, FKBP-12 = FK506-binding protein 12, MMF = mycophenolate mofetil, mTORI = mTOR inhibitor, Rapa = rapamycin

# 2. Objectives

# 2.1. Establishment and characterization of 3D bioprinted cancer models

The quality and physiological relevance of preclinical models are critical determinants of success in the drug development pipeline. Traditional 2D monolayer cell culture models fail to recapitulate the complex architecture, cell—cell interactions, and microenvironmental features of tumors, limiting their predictive value. Therefore, robust and predictive *in vitro* models are essential for predicting *in vivo* and later clinical efficacy and safety outcomes. In this context, 3D bioprinted tumor models represent a promising advancement, offering improved structural and functional resemblance to *in situ* tumors.

Our objectives aim to develop a standardized, physiologically relevant 3D tumor model that enhances the predictive value of preclinical testing and supports the discovery of more effective cancer therapies.

## Accordingly, our main objectives were as follows:

- 1. To establish and optimize a reproducible 3D bioprinting workflow, including the formulation of customized bioinks and the fine-tuning of printing parameters for the generation of 3D bioprinted TMSs.
- 2. To generate 3D bioprinted RCC and breast cancer models from various cell lines (ZR75.1, T47D, MCF7, A498, 786-O, 4T1) and tumor-derived cells.
- 3. To validate the usability of *in vitro* growth-monitoring assays in 3D bioprinted TMSs using a stable mCherry-transfected cell line.
- 4. To investigate tissue morphogenesis and spatial organization within the 3D bioprinted breast cancer TMSs, focusing on cell-cell and cell-ECM interactions.
- 5. To characterize the activity of the mTOR signaling pathway within the 3D bioprinted breast carcinoma TMSs and compare it with conventional 2D monolayer cultures to evaluate differences in baseline signaling.
- 6. To assess the therapeutic sensitivity of the 3D bioprinted breast carcinoma TMSs to mTOR inhibitors and chemotherapeutic agents, and to compare these responses with those observed in 2D monolayer cultures.
- 7. To establish a 3D bioprinted "patient-derived" breast cancer model and compare its drug sensitivity profile with that of other *in vitro* and *in vivo* models.

# 2.2. Tumorigenic role of tacrolimus in post-transplant renal cell carcinoma

The increased risk of malignancies following organ transplantation is well-known. This elevated cancer risk has been attributed to long-term IS therapy, which reduces immune function. However, differences in the tumor-promoting potential of various IS drugs suggest that certain agents may have direct pro-oncogenic effects, independent of immune suppression. These effects may be mediated through the modulation of intracellular signaling pathways, which are known to influence cellular proliferation, metabolism, and survival.

Our objectives aim to elucidate the differential effects of IS agents on oncogenesis and to investigate the molecular pathways underlying post-tx malignancies, with a particular focus on mTOR signaling dynamics.

# To investigate this hypothesis, our specific objectives were as follows:

- 1. To collect a comprehensive RCC cohort of post-tx kidney tumors and *de novo* RCCs from non-transplanted (non-tx) patients.
- 2. To examine the *in situ* effect of CNI- or mTORI-based immunosuppression on mTOR pathway activity in the renal tissue of patients with ESRD, as well as in ischemia-induced murine kidneys *in vivo*.
- 3. To examine the *in situ* effect of CNI- or mTORI-based immunosuppression on mTOR pathway activity in post-tx and *de novo* RCCs, focusing separately on mTORC1 and mTORC2 complexes.
- 4. To evaluate the *in vitro* impact of CNI- or mTORI-based immunosuppression on cell proliferation and mTOR pathway activation in a normal human tubular epithelial cell line and RCC cell lines representing various histological subtypes (2D monolayer cultures and 3D bioprinted TMSs).
- 5. To compare the long-term effects of different IS agents (mTORI- vs. CNI-based) on tumor growth and mTOR pathway activity using a human *in vivo* RCC xenograft mouse model and *in vitro* 3D bioprinted tissue-mimetic structures.

#### 3. Methods

# 3.1. Cell cultures and in vitro reagents

*In vitro* experiments were conducted using a panel of RCC and breast cancer cell lines, as summarized in **Table 3**.

Table 3. Data of the used cell lines.

Cell line	Origin	Subtype	Medium	Source	Reference	Gen. mod.
786-O	H-RCC	clear cell	RPMI-1640	ATCC	#CRL-1932	no
A498	H-RCC	clear cell	MEM	ATCC	#HTB-44	no
ACHN	H-RCC	papillary	DMEM-HG	Sigma	#88100508	no
HK-2	H-PTC	kidney	DMEM-HG	ATCC	#CRL-2190	no
ZR75.1	H-BC	lum. B	RPMI-1640	ATCC	#CRL-1500	no
T47D	H-BC	lum. A	RPMI-1640	gift	(199)	mCherry
MCF7	H-BC	lum. A	RPMI-1640	ATCC	#HTB-22	no
4T1	M-BC	TNBC	DMEM-HG	ATCC	#CRL-2539	no

ATCC = American Type Culture Collection, BC = breast cancer, DMEM = Dulbecco's Modified Eagle Medium, Gen. mod = genetic modification, H = human, HG = high glucose, lum = luminal, M = mouse, MEM = Minimum Essential Medium, PTC = proximal tubular cell, RCC = renal cell carcinoma, RPMI = Roswell Park Memorial Institute (origin), TNBC = triple negative breast cancer

Cells were maintained and cultured at 37 °C in a humidified incubator with 5% CO<sub>2</sub>. All media were supplemented with 10% fetal bovine serum (FBS), 2 mM L-glutamine, and penicillin/streptomycin (100 UI/mL) or gentamycin (80 mg/2 mL) antibiotics (all from Biosera). *In vitro* treatments were performed on cells seeded in 96-well plates (Sarstedt; 2–5 × 10<sup>3</sup> cells/well), T25 flasks (Sarstedt; 2–5 × 10<sup>4</sup> cells/flask), or 6-well plates (Sarstedt; six TMSs/well). For drug sensitivity testing, after 24-hour (2D) or 7-day (3D) preculturing, media was refreshed, and cells were exposed for 72 hours to the treatments (**Table 4**). Concentrations were chosen based on recommended serum levels and former experiments (200, 201). For long-term exposure, TAC (10 ng/mL) or Rapa (10 ng/mL) was reapplied immediately after each medium change over a 21-day period, cells were manually counted, and none were discarded.

Table 4. Characteristics of the *in vitro* treatment substances used in the study.

Substance Target Conc. Source	
-------------------------------	--

tacrolimus (TAC)	CNI	10 ng/mL	Merck-Sigma-Aldrich	
(1110)		50 ng/mL	11101011 2181111 111111011	
ronomyoin (Dono)	allosteric mTORI	10 ng/mL	Merck-Sigma-Aldrich	
rapamycin (Rapa)	(selective mTORC1 inhibitor)	50 ng/mL	Wielek-Sigilia-Aldifeli	
PP242	ATP-competitive mTORI		Tocris Bioscience	
FF2 <b>4</b> 2	(dual mTORC1/C2 inhibitor)	1 μΜ	TOCHS BIOSCIENCE	
ipatasertib (Ipa)	pan-Akt inhibitor	1 μΜ	Selleckchem	
cisplatin (Cis)	DNA cross-linking agent	1 μΜ	Accord Healthcare	
doxorubicin (Doxo)	topoisomerase II inhibitor	50 ng/mL	Teva Hungary	

CNI = calcineurin, Conc. = concentration, mTORI = mTOR inhibitor

## 3.2. *In vitro* proliferation assays (Alamar Blue and Sulforhodamine B)

For 2D assays, cells were seeded in 96-well plates, while 3D bioprinted TMSs were cultured in p-HEMA-coated 6-well plates. Following treatments, cell viability and proliferation were measured using Alamar Blue (AB; Thermo Fisher Scientific) and Sulforhodamine B (SRB) assays. For 3D bioprinted TMSs, proliferation assays were conducted in 96-well plates by transferring the TMSs directly into the wells prior to AB addition. AB was diluted 1:10 in culture medium. Fluorescence was recorded after a 2-4-hour incubation using a Fluoroskan Ascent FL reader (AB: 570–590 nm, mCherry: 530–620 nm, Labsystems International), and data were processed with Ascent software.

For the SRB assay, cells were fixed with trichloroacetic acid (10 %, 4 °C, 60 min), washed with distilled water, and air-dried. Fixed cells were stained with 0.4% SRB in 1% acetic acid (15 min, RT), followed by washing with 1% acetic acid and drying. Protein-bound dye was dissolved in 10 mM Tris buffer, and absorbance was measured at 570 nm using a microplate reader (Labsystems International).

All measurements were performed in six replicates and each experiment was repeated at least three times. Proliferation and viability were expressed relative to untreated controls; vehicle-only wells and cell-free printed constructs served as negative controls.

## 3.3. Preparing hydrogels for 3D bioprinting

Two bioinks were formulated for 3D bioprinting, selected based on their printability, ability to support cell viability, and compatibility with experimental analyses.

For a low-viscosity, cell-containing bioink ("cellular gel"), 3% (w/v) sodium alginate was dissolved in water and sterilized (in autoclave, 121 °C, 120 kPa, 20 min). While still warm, sterile 1% (w/v) gelatin (Sigma-Aldrich) was added under aseptic conditions, then refrigerated at 4 °C for  $\geq$ 24 h. Immediately prior to printing, cells were gently suspended in the gel at  $1\times10^7$  cells/mL and the mixture was maintained at 37 °C. For an acellular "scaffold gel", a 6% (w/v) alginate and 11% (w/v) methylcellulose (Sigma-Aldrich) blend was prepared. The scaffold gel was loaded into printer cartridges and refrigerated at 4 °C for  $\geq$ 24 h to complete gelation, then equilibrated at room temperature (RT) 1 h before use. Each gel was loaded into a separate printhead to enable alternating layer deposition. CaCl<sub>2</sub> (calcium chloride, Sigma-Aldrich) was dissolved in sterile water at 200 mM and subsequently sterilized by filtration (0.22  $\mu$ m).

The rheological behavior of the formulated bioinks was assessed using a Kinexus Pro+ rheometer (Model KNX2100, Malvern Instruments Ltd.). Data analysis was carried out using rSpace software version 2.0. Tests were performed in rotational mode with a cone-plate geometry (CP4/40 SR0207 SS: PL65 S0815 SS), maintaining a 0.15 mm gap. For each measurement, 1.0 g of gel was applied, and three replicates were analyzed. Viscosity was evaluated at two temperatures: RT ( $25.0\pm0.01\,^{\circ}$ C) and physiological temperature ( $37.0\pm0.01\,^{\circ}$ C), across a shear rate range of 0.1 to  $100\,\text{s}^{-1}$ . To determine the influence of temperature on gel properties, additional tests were performed under a constant shear stress of 1 Pa while gradually increasing the temperature from 20 °C to 40 °C. Each condition was assessed in triplicate, and results are presented as mean values with standard deviations.

## 3.4. 3D bioprinting of tissue-mimetic structures

The 3D bioprinted TMSs were designed using GeSiM Robotics software and produced with an extrusion-based bioprinter (Bioscaffolder 3.2, GeSiM) equipped with two independently controlled dispensing units. For proliferation assays, constructs with a 5 mm diameter and a total height of 0.5 mm were printed, consisting of six alternating layers of cell-containing and acellular scaffold gels. For IHC or western blot/WES<sup>TM</sup> Simple analyzes, larger structures (10 mm diameter, 1 mm total height) composed of 10 alternating layers were fabricated. Bioprinting was performed with the following parameters: interlayer angle of 90°, infill distance of 1.5 μm, layer connection set to

"outline plus", and printing speed of 10 mm/s. Needle diameters were 110 μm for the acellular scaffold gel and 50 μm for the cell-containing gel, applied at pressures of 400 kPa and 20 kPa, respectively. Post-printing, the constructs were crosslinked in 200 mM CaCl<sub>2</sub> (2 min), then transferred into fresh medium and refreshed every 2–3 days. To prevent cell attachment to the plate surface, TMSs were maintained in poly-(2-hydroxyethyl methacrylate) (p-HEMA; Sigma-Aldrich)-coated 6-well plates (Sarstedt).

# 3.5. Renal cell carcinoma cohort and tissue microarray construction

The study included post-tx RCCs (n = 44; arising in the remaining kidneys of KTRs) and non-tx RCCs (n = 46; from patients who had not received IS). All tumors were evaluated and classified according to the WHO Classification (117). Additionally, kidney tissues from patients with ESRD (n = 10) and from donor kidneys that were non-transplantable due to surgical reasons (normal kidney; n = 3) were analyzed. All samples were obtained by surgical resection at Semmelweis University (2000-2015), with approval from the Hungarian Scientific Council National Ethics Committee for Scientific Research (No. 7/2006, SE-RKEB - 216/2020).

Tissue microarrays (TMA) were constructed by extracting 2-mm diameter cores from FFPE blocks of RCCs, ESRD tissues, and normal kidney samples. For each case, at least two cores were taken from histologically representative regions, as identified on HE-stained sections by an experienced pathologist. The cores were embedded into recipient paraffin blocks using the TMA Master instrument (3DHistech).

## 3.6. Immunohistochemistry and hematoxylin-eosin staining

For histopathological assessment, formalin-fixed, paraffin-embedded (FFPE) blocks were used. Representative areas were selected by an experienced pathologist for subsequent analysis on routinely hematoxylin-eosin (HE)-stained (4-µm-thick) sections.

For 2D cell cultures, cells were detached using Triple X reagent (Gibco), resuspended in liquid agar, and formalin fixed after the agar had solidified. The 3D bioprinted TMSs were fixed in 10% formalin, then stabilized in 1% agar solution (4 °C, 10 min) and transferred into tissue cassettes. These experimental blocks were dehydrated and embedded in paraffin.

For immunohistochemistry (IHC), sections were deparaffinized, endogenous peroxidase activity was blocked, and antigen retrieval was carried out in a pressure cooker (10 mM citrate buffer; pH 6.0; 10-30 min). Slides were incubated with primary antibodies (**Table 5**), and detection was performed with either the Novolink Polymer detection system (Leica Biosystems) or the Vectastain Universal Quick HRP Kit (Vector Laboratories). 3,3'-Diaminobenzidine (DAB; Dako) was used as chromogen, followed by hematoxylin counterstaining. Stained slides were scanned and independently evaluated by two observers using SlideViewer 2.7 software (3DHistech).

Quantitative evaluation was performed on the RCC cohort. A semi-quantitative H-score was calculated by combining the staining intensity (0, 1+, 2+, or 3+) with the percentage of positive cells (202). Median H-score values defined the cutoffs between "low" and "high" expression (p-mTOR: 130; p-S6: 110; Rictor: 100). mTORC1 activity was estimated based on the expression of p-mTOR and p-S6, while mTORC2 activity was based on p-mTOR and Rictor expression; cases with high expression of p-mTOR and Rictor were classified as mTORC2-high.

Table 5. Primary antibodies used for protein analyzes.

Antibody	Brand	Cat. No	IHC	Dilution WB	WES <sup>TM</sup>	Function
mTOR	CS	#2983	1:100	1:1000	1:50	kinase of mTORC1/C2
p-mTOR	CS	#2976	1:100	-	1:50	activated form of mTOR
(Ser2448)	CS	#2971	-	1:1000	-	
	CS	#5536	-	1:1000	-	
TSC1	GTX	GTX130062	-	1:1000	-	neg.reg. of mTOR
pan-Akt	CS	#4691	1:500	1:1000	1:50	target of mTORC2
p-Akt (Ser473)	CS	#4060	1:50	1:1000	1:50	activated form of Akt
pSAPK/JNK (Thr183/Tyr185)	CS	#4668	-	1:1000	-	stress response
S6	CS	#2317	1:100	1:1000	1:50	target of mTORC1
p-S6	CS	#4858	1:100	1:1000	-	activated form of S6
(Ser235/236)	CS	#2211	1:100	-	-	
p-S6	CS	#2215	-	1:1000	1:50	activated form of S6
(Ser240/244) Rictor	Bethyl	#A500-002A	1:1000	-	-	(mTOR dependent) mTORC2 scaffold prot.
	CS	#2140	-	1:1000	1:50	
Raptor	Abcam	#ab40768	1:100	1:1000	-	mTORC1 scaffold prot.
PTEN	CS	#9188	1:100	-	-	neg.reg. of PI3K/AKT
cleaved-caspase-3	CS	#9664	1:100	-	-	apoptosis

LC3	CS	#3868	1:100	-	-	autophagy
Ki67	TF	#PA5-19462	1:200	-	-	proliferation
N-cadherin	BDB	#610921	1:100	-	-	cell adhesion
E-cadherin	GTX	#GTX629691	1:100	-	-	cell adhesion
β-catenin	Merck	#224M-14	1:50	-	-	cell adhesion and transcr.
fibronectin	TF	#MS-1351	1:100	-	-	EMT
syndecan 1	SB	50641-RP02	1:500	-	-	cell adhesion
β-actin	SA	#A2228	-	1:5000	1:50	loading control

BDB = BD Biosciences, CS = Cell Signaling, GTX = GeneTex, neg.reg. = negative regulator, prot = protein, SA = Sigma-Aldrich, SB = SinoBiological, TF = Thermo Fischer Scientific, transcr. = transcription

# 3.7. Western Blot and WES<sup>TM</sup> Simple analysis

Due to interference caused by the alginate-based bioink, it was removed from the 3D bioprinted TMSs prior to protein extraction. Constructs were rinsed in phosphate-buffered saline (PBS), then incubated in 0.1 mM sodium citrate solution (30 min, on ice), followed by centrifugation (1000 rpm, 10 min, 4 °C). This process effectively dissolved the alginate scaffold while preserving the 3D cellular architecture as spheroid-like aggregates. Cells or residual 3D structures were rinsed with PBS and lysed in ice-cold buffer containing 50 mM Tris, 10% glycerol, 150 mM NaCl, 1% Nonidet-P40, 10 mM NaF, 1 mM PMSF, and 0.5 mM Na<sub>3</sub>VO<sub>4</sub> (30 min, pH 7.5). Protein concentration was quantified using the Bradford assay (Bio-Rad).

When performing western blot (WB), proteins were separated by SDS-PAGE, transferred to polyvinylidene fluoride (PVDF) membranes, and probed with primary antibodies (**Table 5**), followed by incubation with biotinylated secondary antibodies and the avidin–HRP complex (Vectastain Elite ABC HRP Kit; Vector Laboratories). Signal detection and visualization was performed using ECL substrate and iBright FL1000 imaging system (Thermo Fisher Scientific), analyzed in ImageJ software.

Simple Western (WES<sup>TM</sup>) analysis was carried out on a 12–230 kDa Separation Module (ProteinSimple). Samples were diluted (0.2 μg/μl) in Sample Buffer (ProteinSimple), mixed with Fluorescent Master Mix (1:4 ratio, ProteinSimple), and incubated at 95°C (5 min). The samples, Antibody Diluent (ProteinSimple), primary antibodies (**Table 5**), with the Anti-Rabbit/Anti-Mouse Detection Module (ProteinSimple) were loaded into the plate. The following settings were applied: capillary-based stacking and separation (395 V, 30 min), blocking step (5 min), primary

and secondary antibody incubations (30 min), and chemiluminescent detection with luminol/peroxide (15 min). Data analysis was conducted using Compass software (USA).

Protein expression levels were normalized to  $\beta$ -actin. Ratios of phospho-to-total protein were calculated (p-mTOR/mTOR, p-S6/S6, p-Akt/pan-Akt) to assess the activity of mTOR kinase, mTORC1, and mTORC2, respectively. The Raptor/Rictor ratio was used to evaluate the relative abundance of mTORC1 and mTORC2 complexes. All WBs were conducted in at least three replicates.

#### 3.8. Renal ischemia reperfusion mouse model

Eight-week-old male C57BL/6 mice (n = 24) were used to establish a renal ischemia-reperfusion (IR) model. Mice were assigned to six groups (n = 4/group): 1. TAC (3 mg/kg, *intraperitoneal* – *IP*, Advagraf-Astellas Pharma, IR surgery); 2. TAC control (saline, *IP*, IR surgery); 3. TAC SHAM control (saline, *IP*, placebo surgery); 4. Rapa (1.5 mg/kg/day, *per os*, Rapamune — Pfizer, IR surgery); 5. Rapa control (saline, *per os*, IR surgery); 6. Rapa SHAM control (saline, *per os*, placebo surgery).

Anesthesia was induced with ketamine-xylazine (Sigma-Aldrich), body temperature was maintained at 37 °C using a heating pad. IR was induced by clamping the left renal artery and vein for 20 min with an atraumatic vascular clamp. Before reperfusion, the contralateral kidney was removed, and clamp release was followed by visual confirmation of reperfusion. SHAM groups underwent laparotomy without vascular clamping or nephrectomy. Treatments were initiated 24 hours after surgery and continued for three consecutive days. TAC (3 mg/kg/day) maintained therapeutic blood levels (4.5–8.4 ng/mL; Siemens Dimension EXL with LM Integrated Chemistry System). On the fourth day, animals were euthanized, and kidneys were fixed for later processing.

## 3.9. Human xenograft and syngeneic mouse model

Xenograft models were established by subcutaneously injecting  $1-5 \times 10^6$  cells into the flanks/breast region of 8-week-old SCID mice (n = 5/group). To establish the syngeneic tumor model,  $1 \times 10^6$  4T1 cells were injected into the breast region of 8-week-old BALB/c mice. When palpable tumors developed, mice were randomized: 1. *IP* control (saline, *IP*); 2. TAC (3 mg/kg, *IP*, Advagraf); 3. Rapa (1 mg/kg, *per os*, Rapamune); 4. *per os* control (saline, *per os*) or 1. Control (saline, per os); 2. Rapa (3 mg/kg, per os); 3.

Doxo (2 mg/kg, intravenous, Doxorubicin-TEVA); 4. Cis (2 mg/kg, IP, Cisplatin Accord). Treatments were administered three times/week for 21 days (Cis: 1x/week). Tumor size and body weight were monitored throughout the study. At the end, animals were euthanized, and samples were collected for further analyses. For assessing the tumor volumes, the following method was used:

$$\frac{\pi}{6}x\left(\frac{2\ x\ shorter\ diameter + longer\ diameter}{3}\right)^3$$

All procedures were conducted in compliance with animal welfare regulations and were approved by the Institutional Ethical Review Board (PE/EA/801-7/2020; 16 September 2020) and national authorities (PEI/001/1733-2/2015; 14 October 2015).

### 3.10. Isolating cells from in vivo tumor

Solid tumors were excised from euthanized BALB/c mice. Tumor tissues were immediately placed into sterile Petri dishes containing PBS supplemented with penicillin-streptomycin (100 UI/mL). Tumors were chopped into 1–2 mm³ fragments, then subjected to enzymatic digestion in DMEM-HG media containing 1 mg/mL collagenase type IV and 0.1 mg/mL DNase I (45–60 min, 37 °C, gentle agitation, Sigma-Aldrich). After digestion, the resulting cell suspension was passed through a 70 µm cell strainer, to reach a one-cell suspension and eliminate ECM residues, then centrifuged (1000 rpm, 5 min), washed twice with PBS, then directly used for subsequent studies.

### 3.11. Statistical analysis

Expression patterns were evaluated by using contingency tables and chi-square tests on H-scores. For parametric datasets, comparisons between two groups were performed using a two-sample t-test, while one-way ANOVA followed by Tukey's post-hoc test/Fischer's LSD test was applied for analyses involving more than two groups. Data normality was assessed using the D'Agostino-Pearson test. Statistical analyses were carried out using GraphPad Prism version 10.4.1 (532) (GraphPad Software, USA). All results are based on data from at least of three independent experiments.

### 4. Results

### 4.1. Establishment of 3D bioprinted cancer models via Gesim BioScaffolder

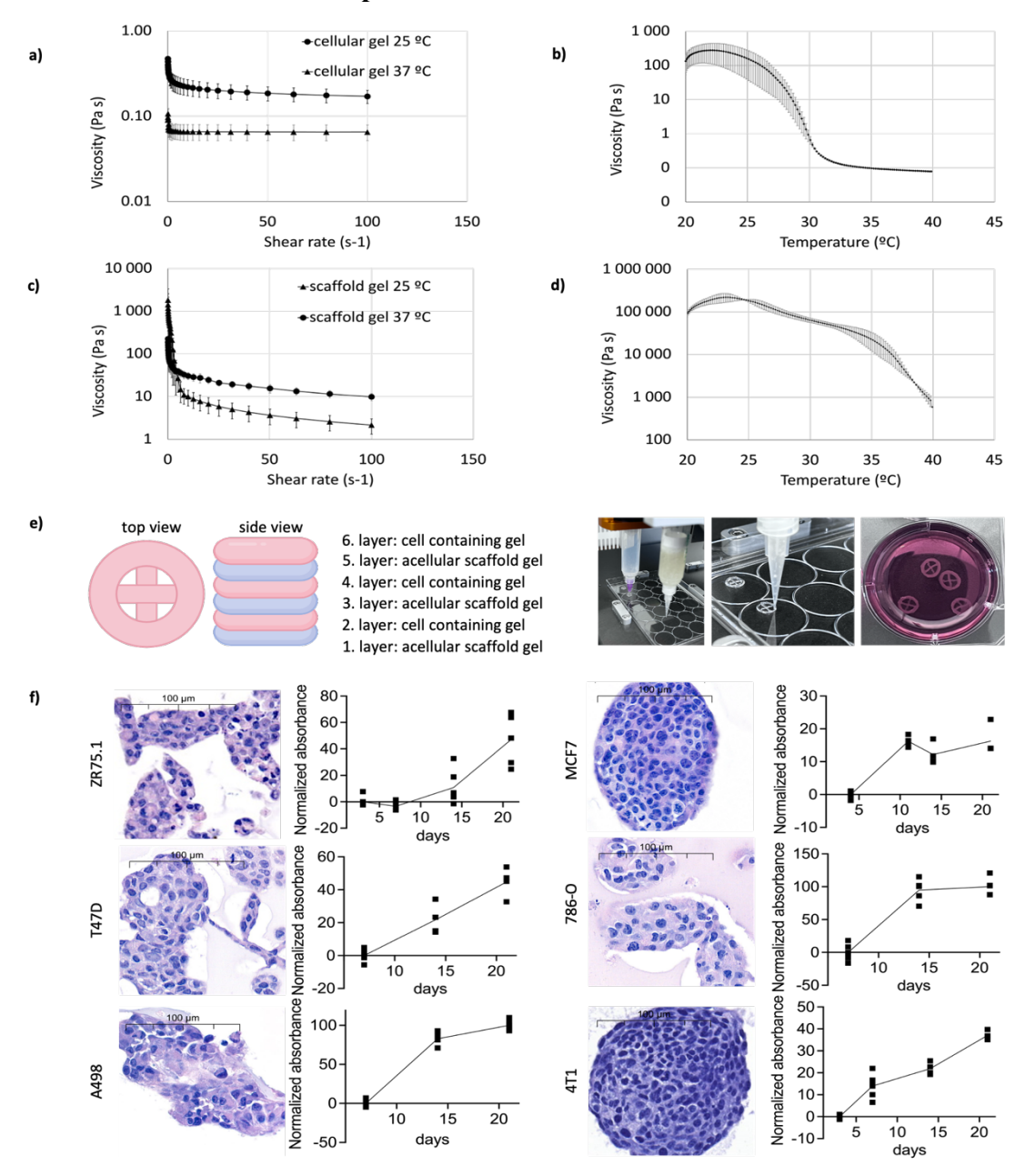


Figure 5. Establishment of 3D bioprinted cancer models from RCC and breast cancer cell lines. Rheological analysis of the bioinks. (a, c) Viscosity curves of the cellular and scaffold gels at various temperatures. Temperature-dependent changes in the viscosity of the (b) cellular and (d) scaffold gels. Data represent three technical replicates (203). (e) Schematic representation of the 3D bioprinted TMSs, composed of six alternating layers of cellular and scaffold gels, along with the bioprinting process. (f) Representative images of 3D TMSs of various RCC and breast cancer cell lines (HE-

staining). Scale bar:  $100 \, \mu m$ . TMS growth was monitored over three weeks using the SRB assay.

Two bioinks were developed for 3D bioprinting: a low-viscosity, cell-containing gel, and a high-viscosity scaffold gel for structural support, deposited in alternating layers. Rheological analysis revealed desirable shear-thinning behavior in both gels, more pronounced in the scaffold gel. Viscosity decreased with rising temperature, supporting printability (**Figure 5a,c**). For the cellular gel, viscosity dropped sharply around 25°C and stabilized near 32°C. The scaffold gel exhibited a more gradual decrease in viscosity across the tested temperature range (**Figure 5b,d**).

The 3D bioprinted TMSs were constructed of six alternating layers of cell-laden and cell-free scaffold gels, followed by CaCl<sub>2</sub> crosslinking (**Figure 5e**). Various cell lines were successfully used, including breast carcinoma (ZR75.1–luminal B, T47D–luminal A, MCF7–luminal A, 4T1–triple-negative) and RCC (A498–ccRCC, 786-O–ccRCC) cell lines (**Table 3**), which were used in subsequent patient-derived model development and renal cancer studies. The bioprinted TMSs were cultured for three weeks with detectable continuous growth in all models. Although the overall growth was consistent, cell line–specific differences in growth kinetics were observed throughout the culture period (**Figure 5f**).

## 4.1.1. Validation of growth and cellular dynamics in 3D bioprinted tissue-mimetic structures

3D bioprinted TMSs were generated using stable mCherry-transfected T47D breast carcinoma cells and cultured for 21 days. Tissue growth was monitored via mCherry fluorescence, AB for metabolic activity and SRB for total protein content. AB and SRB results closely matched mCherry (no significant differences detected), confirming their reliability for assessing proliferation in 3D bioprinted TMSs, which expanded continuously over 21 days (**Figure 6a**).

In the 3D TMSs, apoptotic cells were predominantly localized to central regions, whereas apoptosis was rare in 2D cultures. Autophagy-related protein expression was more prominent in 2D cultures, indicating potentially higher autophagic activity compared to the 3D models. Ki67 staining revealed intense proliferation in 2D cultures,

while in the 3D TMSs, proliferating cells were fewer and distributed heterogeneously throughout the tissue-like constructs (**Figure 6b**).

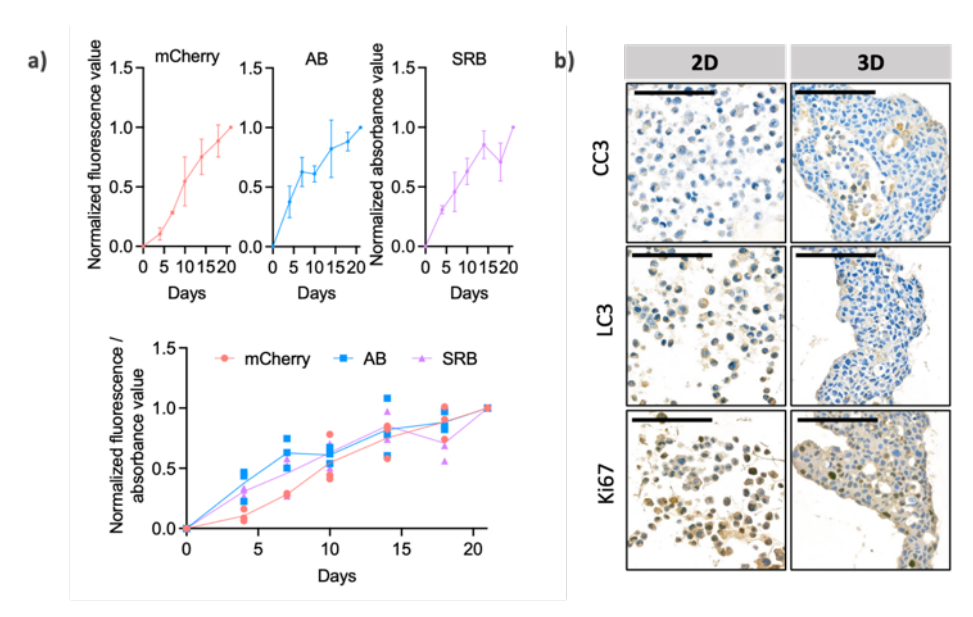


**Figure 6**. **Proliferation and cellular dynamics in 3D-bioprinted T47D tissue-mimetic structures.** (*a*) Growth was quantified via constitutive mCherry fluorescence along with Alamar Blue (AB) and Sulforhodamine B (SRB) assays; no significant differences were detected in the results of these tests (paired t-test, p > 0.05, as shown on multi-line chart). (*b*) Apoptosis (cleaved caspase-3; CC3), autophagy (light chain 3; LC3), and proliferation (Ki-67) were evaluated in 2D cell cultures and 3D-bioprinted TMSs. DAB chromogen, hematoxylin counterstaining. Scale bar: 100 μm. Cell line: T47D.

## 4.1.2. Increase and redistribution of cell-cell and cell-matrix adhesion proteins within 3D bioprinted tissue-mimetic structures

The expression patterns of several key cell–cell adhesion molecules and ECM components were investigated in both 3D bioprinted TMSs and traditional 2D cell monolayers (**Figure 7**). In the 3D bioprinted TMSs, intense membrane-associated staining of  $\beta$ -catenin was detected throughout the entire structure. By contrast, in 2D cultures, only a small subset of cells was found to exhibit  $\beta$ -catenin membrane positivity.

E-cadherin distribution was similar: in the 3D bioprinted TMSs, E-cadherin was predominantly – and specifically – anchored at cell membranes, forming crisp outlines around each cell. In the 2D monolayers, although strong staining was detected, the pattern was less sharp, and the overall intensity of E-cadherin expression was reduced.

Within the 3D bioprinted TMSs, membrane-localized N-cadherin staining was markedly enhanced and was consistently observed on cells throughout the entire structure. In contrast, 2D-cultured cells showed only weak and sporadic N-cadherin positivity, a pattern that closely resembled the β-catenin staining.

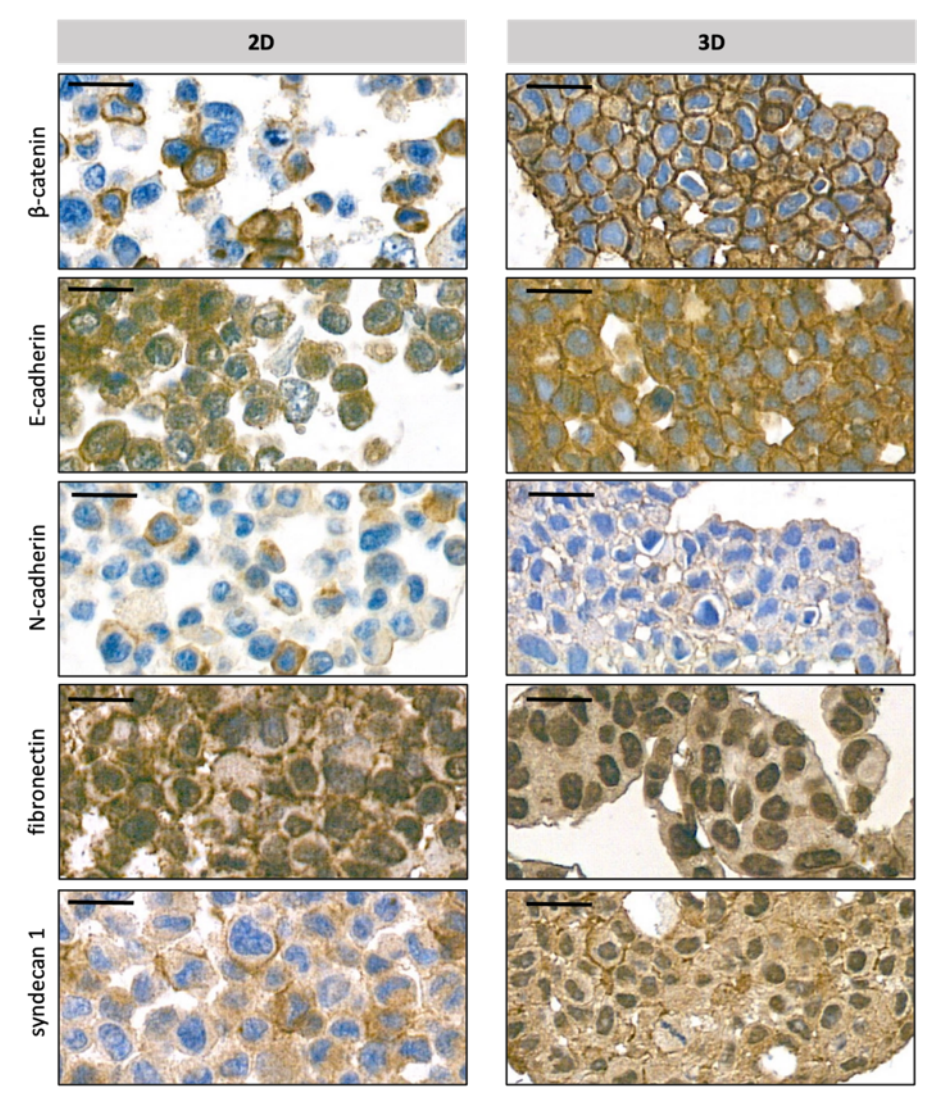


Figure 7. Protein expression pattern associated with cell–cell and cell–ECM adhesion differs between 2D monolayer cultures and 3D bioprinted TMSs. IHC analyzes were performed for membrane and adhesion proteins – including β-catenin, E-cadherin, N-cadherin, fibronectin, and syndecan-1. DAB chromogen, hematoxylin counterstaining. Scale bar: 20 μm. Cell line: T47D.

In the 3D bioprinted TMSs, fibronectin was predominantly detected in a pronounced perinuclear pattern, suggesting active intracellular trafficking or storage

adjacent to the nucleus. Conversely, in 2D cultures, fibronectin was observed at the cell surface, forming a membrane-associated network.

Finally, syndecan expression was distinctly modulated by the dimensionality. In the 3D bioprinted TMSs, a weak but homogeneous cytoplasmic signal was combined with clear membrane positivity, indicating that both intracellular pools and cell-surface reservoirs of syndecan were being utilized. In the 2D monolayers, syndecan-1 staining was weaker overall in the cytoplasm but still retained detectable membrane localization.

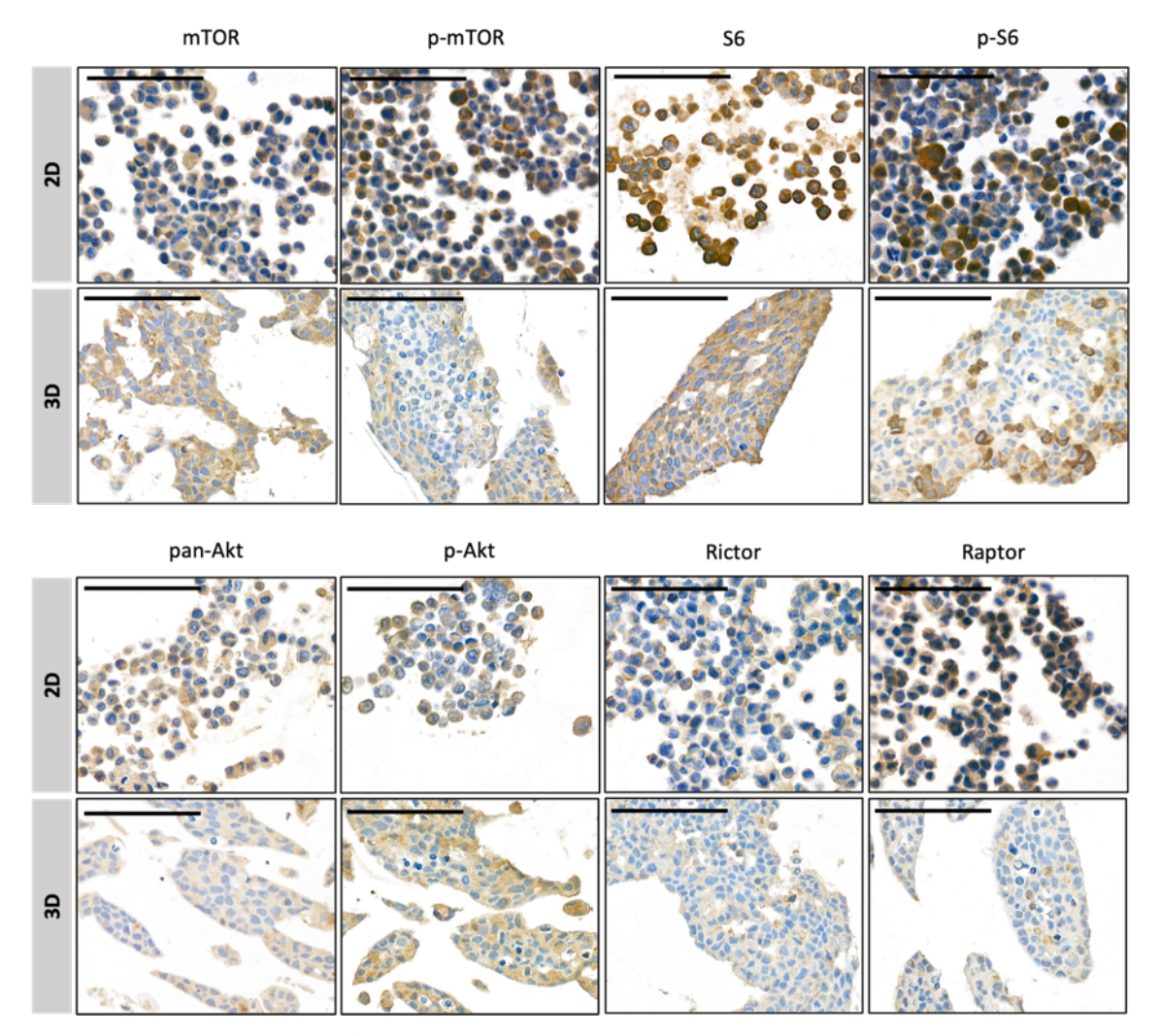
Together, these data illustrate that both the amount and the localization of adhesion molecules and ECM proteins are influenced by the dimensionality of the cell culture environment, with 3D bioprinting fostering more robust membrane localization of adhesion proteins and reconfiguring ECM deposition patterns.

## 4.1.3. Reduced activation and increased heterogeneity of mTOR-pathway components in 3D bioprinted tissue-mimetic structures

The mTOR signaling cascade regulates a wide array of cellular functions – ranging from nutrient sensing and metabolic control to cell growth and division. To investigate how this pathway behaves in a more physiologically relevant context, we compared the expression and activation status of key mTOR-regulated proteins in our 3D bioprinted TMSs versus 2D monolayer cultures.

It was observed that the 3D bioprinted TMSs displayed an overall decrease in the expression of mTOR pathway proteins. Although the total levels of core proteins – including mTOR, S6, and pan-Akt – did not appear to differ significantly between 2D and 3D models by visual inspection, a marked decline was detected in the expression of the phosphorylated (activated) forms of these molecules in the 3D environment. p-mTOR and p-S6 was significantly attenuated in the 3D bioprinted TMSs, as evidenced by weaker staining intensity and a reduced number of positively stained cells. It was further noted that these phospho-proteins were predominantly localized at the outer regions of the 3D bioprinted TMSs, implying that proliferative and growth-related activities were taking place at the periphery. Moreover, the distribution of p-S6 was characterized by pronounced heterogeneity within the 3D bioprinted TMSs, compared to the 2D cultures (**Figure 8**).

This suggests that microenvironmental gradients – such as nutrient availability, oxygen diffusion, or mechanical cues – form within the thicker, cell-rich 3D bioprinted TMSs and directly influence mTOR pathway activation. mTOR signaling is not only downregulated overall but also exhibits a spatial shift, with peripheral activation supporting proliferation, while central regions remain quiescent.



**TMSs versus 2D monolayers.** IHC was performed to compare mTOR pathway activity – including mTOR, p-(Ser2448)-mTOR, S6, p-(Ser235/236)-S6, pan-Akt, p-(Ser473)-Akt, Rictor, and Raptor. DAB chromogen, hematoxylin counterstaining. Scale bar: 100 μm. Cell line: T47D.

## 4.1.4. Quantitative analysis of mTOR signaling in 3D-bioprinted tissue-mimetic structures

mTOR signaling was quantitatively evaluated in 3D bioprinted TMSs. For analysis, the hydrogel matrix was removed by digestion to preserve cell–cell junctions and "tissue" architecture (**Figure 9a**). Following hydrogel removal, the activity of the two mTOR complexes was evaluated in both 3D bioprinted TMSs and the conventional 2D cultures (**Figure 9b**).

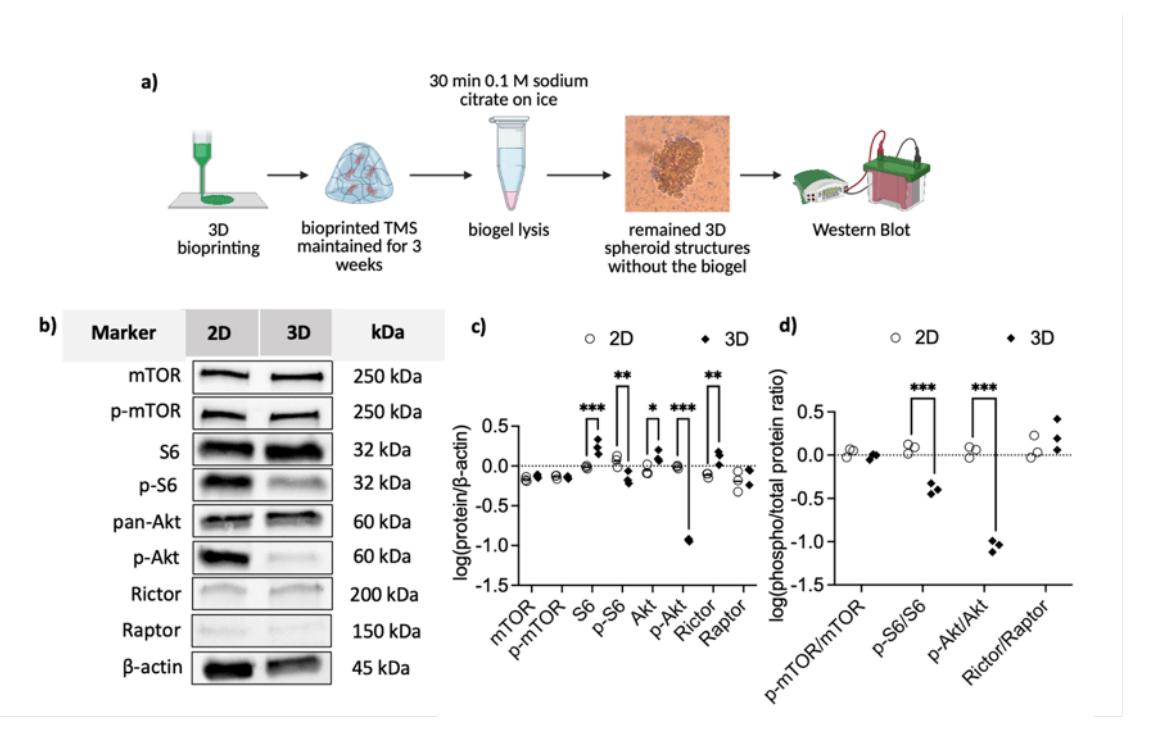


**Figure 9. Comparative quantification of mTOR pathway protein levels in 3D-bioprinted TMSs versus 2D monolayers.** (a) Schematic workflow illustrating how 3D-printed constructs were processed for protein extraction and WB analysis. (b) Representative blots of total and phosphorylated mTOR pathway components (mTOR, p-[Ser2448]-mTOR, S6, p-[Ser235/236]-S6, pan-Akt, p-[Ser473]-Akt, Rictor, and Raptor). (c) Densitometric measurements were normalized to β-actin; \*p<0.05; \*\*p<0.01; \*\*\*p<0.001 (two-way ANOVA with Fisher's LSD post hoc test). (d) Ratios of phosphoto-total proteins. \*p<0.05; \*\*p<0.01; \*\*\*p<0.001 (two-way ANOVA with Fisher's LSD post hoc test). Cell line: T47D.

When normalized to  $\beta$ -actin, elevated levels of S6 (1.75 vs. 0.96), pan-Akt (1.32 vs. 0.89), and Rictor (1.30 vs. 0.77) were detected in the 3D bioprinted TMSs compared

to the 2D monolayers. Conversely, a reduction in p-S6 (0.71 vs. 1.16) and p-Akt (0.11 vs. 0.97) was recorded in the 3D bioprinted TMSs (**Figure 9c**).

Phospho-to-total protein ratios were calculated: a pronounced decrease in p-S6/S6 (0.41 vs. 1.20) and p-Akt/Akt (0.09 vs. 1.11) was observed in the 3D bioprinted TMSs, implicating diminished mTOR kinase activity under 3D culture conditions. Additionally, the ratio of Rictor to Raptor was found to be unchanged between the two model systems, which suggests that the relative abundance of the mTOR complexes remained stable, even though their enzymatic function was attenuated in the 3D bioprinted TMSs (**Figure 9d**).

### 4.1.5. Altered response to mTOR-targeted therapies in 3D bioprinted tissuemimetic structures

The sensitivity of 3D bioprinted TMSs and 2D monolayer cultures to mTOR-targeting and chemotherapeutic agents was evaluated. Treatments were administered *in vitro* using Rapa, Cis, Ipa, and their combinations (Cis + Rapa; Cis + Ipa). In the 2D cultures, a pronounced inhibition in proliferation was induced by Rapa, Ipa, and the combinations, whereas resistance to Cis was demonstrated. By contrast, the 3D bioprinted TMSs exhibited significantly decreased sensitivity to Rapa and a complete insensitivity to Ipa. Notably, even within the 3D bioprinted TMSs, the combination therapies maintained their effectiveness, sensitizing the constructs to Cis and achieving growth suppression comparable to 2D models (**Figure 10a**).

Quantitative densitometry was performed to investigate downstream signaling alterations. In the 2D monolayer cultures, significant reductions in the p-(Ser235/236)-S6 were observed following Rapa (0.005 vs. 0.86) and Ipa (0.10 vs. 0.86) treatments. In the 3D bioprinted TMSs, only Rapa caused a comparable decrease in p-(Ser235/236)-S6 levels (0.003 vs. 0.78), whereas Ipa failed to produce a significant effect. Conversely, p-Akt was found to be elevated upon Ipa exposure in both model systems (2D: 1.82 vs. 0.19; 3D: 1.90 vs. 0.02). Baseline comparisons revealed that TSC1 and activated SAPK/JNK (p54 and p46 isoforms) expression levels were inherently higher in the 3D bioprinted TMSs than in the 2D monolayer cultures (TSC1: 0.78 vs. 0.45; pSAPK/JNK p54: 1.35 vs. 0.12; pSAPK/JNK p46: 1.06 vs. 0.13) (Figure 10b,c).

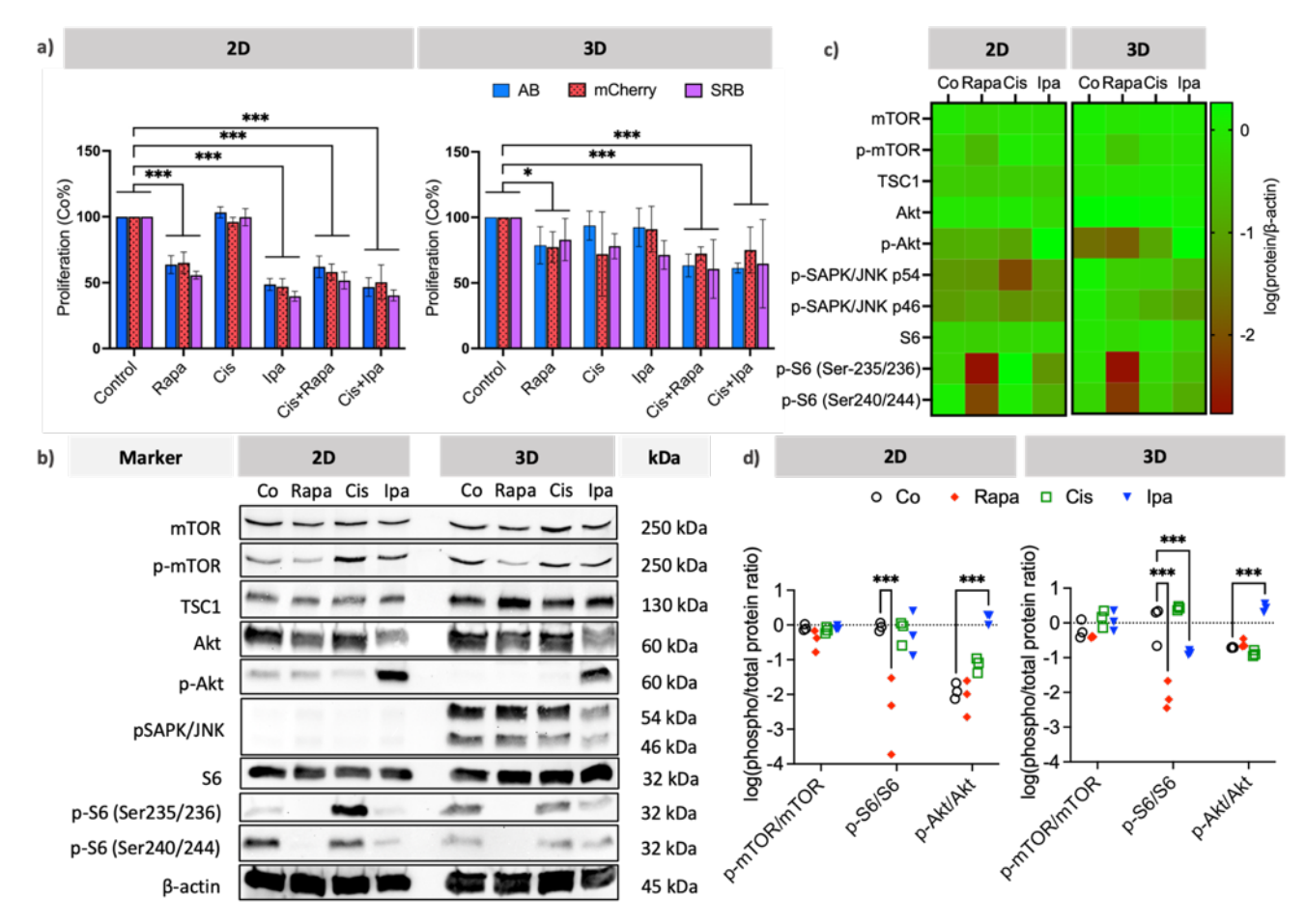


Figure 10. Comparative analysis of mTOR inhibitor sensitivity in 3D bioprinted TMSs versus 2D monolayer cultures. (a) Cells treated with rapamycin were (Rapa), cisplatin (Cis), ipatasertib (Ipa), and their combinations. Viability was measured by AB, SRB, and mCherry. Values were expressed as percentages of controls. Statistical significance was determined by paired t-test (\*p < 0.05; \*\*p < 0.01; \*\*\*p < 0.001).mTOR pathway protein expression after treatments (mTOR, p-[Ser2448]-mTOR, S6, p-[Ser235/236 or Ser240/244]-S6,

pan-Akt, p-[Ser473]-Akt, Rictor, and Raptor) (c) Densitometric heat maps illustrate relative protein levels (green: up-regulation; red: downregulation). (d) Ratios of phospho-to-total proteins (investigated phosphorylation site of p-S6: Ser240/244). Differences between treatment groups were analyzed by two-way ANOVA followed by Fisher's LSD test. Cell line: T47D. (\*p < 0.05; \*\*p < 0.01; \*\*\*p < 0.001).

Further investigation the phospho-to-total protein ratios revealed that in the 2D monolayer cultures, p-(Ser235/236)-S6/S6 ratio was suppressed by Rapa (0.01 vs. 1.46) and Ipa (0.13 vs. 1.46), whereas in 3D bioprinted TMSs only Rapa effected a significant reduction (0.01 vs. 0.90), with Ipa proving ineffective. In both model systems, p-Akt/Akt ratio was elevated upon Ipa treatment (2D: 2.75 vs. 0.20; 3D: 1.60 vs. 0.01), consistent with its ATP-competitive Akt inhibitory mechanism of action (**Figure 10d**). These data illustrate that while monotherapies display differential potency in 2D versus 3D culture conditions, combination regimens can achieve pronounced antitumor effects across both *in vitro* platforms.

### 4.1.6. 3D bioprinted "patient-derived" breast cancer model for drug testing

To enable comparison of tumor behavior in allograft settings – which more closely reflect *in situ* tumor characteristics in patients than xenograft models – a 3D bioprinting-based "patient-derived" cancer model was applied, using the 4T1 mouse breast carcinoma cell line. In these "patient-derived" 3D bioprinting experiments, cells were isolated from *in vivo* growing tumors in BALB/c mice (considered as allograft tumor). Accordingly, cell suspensions and bioinks contained not only tumor cells – the cellular composition of isolated cells were determined by flow cytometry (data not shown). The majority of the cells were identified as tumor cells (~50%), alongside high levels of granulocytes and lymphocytes, indicating a highly inflammatory TME. These tumor-driven cells were applied for drug tests in 2D monolayer cultures, 3D bioprinted TMSs, BALB/c allograft and SCID mice xenograft models.

The effects of Rapa, Doxo and Cis were evaluated. In the syngeneic BALB/c model, Rapa significantly reduced tumor growth, while in the SCID xenograft model, both Rapa and Doxo led to a notable decrease in tumor size. Moreover, drug responses observed in the BALB/c allograft model were consistent with the sensitivity pattern seen in the 3D bioprinted TMSs (**Figure 11**).

Our recent study highlights that this 4T1 "patient-derived" 3D bioprinting technology better mimics the *in situ* environment and drug sensitivity in BALB/c mice compared to the widely used SCID xenografts, which are currently considered the standard for patient-derived tumor studies.

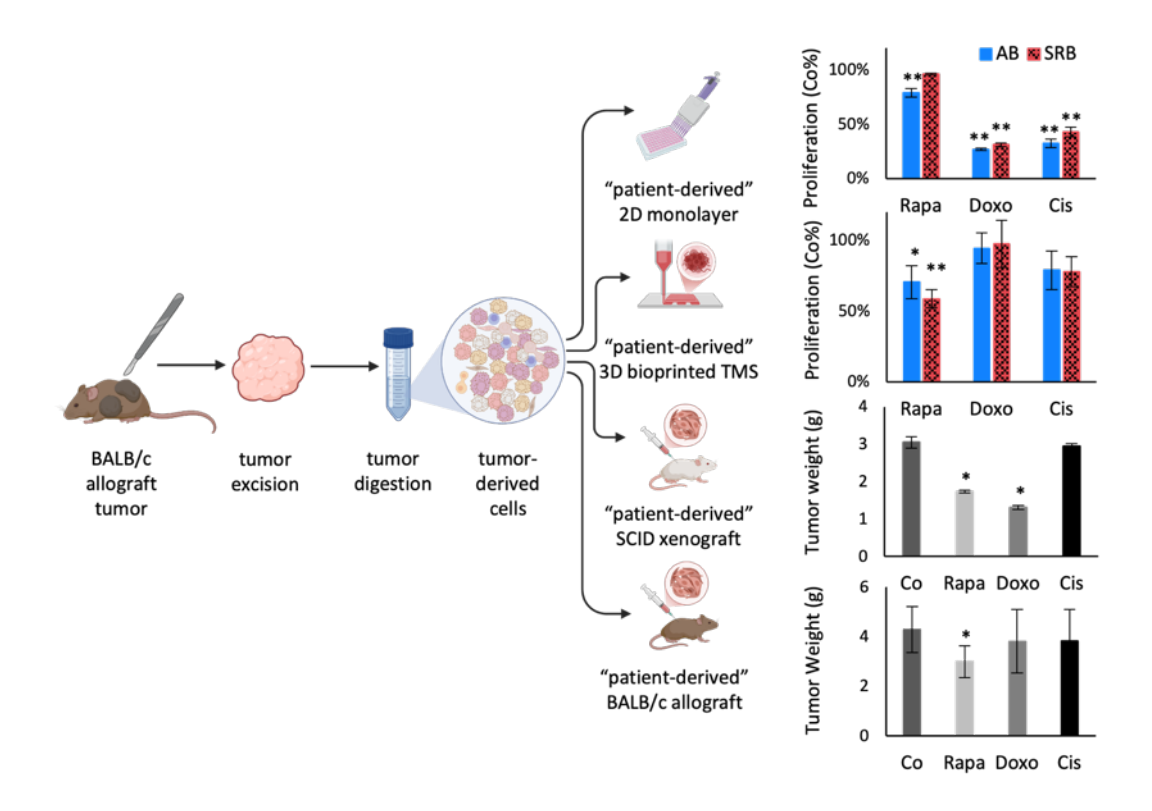


**Figure 11.** Variations in drug response among "patient-derived" breast cancer models. 4T1 tumors were excised from BALB/c mice, and cells were subsequently isolated and cultured under different experimental settings: 2D cultures (24h preculturing +72h treatment), 3D bioprinted TMSs (7 days preculturing + 72h treatment), syngeneic tumors re-implanted into BALB/c mice, and xenografts implanted into SCID mice (21 day after tumors are palpable). \*p<0.05, \*\*p<0.01; three (*in vitro*) or two (*in vivo*) independent experiments with five or six replicates, respectively. Cell line: 4T1 (203).

### 4.2. Metabolic characterization of post-transplant renal cell carcinomas

### 4.2.1. Clinicopathological features of the renal cell carcinoma cohort

Between 2000 and 2015, a total of 2615 renal transplantation surgeries – including 2561 kidney-alone and 54 combined pancreas-kidney transplantations – were carried out at Semmelweis University. The post-tx RCC cohort included 44 cases, which were chosen to represent each common RCC subtype. Additionally, another non-tx RCC cohort (n=46) was included in our study for more accurate analysis (**Table 6**). Consequently, as expected, the resulting subtype distribution among cohorts does not reflect of the actual incidence in general (*de novo*) population.

Table 6. Clinicopathologic characteristics of renal cell carcinoma cohort patients (126).

	No. of cases (%)	
	Post-transplant RCCs (n=44)	Non-transplant RCCs (n=46)
Age (years, mean±SD)	$52 \pm 12.79$	$60 \pm 13.42$
Gender		
Male	35 (80)	28 (61)
Female	9 (20)	18 (39)
Histology		
ccRCC	12 (27)	28 (61)
pRCC	28 (64)	18 (39)
ccpRCC*	4 (9)	0 (0)
Grade		
1	16 (36)	7 (15)
2	24 (55)	27 (59)
3	4 (9)	11 (24)
4	0 (0)	1 (2)
Immunosuppression		
<b>Tacrolimus</b>	22 (50)	_
Cyclosporin A	19 (43)	_
Other**	3 (7)	_

<sup>\*</sup> This group is not involved in further analyses of the study.

<sup>\*\*</sup> One patient received azathioprine treatment, and two patients were treated with mTORC1 inhibitor (rapamycin or combined tacrolimus + everolimus) because of previous malignancies.

ccRCC = clear cell renal cell carcinoma, ccpRCC = clear cell papillary renal cell carcinoma, pRCC = papillary renal cell carcinoma, RCC = renal cell carcinoma, SD = standard deviation

## 4.2.2. Elevated mTOR signaling is detected in end-stage renal disease following immunosuppression compared to healthy kidney tissue

The altered amount and activity of characteristic elements in the mTOR pathway were examined in samples that were obtained from non-transplantable donor kidneys ("Normal"; used as histologically healthy kidney controls) and kidneys affected by ESRD, subdivided into those who had received CNI immunosuppression and those who had not (Figure 12).

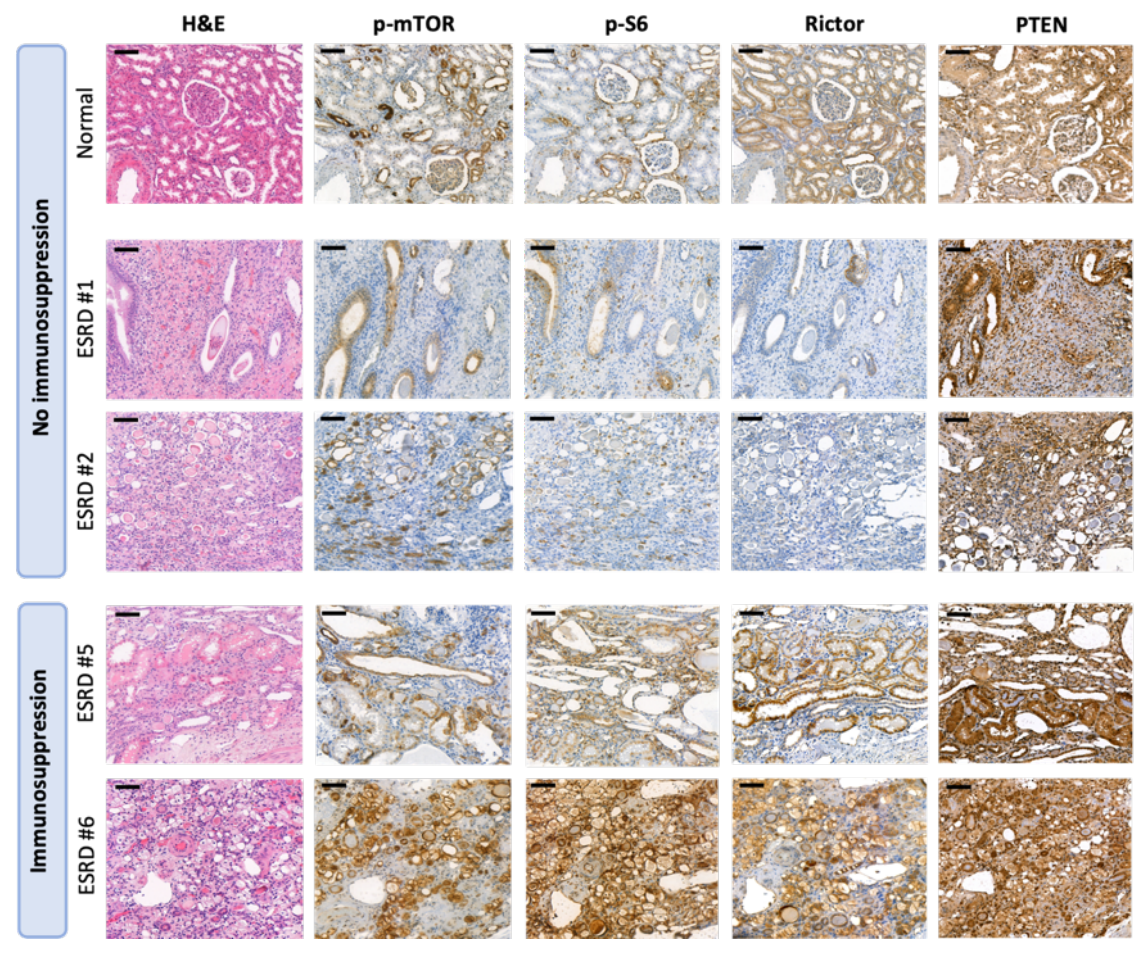


Figure 12. mTORC1/2 activity is increased in end-stage renal disease (ESRD) patients treated with calcineurin-inhibitor (CNI) compared to normal ESRD kidneys without immunosuppression. HE and IHC staining (p-[Ser2448]-mTOR, p-[Ser235/236]-S6, Rictor, PTEN) of representative cases. DAB chromogen, hematoxylin counterstaining. Scale bars: 100 μm (126).

In the "Normal" group, minimal p-mTOR and p-S6 immunoreactivity was observed within the tubular epithelial cells, whereas Rictor expression was maintained at relatively high levels across the non-malignant parenchyma. By contrast, in ESRD kidneys that had not been exposed to CNI immunosuppression, a marked reduction in the staining intensity of p-mTOR, p-S6, and Rictor was noted when compared with the healthy donor controls. These findings suggest that the loss of functional nephrons in ESRD is associated with a downregulation of both mTORC1 and mTORC2 signaling components.

Remarkably, KTRs receiving CNI-based immunosuppression exhibited a pronounced upregulation of mTOR pathway markers. Tissue sections exhibited robust p-mTOR and p-S6 immunopositivity, accompanied by enhanced Rictor staining, exceeding levels in both the normal control kidneys and the untreated ESRD group. These data indicate that CNI-mediated immunosuppression in the context of ESRD drives a reactivation or overcompensation of mTOR complex signaling within the renal epithelium.

### 4.2.3. Tacrolimus enhances the mTOR activity in the ischemic kidney of mice

To model ESRD *in vivo*, a murine renal ischemic model was established: ischemia was surgically induced in mice, followed by administration of TAC or Rapa, and the kidneys were subsequently analyzed for expression of p-mTOR, p-S6, Rictor, and p-Akt.

Ischemia alone (IR group, without TAC treatment), slightly increased the expression of all examined mTOR markers – upregulation of p-mTOR, p-S6, and Rictor was detected. However, the effect was markedly enhanced by TAC treatment. Particularly intense mTORC1 activation (as evidenced by robust p-mTOR and p-S6 expression) was observed within discrete tubular segments of the TAC-treated IR kidneys, whereas mTORC2 activity (assessed via p-mTOR, Rictor, and p-Akt) was also enhanced but to a more moderate extent. In contrast, slight attenuation of both mTORC1 and mTORC2 signaling was noted in Rapa-treated ischemic kidneys (**Figure 13**).

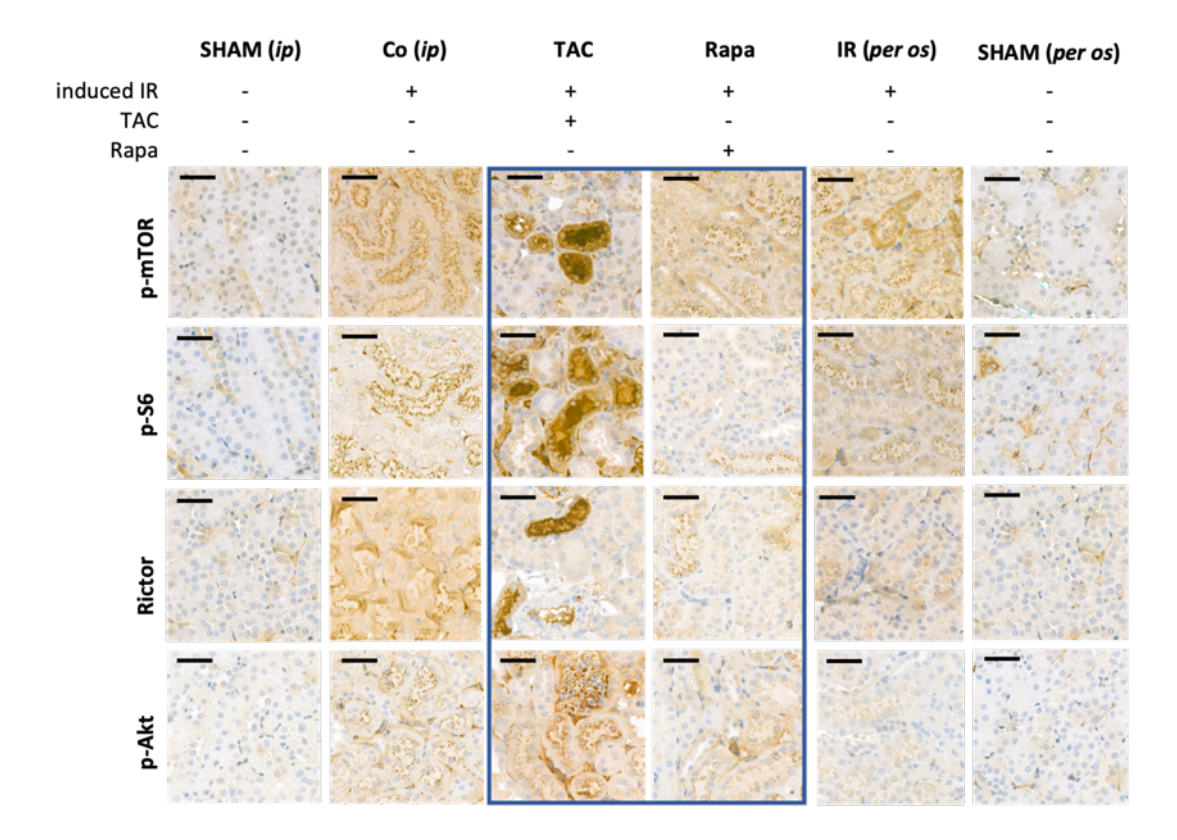


**Figure 13.** Tacrolimus enhances the mTOR activity in *in vivo* end-stage renal disease model. A murine ischemia-reperfusion model (*in vivo* ESRD model) was established in C57BL/6 mice (SHAM = placebo surgery, IR = induced ischemia). Following surgery, mice were treated for three consecutive days with TAC (3 mg/kg) and Rapa (1.5 mg/kg). IHC was performed on renal tissue sections using antibodies against p-(Ser2448)-mTOR, p-(Ser235-236)-S6, Rictor and p-(Ser473)-Akt. The dark blue frame indicates the TAC-or Rapa-treated groups; the SHAM group was only sham-operated and received no treatment, while the Co group was IR-operated but not treated (received vehicle *intraperitoneal - ip* or *per os*). Scale bars: 50 μm (126).

# 4.2.4. Pronounced activation of the mTORC2 signaling axis in post-transplant renal cell carcinomas compared to non-transplant, *de novo* renal cell carcinomas

To assess the activation pattern of mTOR complexes, IHC was performed on post-tx and non-tx RCC samples, examining p-mTOR, p-S6, and Rictor levels (**Figure 14a**).

In ccRCC, p-mTOR expression was higher in post-tx cases but did not reach significance (p = 0.09). In contrast, within the pRCC subgroup, both p-mTOR and Rictor expression levels were found to be significantly elevated in tissues derived from post-tx

patients (p = 0.03 for p-mTOR; p < 0.01 for Rictor). No significant differences in p-S6 levels were observed in either subtype (**Figure 14b**).

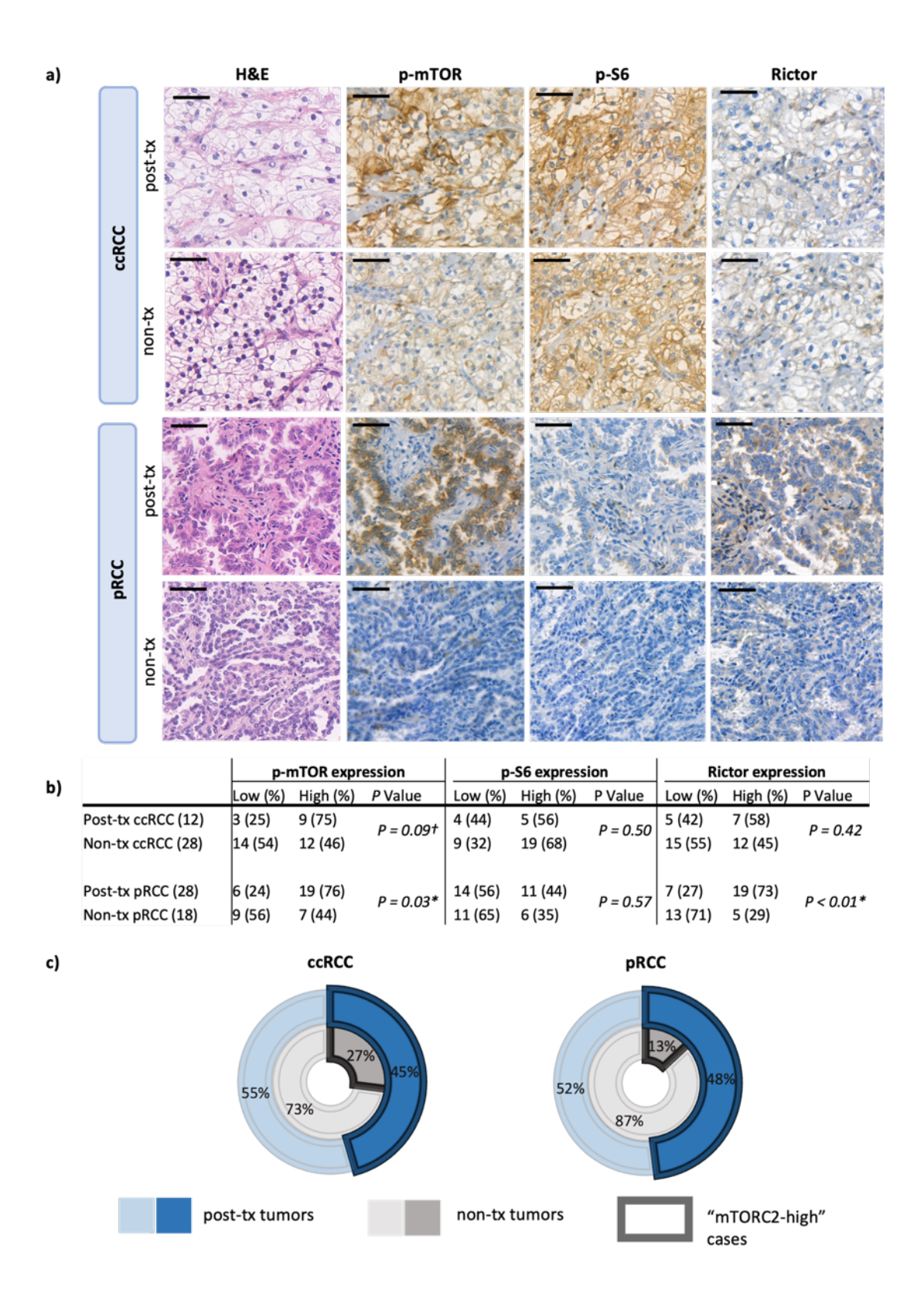


Figure 14. mTORC2 activity is elevated in post-transplant (post-tx) compared to non-transplant (non-tx) RCCs of both subtypes (clear cell – ccRCC, papillary – pRCC). (a) IHC staining for p-(Ser2448)-mTOR, p-(Ser235/236)-S6, and Rictor was performed. DAB chromogen, hematoxylin counterstaining. Scale bars:  $50 \,\mu\text{m}$ . (b) Expression of mTORC1/C2 markers in post-tx (immunosuppressed) and non-tx (without immunosuppression) RCCs. Marker expression was categorized as high or low based on whether the H-score deviated above or below the median. Statistical significance was defined as \*p < 0.05, with †p < 0.1 indicating a trend. (c) Case distribution based on mTORC2 activity. "mTORC2-high" cases were defined by high (above median H-score) expression of both the active form of the catalytic subunit of mTORC1/C2 and the scaffold protein of mTORC2 (p-[Ser2448]-mTOR and Rictor, respectively) (126).

Post-tx RCCs of both subtypes exhibited increased mTORC2 activity, as evidenced by the increased activity of the catalytic subunit of both complexes (p-mTOR) and elevated levels of Rictor (scaffold protein of mTORC2) together (**Figure 14c**). These findings indicate that mTORC2 activity is preferentially enhanced in RCCs occurring after transplantation, likely due to immunosuppressive therapy.

## 4.2.5. mTOR signal activating effects of tacrolimus on normal tubular epithelial cell line *in vitro*

*In vitro* effects of TAC on cell growth and mTOR signaling were investigated by using an immortalized human proximal tubular epithelial cell line (HK-2).

The effects of TAC, Rapa, and PP242 on HK-2 cell proliferation were studied using AB and SRB assays. Proliferation was not significantly altered by TAC following a 72-hour treatment, whereas Rapa and PP242 had moderate antiproliferative effects. Moreover, no significant changes in proliferation were observed when TAC was combined with Rapa or PP242 (**Figure 15a**). No further increase in proliferation was observed following long-term (21-day) treatment (**Figure 15b**).

Following a 72-hour exposure to TAC, Rapa and PP242, mTOR pathway activation in cells was assessed by WB. Quantification revealed that the ratio of p-S6/S6 was significantly elevated in TAC-treated samples compared to controls (0.62 vs. 0.45), indicating acute enhancement of mTORC1 activity. In contrast, no significant changes

were detected in the phosphorylation ratios of mTOR or p-Akt/Akt, suggesting that upstream Akt signaling and mTORC2 remained largely unaffected by short-term TAC exposure. Rapa (a selective mTORC1 inhibitor) and PP242 (a dual mTORC1/mTORC2 inhibitor) caused decreases in both p-mTOR/mTOR and p-S6/S6 ratios (**Figure 15c**). To assess whether the observed mTORC1 stimulation was sustained over longer periods, HK-2 cells were maintained in the presence of TAC for 21 days. Under these conditions, an enduring increase in mTORC1 activation was detected: elevated p-S6/S6 ratio (1.03 vs. 0.66) and a trend toward higher p-mTOR/mTOR levels (1.14 vs. 0.54), implying that long-term TAC treatment may activate mTORC1 signaling over time (**Figure 15d**).

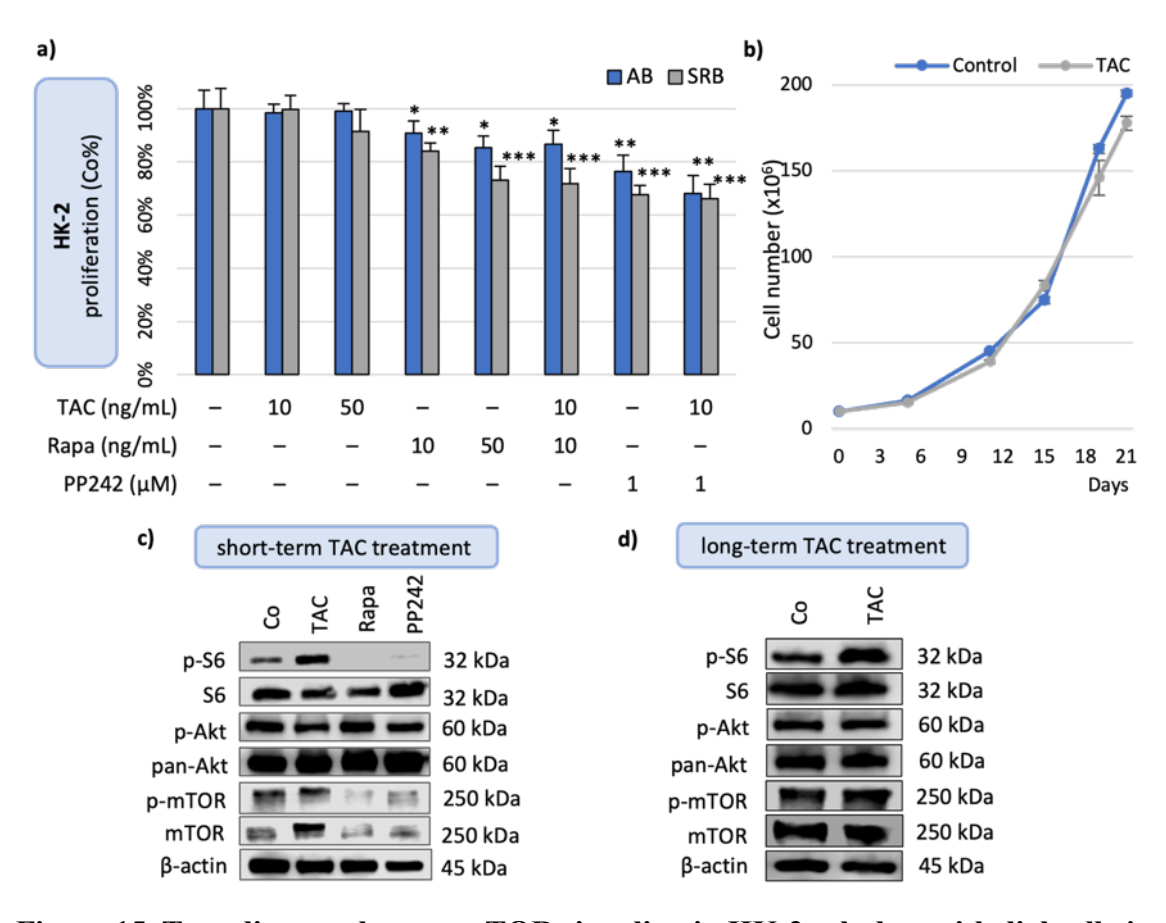


Figure 15. Tacrolimus enhances mTOR signaling in HK-2 tubular epithelial cells in vitro (2D monolayer). (a) Cell proliferation was examined using AB and SRB assays after short-term (72 h) treatment with TAC, Rapa, or PP242 in the HK-2 cell line. Results were expressed as a percentage of the control. Statistical significance was determined by one-way ANOVA with Tukey's post hoc test (\*p < 0.05; \*\*p < 0.01; \*\*\*p < 0.001). (b) Effects of long-term (21–day) exposure to TAC (10 ng/mL) on the growth of HK-2 were

monitored by cell counts; no cells were discarded throughout the experiment (ns). (c) WB was used to assess the effects of short-term (72 h) treatment with TAC (10 ng/mL), Rapa (10 ng/mL), and PP242 (1 μM) on mTOR activity of HK-2 cell line (phosphorylation sites: p-mTOR – Ser2448; p-S6 – Ser235/236; p-Akt – Ser473). (d) Effects of long-term (21–day) exposure to TAC (10 ng/mL) on the mTOR pathway in HK-2 cells (phosphorylation sites: p-mTOR – Ser2448; p-S6 – Ser235/236 or Ser 240/244; p-Akt – Ser473) (126).

## 4.2.6. *In vitro* effects of tacrolimus on renal cell carcinoma cell lines: activation of mTOR signaling and increasing proliferation

Treatment with low- and high-dose TAC for 72 hours was associated with increased proliferation in one RCC cell line (A498). PP242 elicited a robust antiproliferative effect across all cell lines. However, resistance to Rapa was noted in A498, whereas the 786-O and ACHN remained sensitive (**Figure 16a**). Given the proliferation enhancement observed in A498 after short-term TAC exposure, the experiment was extended to long-term (21–day) treatment. A 10% increase in cell number was recorded as a trend (ns; p = 0.07) (**Figure 16b**).

To assess the effects of long-term immunosuppressant exposure, A498 cells were maintained under TAC for 21 days, where further increases in phospho-to-total ratios were detected: p-S6/S6 (0.81 vs. 0.25), p-mTOR/mTOR (3.90 vs. 1.30), indicating that both mTORC1 and mTORC2 complexes were activated during extended TAC exposure (**Figure 16c**).

Following a 72-hour exposure to TAC, a modest but consistent increase in p-mTOR/mTOR ratio was observed across RCC cell lines; however, the increase reached statistical significance only in the case of A498 (1.71 vs. 0.61). In contrast, treatment with Rapa or PP242 led to a suppression of mTOR pathway signaling. p-S6 (downstream marker of mTORC1) expression was nearly undetectable following Rapa administration, while the impact of Rapa on mTORC2 activity – as measured by the p-Akt/Akt ratio – was found to be negligible (**Figure 16d**).

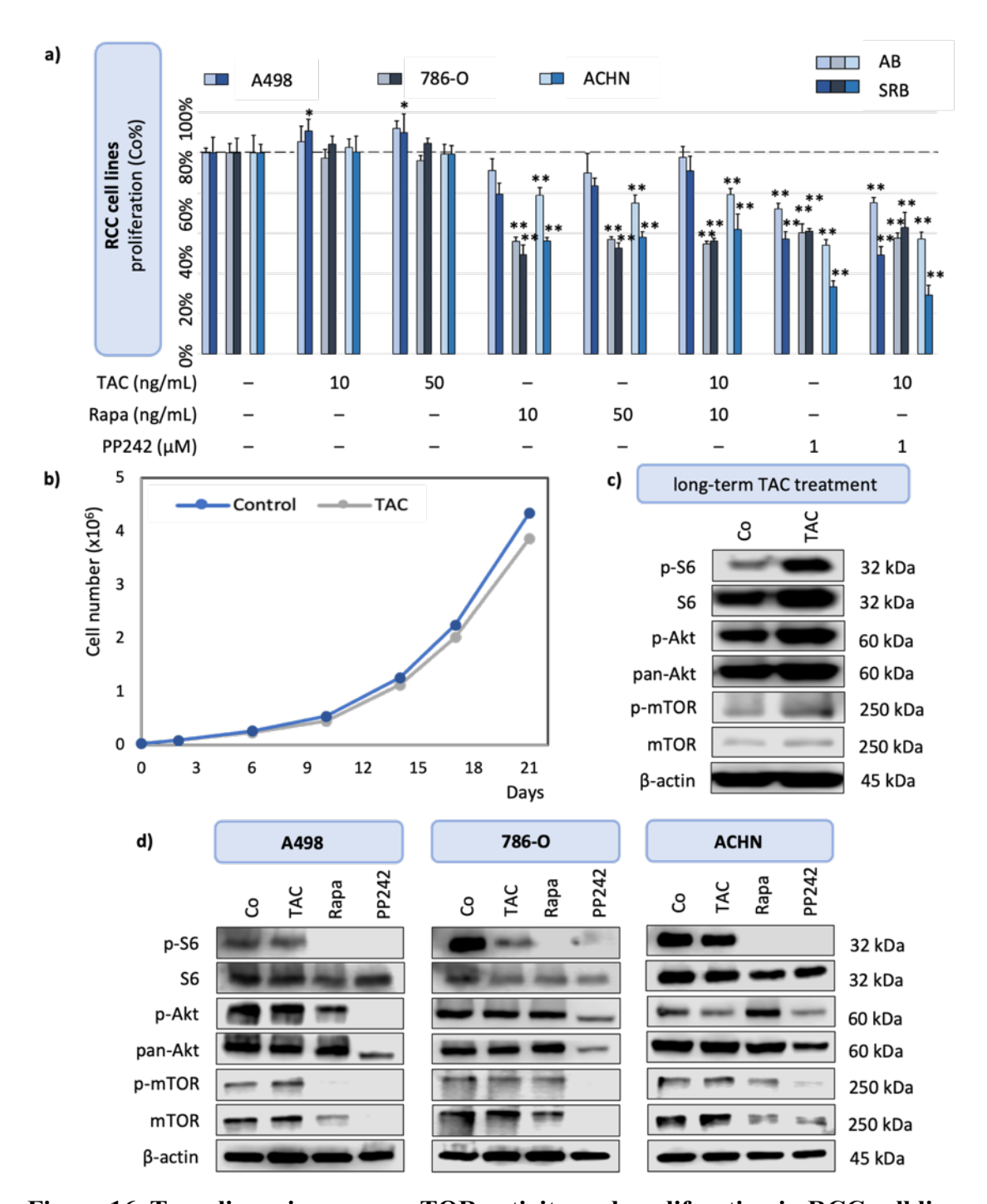


Figure 16. Tacrolimus increases mTOR activity and proliferation in RCC cell lines in vitro (2D monolayer). (a) Cell proliferation was examined using AB and SRB assays after short-term (72 h) treatments with TAC, Rapa, or PP242 on RCC cell lines. Results were expressed as a percentage of the control. Statistical significance was determined by one-way ANOVA with Tukey's post hoc test (\*p < 0.05; \*\*p < 0.01; \*\*\*p < 0.001). (b) Effects of long-term (21-day) exposure to TAC (10 ng/mL) on the proliferation of the A498 cell line (p = 0.07). (c, d) WB analysis of short- and long-term (72 h, 21-day) effects

of treatments with TAC (10 ng/mL), Rapa (10 ng/mL), and PP242 (1 μM) on mTOR activity (phosphorylation sites: p-mTOR – Ser2448; p-S6 – Ser235/236; p-Akt – Ser473). A498, 786-O (ccRCC subtype), and ACHN (pRCC subtype) cell lines were used for short-term and A498 for long-term experiments (126).

## 4.2.7. 3D effects of tacrolimus on renal cell carcinoma cell lines: increasing proliferation and tumor growth

The detected increase in cell proliferation in conventional 2D monolayer cultures of A498 following TAC treatment highlights the potential importance of TAC-induced tumor growth in certain post-tx renal cancers. To determine whether this proliferative response could be detected in 3D environment, the effects of IS agents were also tested on the previously established 3D bioprinted TMSs and in *in vivo* xenograft models.

72-hour TAC treatment resulted in a significant increase in proliferation in 3D bioprinted A498 TMSs, which mirrored the proliferative effect previously detected in 2D cultures. For mTOR inhibitors, resistance was observed under 3D maintenance conditions: the sensitivity (previously detected in 2D monolayer cultures) of A498 to PP242 and 786-O to Rapa was lost or significantly decreased. In the case of combination therapy (TAC + PP242), a significant reduction in cell proliferation was detected in both cell lines (**Figure 17a**).

During long-term (21-day) TAC treatment, significantly higher proliferation was observed in 3D bioprinted A498 TMSs. In 3D bioprinted 786-O TMSs, the results were not entirely conclusive: on certain days of growth, higher proliferation was observed, whereas on others no significant difference was found. Both cell lines showed long-term Rapa sensitivity, suggesting that, in the 3D environment a 72-hour exposure is insufficient for the full manifestation of Rapa's effect. While the A498 cells were resistant to Rapa after 72 hours in both 2D culture and 3D bioprinted TMSs, a significant inhibition of proliferation was observed in the TMSs after 21 days of treatment (**Figure 17b**).

Our 3D bioprinted *in vitro* results underline the importance of the potential TAC induced tumor growth and this was also confirmed in *in vivo* human xenograft mouse model of A498. A 21-day regimen of TAC was found to dramatically accelerate tumor growth. Mean tumor volumes and weights in the TAC cohort reached  $211.17 \pm 60.45 \text{ mm}^3$  and  $1.25 \pm 0.64 \text{ g}$ , respectively, whereas control tumors measured only  $61.34 \pm 22.37 \text{ mm}^3$  and  $0.60 \pm 0.27 \text{ g}$ . By contrast, Rapa treatment produced suppression of tumor growth,

with treated tumors averaging  $45.17 \pm 29.16$  mm<sup>3</sup> and  $0.32 \pm 0.18$  g, compared to control values of  $85.53 \pm 18.34$  mm<sup>3</sup> and  $1.18 \pm 0.36$  g (**Figure 17c**).

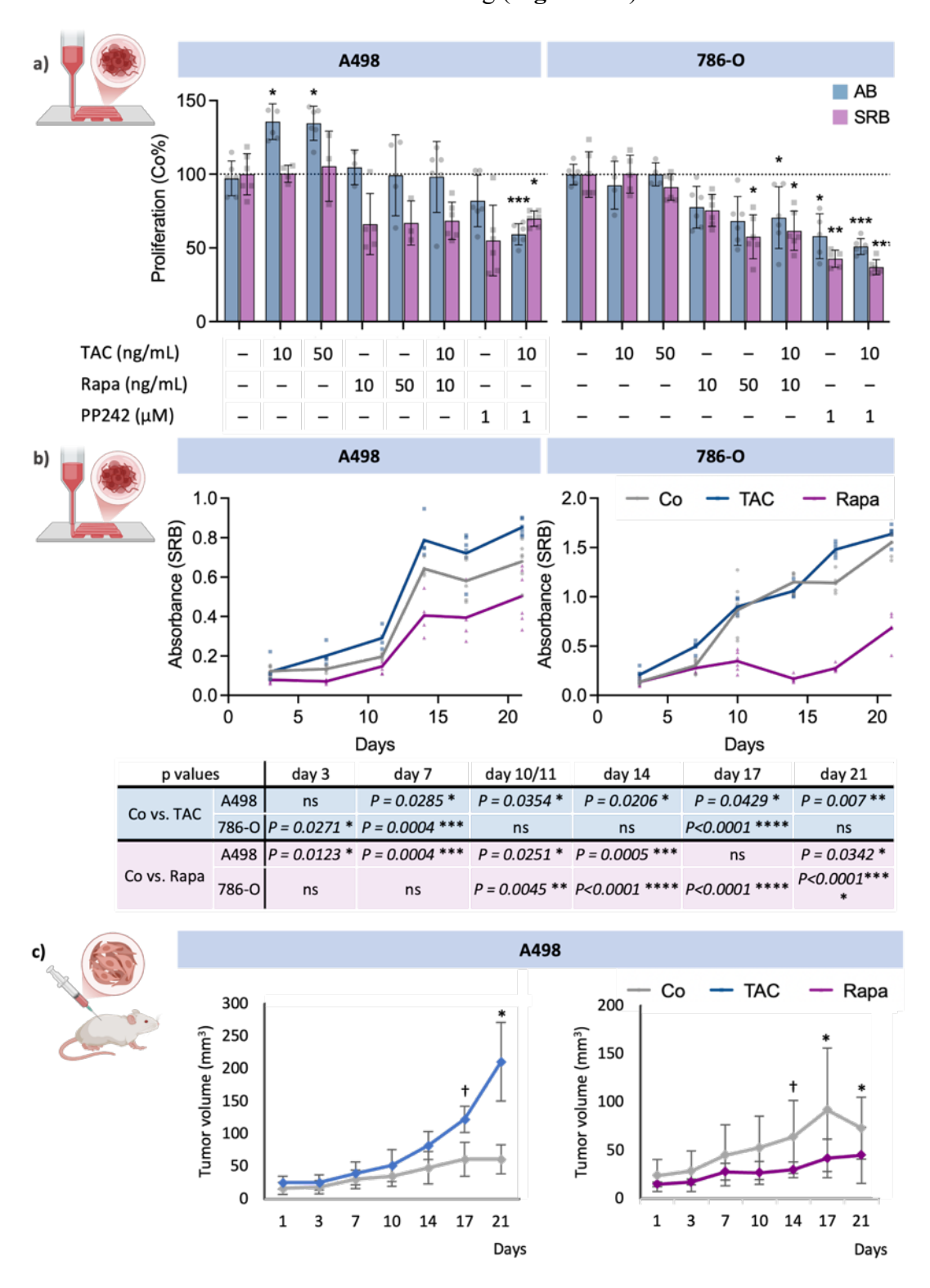


Figure 17. Tacrolimus enhances the proliferation *in* 3D bioprinted tissue-mimetic structures and the tumor growth in *in vivo* xenografts of A498 RCC cell line. (a) Cell

proliferation was examined using AB and SRB assays after short-term (72 h) treatments of 3D bioprinted TMSs with TAC, Rapa, or PP242 on the RCC cell lines A498 and 786-O. Results were expressed as a percentage of the control. Statistical significance was determined by one-way ANOVA with Fisher's LSD test (\*p < 0.05; \*\*p < 0.01; \*\*\*p < 0.001). (b) Effects of long-term (21-day) exposure to TAC (10 ng/mL) or Rapa (10 ng/mL) on the proliferation of A498 and 786-O 3D bioprinted TMSs. Statistical significance was determined by one-way ANOVA with Fisher's LSD test (\*p < 0.05; \*\*p < 0.01; \*\*\*p < 0.001; \*\*\*\*p < 0.0001; ns = not significant) (c) Tumor growth in A498 RCC human xenografts after 21–day (TAC/ Rapa) treatment. †p < 0.1, \*p < 0.05; (paired t-test) (126).

Taken together, these findings demonstrate that: a) TAC can induce tumor growth in a cell-type dependent manner both *in vitro* and *in vivo*; b) the proliferative and drugsensitivity profiles of RCC cell lines are significantly altered when cultured within 3D bioprinted environments, better simulating the *in vivo* context.

## 4.2.8. Tacrolimus-mediated activation of mTOR signaling in 3D bioprinted renal cell carcinoma model and in tumors of xenograft mice

To mimic the longer duration of the *in vivo* experiments, 3D bioprinted A498 renal carcinoma TMSs were treated for 21 days. Evaluation of phospho-to-total protein ratios following TAC treatment revealed a significant increase in p-S6/S6 (3.84 vs. 0.35) and p-Akt/Akt (0.06 vs. 0.02) ratios, whereas a decrease was detected in the p-mTOR/mTOR (1.16 vs. 6.28) ratio. The latter was likely due to elevated total mTOR levels (0.10 vs. 0.01) in the presence of unchanged p-mTOR expression. These findings suggest that the amount of activated mTOR remained constant, while the pool of mTOR capable of responding to external stimuli was expanded. Furthermore, increased activity of the downstream mTORC1 (p-S6; 0.03 vs. 0.006) and mTORC2 targets (p-Akt; 0.09 vs. 0.04) was also demonstrated (**Figure 18a,b**). A similar increase in activity could not be detected in the case of the 786-O cells (data not shown).

IHC evaluation of the xenograft tumors revealed increased mTORC1 activity (reflected by significantly elevated p-mTOR and p-S6 staining) and modest rises in Rictor and p-Akt expression within TAC-treated tumors (**Figure 18c**). These 3D bioprinted and

*in vivo* findings are consistent with the *in vitro* observations of TAC-driven proliferation in A498 cells. This effect appeared to be cell-type dependent, as TAC had no impact on the *in vivo* growth of the 786-O cell line (data not shown).

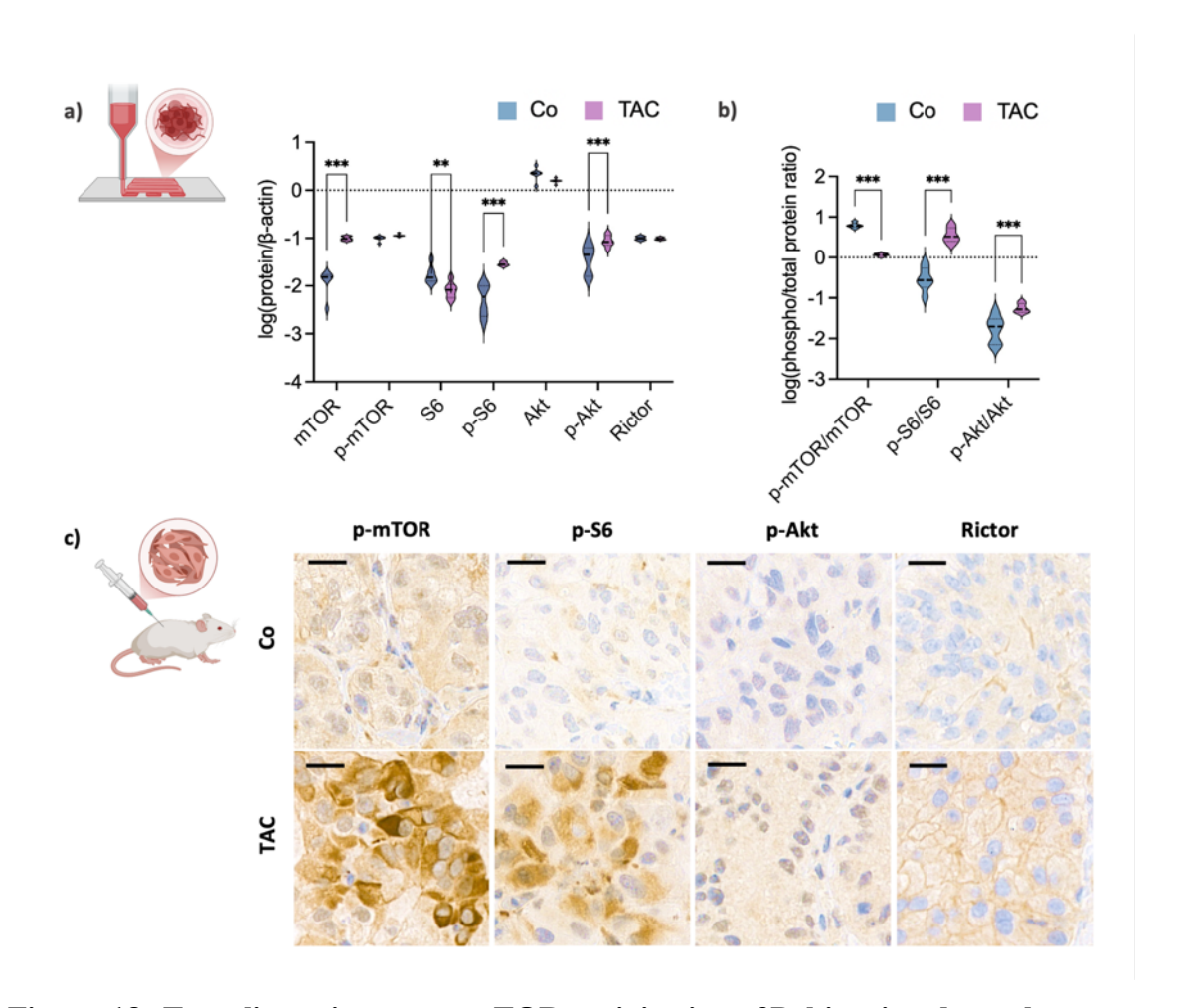


Figure 18. Tacrolimus increases mTOR activity in a 3D bioprinted renal cancer model and in *in vivo* xenograft tumors of the A498 cell line. (a) Wes<sup>TM</sup> Simple analysis of long-term (21–day) effects of TAC treatment (10 ng/mL) on mTOR activity of A498 cell line (phosphorylation sites: p-mTOR – Ser2448; p-S6 – Ser240/244; p-Akt – Ser473). Statistical significance was determined by two-way ANOVA with Fisher's LSD test (\*p < 0.05; \*\*p < 0.01; \*\*\*p < 0.001). (b) Ratios of phospho-to-total proteins. Differences between treatment groups were analyzed by two-way ANOVA followed by Fisher's LSD test (\*p < 0.05; \*\*p < 0.01; \*\*\*p < 0.001). (c) mTOR pathway activity analysis was performed on A498 xenograft tumors sections. DAB chromogen, hematoxylin counterstaining. Scale bars: 20 µm (126).

### 5. Discussion

### 5.1. Establishment and investigation of 3D bioprinted cancer models

The primary goal of 3D bioprinting in cancer research is to model the *in situ* tumor behavior and drug responsiveness. However, standardization remains a major challenge due to variable factors, including bioink composition, rheology, bioprinting parameters (e.g., nozzle size, temperature, pressure, speed, and cross-linking), and post-printing culture conditions (medium type, incubation time). The diversity in methods makes it difficult to compare findings across studies (86).

After testing several different cancer cell lines including breast and renal cancers, we developed a 3D bioprinted breast cancer model using mainly a stable mCherry-transfected T47D human breast carcinoma cell line. The 3D bioprinted TMSs could be maintained for 21 days, during this period their growth was monitored using intrinsic mCherry fluorescence. In parallel, this auto-fluorescent signal also served to validate other proliferation assays, such as AB and SRB, ensuring their suitability for 3D bioprinted systems.

Histopathological analysis revealed apoptosis in the central regions of the 3D bioprinted TMSs and heterogeneous Ki67 staining, indicating spatial variation in proliferative activity that resembles *in situ* breast carcinoma (204). Interestingly, expression of the autophagy marker LC3 was higher in 2D cultures, suggesting that the lack of a 3D microenvironment may induce cellular stress and trigger autophagy, despite constant access to nutrients and oxygen. These observations are consistent with prior reports showing that autophagic activity is more dependent on cell type than on culture dimensionality (205).

In 2D monolayer cultures,  $\beta$ -catenin, E-cadherin, and N-cadherin showed diffuse cytoplasmic localization, indicative of weak or absent cell-cell adhesion (206, 207). These proteins are essential for maintaining tissue architecture, and  $\beta$ -catenin, through its nuclear translocation could promote tumor cell survival (208, 209). In contrast, 3D bioprinted TMSs showed increased and more specific membranous localization of cadherins and  $\beta$ -catenin, indicating enhanced adhesion in the forming "tissue". This may contribute to altered downstream signaling pathways and help explain the increased resistance to mTOR inhibitors observed in 3D bioprinted TMSs (210). Changes in the expression pattern of fibronectin and syndecan-1, may also be associated with

tumorigenicity and metastatic potential (211, 212). Loss of the detected cell-surface fibronectin, coupled with its nuclear translocation during EMT progression (213), has been also linked to Rapa-resistance (214). Similarly, the predominant cytoplasmic localization of syndecan-1 in the 3D bioprinted TMSs may suggest a non-canonical role in transcriptional regulation (215, 216), potentially contributing to progression or resistance – consistent with its association with poor prognosis in human breast cancer (217, 218). One study reported that syndecan-1 internalization is in correlation with tumor dedifferentiation and grade (219). The recently described changes in the localization and expression of adhesion and ECM proteins, along with altered signaling networks, may underlie the increased tumorigenic potential and reduced drug sensitivity in the 3D bioprinted TMSs.

Alongside these structural and adhesion-related changes, we observed modifications in key signaling pathways. Notably, the phospho-to-total protein ratios of mTOR pathway components were lower in 3D bioprinted TMSs compared to 2D monolayer cultures, indicating a baseline downregulation of mTOR signaling. Although total protein levels were higher, the phosphorylated (active) forms were significantly reduced, suggesting the presence of a larger, yet predominantly inactive protein pool. This inactive reservoir may render the cells more responsive to external stimuli. In parallel, elevated levels of pSAPK/JNK and TSC1 were observed in 3D bioprinted TMSs. JNK signaling, known for its dual pro- and anti-survival roles (220), can suppress mTOR activity, thereby influencing drug sensitivity (221). These changes may be driven by the 3D architecture, including metabolic gradients and biomechanical cues that are absent in 2D systems. Supporting this hypothesis, previous studies have reported similar upregulation of TSC1 in 3D as part of a compensatory feedback mechanism to modulate mTOR signaling (222).

These structural and signaling alterations were accompanied by decreased therapeutic sensitivity in 3D bioprinted TMSs. While Cis resistance was also observed in 2D monolayers, additional Rapa and Ipa resistance was observed in the 3D bioprinted TMSs, which may be a consequence of the reduced mTOR pathway activity. Interestingly, Ipa led to increased phosphorylation of Akt in both 2D and 3D settings – a well-characterized effect of ATP-competitive inhibitors, which prevent phosphatase access to the activation site while maintaining downstream pathway inhibition (223-226).

Notably, combination therapies involving Cis were able to sensitize both culture models, suggesting a potential strategy to overcome resistance mechanisms.

Our findings are consistent with those of *Riedl et al.*, who reported reduced mTOR signaling in 3D colon cancer spheroids compared to 2D cultures, although in their case, drug responsiveness increased (227). Other studies have shown that 3D spheroids resemble 2D cultures more closely in protein expression and drug response, while 3D bioprinted TMSs more accurately model the *in situ* tumors (228). *Weigelt et al.* found reduced Akt phosphorylation and altered PI3K-Akt and MAPK signaling in 3D breast cancer culture (229), while *Frtús et al.* observed lower p-mTOR expression in 3D collagen scaffolds of hepatocellular carcinoma compared to 2D monolayers (230).

In a complementary experiment, tumor heterogeneity within 3D bioprinted TMSs was assessed using an approach analogous to "patient-derived" models. Cells isolated from *in vivo*-grown tumors were tested across multiple drug-testing platforms, including *in vitro* 2D cultures, 3D bioprinted TMSs, and *in vivo* allograft and xenograft models. The results demonstrated that the drug response observed in the 3D bioprinted TMSs most closely mirrored that of the original tumors in 4T1 allograft-bearing BALB/c mice. Notably, the 3D bioprinted TMSs more accurately reproduced both the drug response and morphological characteristics of the allograft tumors, than the SCID mouse xenografts, underscoring their potential utility in future patient-derived tumor models (203).

Taken together, alterations in the localization and expression of adhesion and ECM proteins, together with changes in signaling networks, may contribute to the increased tumorigenic potential and reduced drug sensitivity of 3D bioprinted TMSs. Here, we developed and characterized a novel 3D bioprinted breast cancer model that recapitulates key features of the *in vivo* TME, including ECM dynamics, cell–cell interactions, and spatial signaling heterogeneity. These findings provide a basis for standardization of 3D cancer modeling and highlight the added predictive value of 3D bioprinted systems over traditional 2D monolayer cell cultures. Such advantages could accelerate the development of patient-derived tumor models for personalized drug testing. Patient-derived models play a key role in cancer research because they preserve the unique molecular and phenotypic characteristics of each patient's tumor (231, 232). In the future, these models could form the basis of personalized therapy by helping oncologists identify and choose the most effective treatment for each patient.

### 5.2. Tumorigenic role of tacrolimus in post-transplant renal cell carcinoma

As chronic kidney disease progresses, structural and functional decline leads to fibrosis and loss of renal function. Fibrosis, initially a protective response, becomes pathological when regeneration fails, leading to accumulation of ECM and replacement of parenchyma (233). This results in irreversible organ failure and progression to ESRD. The fibrotic transformation is driven by chronic inflammation, characterized by immune cell infiltration (234) and the release of pro-fibrotic cytokines such as TGF-β1. It further stimulates ECM production and promotes this cycle until the kidney completely loses its function (235, 236). In kidney transplantation, non-functioning end-stage kidneys are usually left *in situ* (in their original location), where they continue to exhibit chronic inflammatory and fibrotic activity, creating a tumor-promoting microenvironment (237, 238). IS therapy is inevitable after transplantation, with TAC remaining a cornerstone of maintenance therapy. Although alternative agents such as mTORIs are gaining clinical relevance, TAC continues to be widely used in current practice.

In our experiments, TAC promoted tumorigenic signaling through mTOR pathway activation both *in vitro* and *in vivo*. Specifically, TAC enhanced mTORC1 and mTORC2 activity in RCC cell lines and in the induced ischemic kidneys of mice. TAC significantly increased both mTOR pathway activation and tumor growth in A498 3D bioprinted RCC TMSs and *in vivo* xenografts. These findings suggest that the protumorigenic effects of TAC are influenced by both the cell type and the surrounding ischemic or fibrotic microenvironment. This may provide a mechanistic basis for the elevated cancer risk observed in KTRs receiving CNI-based immunosuppression.

Beyond its IS effects, TAC has also been shown to upregulate TGF-β expression in a dose-dependent manner via activation of the ERK signaling pathway (168, 169). Once activated, TGF-β can engage multiple downstream signaling cascades – including the canonical SMAD pathway and non-canonical pathways such as MAPK, ERK1/2, PI3K/AKT, and JNK – thereby promoting EMT, ECM accumulation, immune evasion, and tumor progression (239, 240). Emerging evidence also supports a role of TAC in promoting oncogenesis through direct modulation of the mTOR signaling network. For instance, CNI therapy has been linked to activation of the proto-oncogene Ras and phosphorylation of PRAS40, thus enhancing mTOR signaling (170, 241). While some studies have reported mTORC1 inhibition by TAC in non-tumor settings (e.g., pancreatic

islets), these observations are not applicable to cancer models (242). These findings underscore the complexity and cell-type specificity of TAC's molecular effects and suggest that it can promote tumorigenic mTOR activation in susceptible tissues. These mechanisms, alongside chronic inflammation and fibrosis, may contribute to the development of post-tx RCCs, warranting further investigation.

In KTRs who develop malignancies, switching to mTORI is often considered. Although rapalogs are commonly used to lower the risk of post-tx malignancies (192, 243), recent studies question the effectiveness of early switching to mTORI-based regimen for cancer prevention. A study reported no significant reduction in cancer incidence following early mTORI conversion (195). However, after 12 years of follow-up, similar graft function and survival rates in the everolimus and CNI groups suggest that mTORI-based IS is safe for patients with increased cancer risk (244).

Our results suggest that not only mTORC1, but also mTORC2 contributes to the development of post-tx RCCs. Additionally, a significantly higher prevalence of mTORC2 hyperactivation in post-tx tumors was observed. Elevated mTORC2 activity has been associated with aggressive tumor behavior and poor prognosis (245-248). The increased cancer-specific mortality observed in KTRs with malignancies may, at least in part, be explained by the pro-metastatic and metabolic functions of mTORC2. Our findings revealed upregulation of mTORC2 in ischemic renal tissue, suggesting its role in the cellular response to injury and fibrosis. In this context, mTORC2 activity may influence the delicate balance between cell death, proliferation, and tissue regeneration. Dysregulation of this balance through Rictor-mediated mTORC2 activation could promote aberrant cell growth and fibrogenesis.

While mTORC1 inhibition alone may not greatly reduce tumor incidence, combining everolimus with TAC may suppress TAC-induced fibrosis and reduce rapalog-related adverse effects, as well. Everolimus inhibits fibroblast activation and ECM protein expression in the kidney, supporting its antifibrotic potential (249).

Given the role of mTORC2 in tumor progression and the limitations of selective mTORC2 inhibition, there is potential in exploring dual mTORC1/2 inhibitors in the post-tx setting. Dual inhibitors may offer improved control of pro-oncogenic signaling pathways and represent a promising strategy for preventing or treating post-tx RCCs.

### 6. Conclusions

### I. Establishment and characterization of 3D bioprinted cancer models

In this part of the work, we developed 3D bioprinted in vitro breast and renal cancer models to better recapitulate the in vivo tumor microenvironment, with model characterization performed using the T47D breast cancer cell line.

Specifically, our original findings were that we:

- Established a 3D bioprinting protocol using two custom-made hydrogel formulations, generating 3D bioprinted models suitable for proliferation assays and further analyzes.
- 2) Generated 3D bioprinted RCC and breast cancer models from various cell lines (ZR75.1, T47D, MCF7, A498, 786-O, 4T1) and tumor-derived cells representing distinct pathological subtypes, which exhibited growth over three weeks with tissue-like organization.
- 3) Validated additional proliferation assays (Alamar Blue, Sulforhodamine B) using the constitutive fluorescence of stable mCherry-expressing cells, confirming their applicability in the 3D bioprinted context.
- 4) Characterized tissue morphogenesis in the 3D bioprinted breast cancer model by analyzing several cell-cell and cell-ECM markers, revealing *in situ* tumor-like spatial organization and potential transcriptional regulation associated with the nuclear translocation of fibronectin and syndecan-1.
- 5) Identified upregulation of pSAPK/JNK and TSC1, indicating an adaptive response to 3D stressors (e.g., nutrient/oxygen gradients, architecture) alongside reduced mTOR pathway activity (elevated total S6, Akt, but decreased phospho-proteins resulting in lower p-S6/S6 and p-Akt/Akt ratios), suggesting the presence of a larger but inactive protein pool that may allow rapid response to external stimuli.
- 6) Observed reduced drug sensitivity of 3D bioprinted breast cancer structures to mTOR inhibitors compared to conventional 2D monolayers, likely due to lower baseline mTOR activity.
- 7) Demonstrated that 3D bioprinted structures, particularly tumor-derived 3D bioprinted TMSs, more accurately mimic *in situ* drug responses than 2D monolayer cultures or even xenograft models.

### II. The tumorigenic role of tacrolimus in post-transplant renal cell carcinoma

In this part of the work, we investigated the tumorigenic role of tacrolimus in post-transplant renal cell carcinoma using patient samples and experimental models.

Specifically, our original findings were that we:

- 1) Described for the first time that CNI-based immunosuppression (mainly TAC) increases mTOR pathway activity in the kidneys of ESRD patients.
- 2) Confirmed *in vivo*, using an ischemia-induced murine ESRD model, that TAC enhances mTOR activity in the ischemic kidneys of mice, particularly affecting mTORC1.
- 3) Detected, that mTORC2 activity is elevated in post-tx RCCs compared to *de novo* RCCs under CNI-based immunosuppression, in both pRCC and ccRCC.
- 4) Demonstrated that TAC enhances mTOR activity or proliferation *in vitro* in both a normal tubular epithelial cell line (HK-2) and RCC cell lines (A498, 786-O) in a cell line-dependent manner, suggesting a direct tumorigenic effect.
- 5) Found that TAC promotes, while Rapa inhibits tumor growth in both 3D bioprinted and *in vivo* A498 renal cell carcinoma models, through strong mTORC1 and moderate mTORC2 activation. This effect was cell line-specific and not observed in other tested RCC models.
- 6) Showed that RCC cell lines that were sensitive to mTOR inhibitors in 2D became resistant in 3D after 72 hours, but this resistance decreased with long-term (21–day) treatment, suggesting that short-term exposure may underestimate drug efficacy.

### 7. Summary

Tumor metabolism is key in cancer development, and understanding its plasticity is necessary for developing improved therapies. This study aimed to (1) develop and investigate 3D bioprinted preclinical cancer models and (2) examine mTOR activity and the tumorigenic potential of tacrolimus (TAC) in post-transplant (post-tx) and *de novo* renal cell carcinoma (RCC).

3D bioprinted cancer models were created using breast cancer and RCC cell lines, as well as tumor-derived cells. 3D bioprinted tissue-mimetic structures (TMSs) were analyzed through validated proliferation assays, histology, and molecular profiling. mTOR pathway activity was examined in patients with end-stage renal disease (ESRD), post-tx and *de novo* RCCs, while the effects of TAC were assessed *in vitro* and *in vivo*.

- (1) The 3D bioprinted TMSs exhibited heterogenous expression of apoptosis and proliferation markers, and showed reduced autophagy compared to 2D cultures, closely mimicking *in situ* tumor characteristics. Enhanced membranous localization of β-catenin, E-cadherin, and N-cadherin indicated improved cell–cell interactions, while nuclear translocation of fibronectin and syndecan-1 suggested altered gene expression patterns in the 3D bioprinted TMSs. Reduced sensitivity to mTOR inhibitors correlated with stress-mediated feedback and lower baseline mTOR activity, as evidenced by decreased phospho-to-total ratios of mTOR-related proteins and elevated pSAPK/JNK and TSC1 levels. Additionally, tumor-derived 3D bioprinted TMSs more accurately replicated *in situ* drug responses compared to 2D monolayer cultures and xenograft models.
- (2) TAC treatment induced mTOR activation *in situ*, *in vitro* and *in vivo*, and promoted growth in certain RCC cells. Notably, mTORC2 hyperactivation was more prevalent in post-tx tumors compared to *de novo* RCCs and was also observed in ESRD kidneys, implicating mTORC2 in both fibrosis and oncogenesis. Given mTORC2's role in regulating cell survival, metabolism, and metastasis, these findings underscore its importance in the pathology of post-tx malignancies.

In summary, 3D bioprinted cancer models provide a robust and physiologically relevant platform for investigating tumor progression mechanisms and drug responses. In parallel, our *in situ* tissue characterization and experimental data – further supported by *in vitro* and *in vivo* findings – highlight the oncogenic potential of TAC-induced mTORC2 activation in RCC, particularly in post-tx RCCs.

### 8. References

- 1. Warburg O, Minami S. Versuche an Überlebendem Carcinom-gewebe. Klinische Wochenschrift. 1923;2(17):776-7.
- 2. Pavlova NN, Thompson CB. The Emerging Hallmarks of Cancer Metabolism. Cell Metab. 2016;23(1):27-47.
- 3. Tufail M, Jiang CH, Li N. Altered metabolism in cancer: insights into energy pathways and therapeutic targets. Mol Cancer. 2024;23(1):203.
- 4. Schiliro C, Firestein BL. Mechanisms of Metabolic Reprogramming in Cancer Cells Supporting Enhanced Growth and Proliferation. Cells. 2021;10(5).
- 5. Warburg O. The Metabolism of Carcinoma Cells1. The Journal of Cancer Research. 1925;9(1):148-63.
- 6. Vazquez A, Liu J, Zhou Y, Oltvai ZN. Catabolic efficiency of aerobic glycolysis: the Warburg effect revisited. BMC Syst Biol. 2010;4:58.
- 7. Gatenby RA, Smallbone K, Maini PK, Rose F, Averill J, Nagle RB, et al. Cellular adaptations to hypoxia and acidosis during somatic evolution of breast cancer. Br J Cancer. 2007;97(5):646-53.
- 8. Pérez-Tomás R, Pérez-Guillén I. Lactate in the Tumor Microenvironment: An Essential Molecule in Cancer Progression and Treatment. Cancers. 2020;12(11):3244.
- 9. Jin J, Byun JK, Choi YK, Park KG. Targeting glutamine metabolism as a therapeutic strategy for cancer. Exp Mol Med. 2023;55(4):706-15.
- 10. Gong T, Zheng C, Ou X, Zheng J, Yu J, Chen S, et al. Glutamine metabolism in cancers: Targeting the oxidative homeostasis. Front Oncol. 2022;12:994672.
- 11. Eniafe J, Jiang S. The functional roles of TCA cycle metabolites in cancer. Oncogene. 2021;40(19):3351-63.
- 12. Newman AC, Maddocks ODK. One-carbon metabolism in cancer. Br J Cancer. 2017;116(12):1499-504.
- 13. Jiang P, Du W, Wu M. Regulation of the pentose phosphate pathway in cancer. Protein Cell. 2014;5(8):592-602.
- 14. Koundouros N, Poulogiannis G. Reprogramming of fatty acid metabolism in cancer. Br J Cancer. 2020;122(1):4-22.
- 15. Schug ZT, Vande Voorde J, Gottlieb E. The metabolic fate of acetate in cancer. Nat Rev Cancer. 2016;16(11):708-17.

- 16. Hanahan D. Hallmarks of Cancer: New Dimensions. Cancer Discov. 2022;12(1):31-46.
- 17. Swanton C, Bernard E, Abbosh C, André F, Auwerx J, Balmain A, et al. Embracing cancer complexity: Hallmarks of systemic disease. Cell. 2024;187(7):1589-616.
- 18. Zoncu R, Efeyan A, Sabatini DM. mTOR: from growth signal integration to cancer, diabetes and ageing. Nature Reviews Molecular Cell Biology. 2011;12(1):21-35.
- 19. Martini M, De Santis MC, Braccini L, Gulluni F, Hirsch E. PI3K/AKT signaling pathway and cancer: an updated review. Ann Med. 2014;46(6):372-83.
- 20. Yu L, Wei J, Liu P. Attacking the PI3K/Akt/mTOR signaling pathway for targeted therapeutic treatment in human cancer. Semin Cancer Biol. 2022;85:69-94.
- 21. Vivanco I, Sawyers CL. The phosphatidylinositol 3-Kinase AKT pathway in human cancer. Nat Rev Cancer. 2002;2(7):489-501.
- 22. Johnson SC, Rabinovitch PS, Kaeberlein M. mTOR is a key modulator of ageing and age-related disease. Nature. 2013;493(7432):338-45.
- 23. Dai DF, Kang P, Bai H. The mTOR signaling pathway in cardiac aging. J Cardiovasc Aging. 2023;3(3).
- 24. Kim DH, Sarbassov DD, Ali SM, King JE, Latek RR, Erdjument-Bromage H, et al. mTOR interacts with raptor to form a nutrient-sensitive complex that signals to the cell growth machinery. Cell. 2002;110(2):163-75.
- 25. Glaviano A, Foo ASC, Lam HY, Yap KCH, Jacot W, Jones RH, et al. PI3K/AKT/mTOR signaling transduction pathway and targeted therapies in cancer. Mol Cancer. 2023;22(1):138.
- 26. Hartung J, Müller C, Calkhoven CF. The dual role of the TSC complex in cancer. Trends Mol Med. 2025;31(5):452-65.
- 27. Rahman M, Nguyen TM, Lee GJ, Kim B, Park MK, Lee CH. Unraveling the Role of Ras Homolog Enriched in Brain (Rheb1 and Rheb2): Bridging Neuronal Dynamics and Cancer Pathogenesis through Mechanistic Target of Rapamycin Signaling. International Journal of Molecular Sciences. 2024;25(3):1489.
- 28. Ghosh AP, Marshall CB, Coric T, Shim EH, Kirkman R, Ballestas ME, et al. Point mutations of the mTOR-RHEB pathway in renal cell carcinoma. Oncotarget. 2015;6(20):17895-910.

- 29. Li TT, Zhu HB. LKB1 and cancer: The dual role of metabolic regulation. Biomed Pharmacother. 2020;132:110872.
- 30. Sztankovics D, Moldvai D, Petővári G, Dankó T, Szalai F, Miyaura R, et al. mTOR hyperactivity and RICTOR amplification as targets for personalized treatments in malignancies. Pathol Oncol Res. 2024;30:1611643.
- 31. Saxton RA, Sabatini DM. mTOR Signaling in Growth, Metabolism, and Disease. Cell. 2017;168(6):960-76.
- 32. Golebiewska A, Fields RC. Advancing preclinical cancer models to assess clinically relevant outcomes. BMC Cancer. 2023;23(1):230.
- 33. Neufeld L, Yeini E, Pozzi S, Satchi-Fainaro R. 3D bioprinted cancer models: from basic biology to drug development. Nat Rev Cancer. 2022;22(12):679-92.
- 34. Wouters OJ, McKee M, Luyten J. Estimated Research and Development Investment Needed to Bring a New Medicine to Market, 2009-2018. Jama. 2020;323(9):844-53.
- 35. Wong CH, Siah KW, Lo AW. Corrigendum: Estimation of clinical trial success rates and related parameters. Biostatistics. 2018;20(2):366-.
- 36. Craveiro NS, Lopes BS, Tomás L, Almeida SF. Drug Withdrawal Due to Safety: A Review of the Data Supporting Withdrawal Decision. Curr Drug Saf. 2020;15(1):4-12.
- 37. Lexchin J. How safe are new drugs? Market withdrawal of drugs approved in Canada between 1990 and 2009. Open Med. 2014;8(1):e14-9.
- 38. Kim E, Yang J, Park S, Shin K. Factors Affecting Success of New Drug Clinical Trials. Ther Innov Regul Sci. 2023;57(4):737-50.
- 39. Schachter AD, Ramoni MF, Baio G, Roberts TG, Jr., Finkelstein SN. Economic evaluation of a Bayesian model to predict late-phase success of new chemical entities. Value Health. 2007;10(5):377-85.
- 40. Kapałczyńska M, Kolenda T, Przybyła W, Zajączkowska M, Teresiak A, Filas V, et al. 2D and 3D cell cultures a comparison of different types of cancer cell cultures. Arch Med Sci. 2018;14(4):910-9.
- 41. Akhtar A. The flaws and human harms of animal experimentation. Camb Q Healthc Ethics. 2015;24(4):407-19.

- 42. Van Norman GA. Limitations of Animal Studies for Predicting Toxicity in Clinical Trials: Is it Time to Rethink Our Current Approach? JACC Basic Transl Sci. 2019;4(7):845-54.
- 43. Bracken MB. Why animal studies are often poor predictors of human reactions to exposure. J R Soc Med. 2009;102(3):120-2.
- 44. Knight A. Animal experiments scrutinised: systematic reviews demonstrate poor human clinical and toxicological utility. Altex. 2007;24(4):320-5.
- 45. Hutchinson I, Owen C, Bailey J. Modernizing Medical Research to Benefit People and Animals. Animals (Basel). 2022;12(9).
- 46. Regulation (EC) No 1223/2009 of the European Parliament and of the Council of 30 November 2009 on cosmetic products (recast) (Text with EEA relevance), 1223/2009 (2009, Current consolidated version: 01/05/2025).
- 47. Wadman M. FDA no longer has to require animal testing for new drugs. Science. 2023;379(6628):127-8.
- 48. Niazi SK. End animal testing for biosimilar approval. Science. 2022;377(6602):162-3.
- 49. Han JJ. FDA Modernization Act 2.0 allows for alternatives to animal testing. Artificial Organs. 2023;47(3):449-50.
- 50. Administration USFaD. FDA Announces Plan to Phase Out Animal Testing Requirement for Monoclonal Antibodies and Other Drugs: U.S. Food and Drug Administration; 2025 [Press release regarding regulatory policy change on preclinical animal testing.].
- 51. Honkala A, Malhotra SV, Kummar S, Junttila MR. Harnessing the predictive power of preclinical models for oncology drug development. Nat Rev Drug Discov. 2022;21(2):99-114.
- 52. Sajjad H, Imtiaz S, Noor T, Siddiqui YH, Sajjad A, Zia M. Cancer models in preclinical research: A chronicle review of advancement in effective cancer research. Animal Model Exp Med. 2021;4(2):87-103.
- 53. Pozzi S, Scomparin A, Israeli Dangoor S, Rodriguez Ajamil D, Ofek P, Neufeld L, et al. Meet me halfway: Are in vitro 3D cancer models on the way to replace in vivo models for nanomedicine development? Adv Drug Deliv Rev. 2021;175:113760.

- 54. Choi JR, Kozalak G, di Bari I, Babar Q, Niknam Z, Rasmi Y, et al. In Vitro Human Cancer Models for Biomedical Applications. Cancers (Basel). 2022;14(9).
- 55. Kim JH, Verwilst P, Won M, Lee J, Sessler JL, Han J, et al. A Small Molecule Strategy for Targeting Cancer Stem Cells in Hypoxic Microenvironments and Preventing Tumorigenesis. J Am Chem Soc. 2021;143(35):14115-24.
- 56. Obeagu EI. Oxygen gradients in tumor tissues implications for breast cancer metastasis a narrative review. Ann Med Surg (Lond). 2025;87(6):3372-80.
- 57. Lobel GP, Jiang Y, Simon MC. Tumor microenvironmental nutrients, cellular responses, and cancer. Cell Chem Biol. 2023;30(9):1015-32.
- 58. Griffiths JI, Cosgrove PA, Medina EF, Nath A, Chen J, Adler FR, et al. Cellular interactions within the immune microenvironment underpins resistance to cell cycle inhibition in breast cancers. Nat Commun. 2025;16(1):2132.
- 59. Prakash J, Shaked Y. The Interplay between Extracellular Matrix Remodeling and Cancer Therapeutics. Cancer Discov. 2024;14(8):1375-88.
- 60. Box GEP. Robustness in the Strategy of Scientific Model Building. In: Launer RL, Wilkinson GN, editors. Robustness in Statistics: Academic Press; 1979. p. 201-36.
- 61. Moldvai D. Effects of 3D tissue structure on drug sensitivity 3D bioprinted tissue mimetic structures in cancer research. Magy Onkol. 2023;67(3):237-46.
- 62. Mohebi MM, Evans JR. A drop-on-demand ink-jet printer for combinatorial libraries and functionally graded ceramics. J Comb Chem. 2002;4(4):267-74.
- 63. Klebe RJ. Cytoscribing: A method for micropositioning cells and the construction of two- and three-dimensional synthetic tissues. Experimental Cell Research. 1988;179(2):362-73.
- 64. Mironov V, Boland T, Trusk T, Forgacs G, Markwald RR. Organ printing: computer-aided jet-based 3D tissue engineering. Trends Biotechnol. 2003;21(4):157-61.
- 65. Groll J, Boland T, Blunk T, Burdick JA, Cho DW, Dalton PD, et al. Biofabrication: reappraising the definition of an evolving field. Biofabrication. 2016;8(1):013001.
- 66. Lam EHY, Yu F, Zhu S, Wang Z. 3D Bioprinting for Next-Generation Personalized Medicine. Int J Mol Sci. 2023;24(7).
- 67. Tripathi S, Mandal SS, Bauri S, Maiti P. 3D bioprinting and its innovative approach for biomedical applications. MedComm (2020). 2023;4(1):e194.

- 68. Fatimi A, Okoro OV, Podstawczyk D, Siminska-Stanny J, Shavandi A. Natural Hydrogel-Based Bio-Inks for 3D Bioprinting in Tissue Engineering: A Review. Gels. 2022;8(3).
- 69. Gu Z, Fu J, Lin H, He Y. Development of 3D bioprinting: From printing methods to biomedical applications. Asian J Pharm Sci. 2020;15(5):529-57.
- 70. Landers R, Hübner U, Schmelzeisen R, Mülhaupt R. Rapid prototyping of scaffolds derived from thermoreversible hydrogels and tailored for applications in tissue engineering. Biomaterials. 2002;23(23):4437-47.
- 71. Ozbolat IT, Hospodiuk M. Current advances and future perspectives in extrusion-based bioprinting. Biomaterials. 2016;76:321-43.
- 72. Trachtenberg JE, Placone JK, Smith BT, Piard CM, Santoro M, Scott DW, et al. Extrusion-Based 3D Printing of Poly(propylene fumarate) in a Full-Factorial Design. ACS Biomater Sci Eng. 2016;2(10):1771-80.
- 73. Ozbolat IT, Moncal KK, Gudapati H. Evaluation of bioprinter technologies. Additive Manufacturing. 2017;13:179-200.
- 74. Groll J, Burdick JA, Cho DW, Derby B, Gelinsky M, Heilshorn SC, et al. A definition of bioinks and their distinction from biomaterial inks. Biofabrication. 2018;11(1):013001.
- 75. Baumann B, Jungst T, Stichler S, Feineis S, Wiltschka O, Kuhlmann M, et al. Control of Nanoparticle Release Kinetics from 3D Printed Hydrogel Scaffolds. Angew Chem Int Ed Engl. 2017;56(16):4623-8.
- 76. Narayanan LK, Huebner P, Fisher MB, Spang JT, Starly B, Shirwaiker RA. 3D-Bioprinting of Polylactic Acid (PLA) Nanofiber-Alginate Hydrogel Bioink Containing Human Adipose-Derived Stem Cells. ACS Biomater Sci Eng. 2016;2(10):1732-42.
- 77. Kamperman T, Henke S, van den Berg A, Shin SR, Tamayol A, Khademhosseini A, et al. Single Cell Microgel Based Modular Bioinks for Uncoupled Cellular Micro- and Macroenvironments. Adv Healthc Mater. 2017;6(3).
- 78. Sharma R, Smits IPM, De La Vega L, Lee C, Willerth SM. 3D Bioprinting Pluripotent Stem Cell Derived Neural Tissues Using a Novel Fibrin Bioink Containing Drug Releasing Microspheres. Front Bioeng Biotechnol. 2020;8:57.

- 79. Ribeiro A, Blokzijl MM, Levato R, Visser CW, Castilho M, Hennink WE, et al. Assessing bioink shape fidelity to aid material development in 3D bioprinting. Biofabrication. 2017;10(1):014102.
- 80. Paxton N, Smolan W, Böck T, Melchels F, Groll J, Jungst T. Proposal to assess printability of bioinks for extrusion-based bioprinting and evaluation of rheological properties governing bioprintability. Biofabrication. 2017;9(4):044107.
- 81. Mouser VH, Melchels FP, Visser J, Dhert WJ, Gawlitta D, Malda J. Yield stress determines bioprintability of hydrogels based on gelatin-methacryloyl and gellan gum for cartilage bioprinting. Biofabrication. 2016;8(3):035003.
- 82. Rutz AL, Hyland KE, Jakus AE, Burghardt WR, Shah RN. A multimaterial bioink method for 3D printing tunable, cell-compatible hydrogels. Adv Mater. 2015;27(9):1607-14.
- 83. Blaeser A, Duarte Campos DF, Puster U, Richtering W, Stevens MM, Fischer H. Controlling Shear Stress in 3D Bioprinting is a Key Factor to Balance Printing Resolution and Stem Cell Integrity. Adv Healthc Mater. 2016;5(3):326-33.
- 84. Gopinathan J, Noh I. Recent trends in bioinks for 3D printing. Biomater Res. 2018;22:11.
- 85. Ouyang L, Yao R, Zhao Y, Sun W. Effect of bioink properties on printability and cell viability for 3D bioplotting of embryonic stem cells. Biofabrication. 2016;8(3):035020.
- 86. Sztankovics D, Moldvai D, Petővári G, Gelencsér R, Krencz I, Raffay R, et al. 3D bioprinting and the revolution in experimental cancer model systems-A review of developing new models and experiences with in vitro 3D bioprinted breast cancer tissue-mimetic structures. Pathol Oncol Res. 2023;29:1610996.
- 87. Chang R, Nam J, Sun W. Effects of dispensing pressure and nozzle diameter on cell survival from solid freeform fabrication-based direct cell writing. Tissue Eng Part A. 2008;14(1):41-8.
- 88. Smith CM, Stone AL, Parkhill RL, Stewart RL, Simpkins MW, Kachurin AM, et al. Three-dimensional bioassembly tool for generating viable tissue-engineered constructs. Tissue Eng. 2004;10(9-10):1566-76.
- 89. LI M, TIAN X, KOZINSKI JA, CHEN X, HWANG DK. MODELING MECHANICAL CELL DAMAGE IN THE BIOPRINTING PROCESS EMPLOYING

- A CONICAL NEEDLE. Journal of Mechanics in Medicine and Biology. 2015;15(05):1550073.
- 90. Nair K, Gandhi M, Khalil S, Yan KC, Marcolongo M, Barbee K, et al. Characterization of cell viability during bioprinting processes. Biotechnology Journal. 2009;4(8):1168-77.
- 91. Sarker M, Chen XB. Modeling the Flow Behavior and Flow Rate of Medium Viscosity Alginate for Scaffold Fabrication With a Three-Dimensional Bioplotter. Journal of Manufacturing Science and Engineering. 2017;139(8).
- 92. Chen XB, Li MG, Ke H. Modeling of the Flow Rate in the Dispensing-Based Process for Fabricating Tissue Scaffolds. Journal of Manufacturing Science and Engineering. 2008;130(2).
- 93. Skardal A, Devarasetty M, Kang HW, Mead I, Bishop C, Shupe T, et al. A hydrogel bioink toolkit for mimicking native tissue biochemical and mechanical properties in bioprinted tissue constructs. Acta Biomater. 2015;25:24-34.
- 94. Schwab A, Levato R, D'Este M, Piluso S, Eglin D, Malda J. Printability and Shape Fidelity of Bioinks in 3D Bioprinting. Chem Rev. 2020;120(19):11028-55.
- 95. Cheng F, Cao X, Li H, Liu T, Xie X, Huang D, et al. Generation of Cost-Effective Paper-Based Tissue Models through Matrix-Assisted Sacrificial 3D Printing. Nano Lett. 2019;19(6):3603-11.
- 96. Reid JA, Palmer X-L, Mollica PA, Northam N, Sachs PC, Bruno RD. A 3D bioprinter platform for mechanistic analysis of tumoroids and chimeric mammary organoids. Scientific Reports. 2019;9(1):7466.
- 97. Zhou X, Zhu W, Nowicki M, Miao S, Cui H, Holmes B, et al. 3D Bioprinting a Cell-Laden Bone Matrix for Breast Cancer Metastasis Study. ACS Appl Mater Interfaces. 2016;8(44):30017-26.
- 98. Horder H, Guaza Lasheras M, Grummel N, Nadernezhad A, Herbig J, Ergün S, et al. Bioprinting and Differentiation of Adipose-Derived Stromal Cell Spheroids for a 3D Breast Cancer-Adipose Tissue Model. Cells. 2021;10(4).
- 99. Wang Y, Shi W, Kuss M, Mirza S, Qi D, Krasnoslobodtsev A, et al. 3D Bioprinting of Breast Cancer Models for Drug Resistance Study. ACS Biomater Sci Eng. 2018;4(12):4401-11.

- 100. Dey M, Ayan B, Yurieva M, Unutmaz D, Ozbolat IT. Studying Tumor Angiogenesis and Cancer Invasion in a Three-Dimensional Vascularized Breast Cancer Micro-Environment. Adv Biol (Weinh). 2021;5(7):e2100090.
- 101. Paškevičiūtė M, Petrikaitė V. Proton Pump Inhibitors Modulate Transport Of Doxorubicin And Its Liposomal Form Into 2D And 3D Breast Cancer Cell Cultures. Cancer Manag Res. 2019;11:9761-9.
- 102. Paškevičiūtė M, Petrikaitė V. Application of carbonic anhydrase inhibitors to increase the penetration of doxorubicin and its liposomal formulation into 2D and 3D triple negative breast cancer cell cultures. Am J Cancer Res. 2020;10(6):1761-9.
- 103. Perini G, Rosenkranz A, Friggeri G, Zambrano D, Rosa E, Augello A, et al. Advanced usage of Ti(3)C(2)T(x) MXenes for photothermal therapy on different 3D breast cancer models. Biomed Pharmacother. 2022;153:113496.
- 104. Nam KH, Jeong CB, Kim H, Ahn M, Ahn SJ, Hur H, et al. Quantitative Photothermal Characterization with Bioprinted 3D Complex Tissue Constructs for Early-Stage Breast Cancer Therapy Using Gold Nanorods. Adv Healthc Mater. 2021;10(18):e2100636.
- 105. Dey M, Kim MH, Nagamine M, Karhan E, Kozhaya L, Dogan M, et al. Biofabrication of 3D breast cancer models for dissecting the cytotoxic response of human T cells expressing engineered MAIT cell receptors. Biofabrication. 2022;14(4).
- 106. Singh NK, Han W, Nam SA, Kim JW, Kim JY, Kim YK, et al. Three-dimensional cell-printing of advanced renal tubular tissue analogue. Biomaterials. 2020;232:119734.
- 107. King SM, Higgins JW, Nino CR, Smith TR, Paffenroth EH, Fairbairn CE, et al. 3D Proximal Tubule Tissues Recapitulate Key Aspects of Renal Physiology to Enable Nephrotoxicity Testing. Front Physiol. 2017;8:123.
- 108. Lin NYC, Homan KA, Robinson SS, Kolesky DB, Duarte N, Moisan A, et al. Renal reabsorption in 3D vascularized proximal tubule models. Proc Natl Acad Sci U S A. 2019;116(12):5399-404.
- 109. Lawlor KT, Vanslambrouck JM, Higgins JW, Chambon A, Bishard K, Arndt D, et al. Cellular extrusion bioprinting improves kidney organoid reproducibility and conformation. Nat Mater. 2021;20(2):260-71.

- 110. Shen JX, Youhanna S, Zandi Shafagh R, Kele J, Lauschke VM. Organotypic and Microphysiological Models of Liver, Gut, and Kidney for Studies of Drug Metabolism, Pharmacokinetics, and Toxicity. Chem Res Toxicol. 2020;33(1):38-60.
- 111. Fransen MFJ, Addario G, Bouten CVC, Halary F, Moroni L, Mota C. Bioprinting of kidney in vitro models: cells, biomaterials, and manufacturing techniques. Essays Biochem. 2021;65(3):587-602.
- 112. Herrada-Manchón H, Celada L, Rodríguez-González D, Alejandro Fernández M, Aguilar E, Chiara MD. Three-dimensional bioprinted cancer models: A powerful platform for investigating tunneling nanotube-like cell structures in complex microenvironments. Mater Sci Eng C Mater Biol Appl. 2021;128:112357.
- 113. Virumbrales-Muñoz M, Chen J, Ayuso J, Lee M, Abel EJ, Beebe DJ. Organotypic primary blood vessel models of clear cell renal cell carcinoma for single-patient clinical trials. Lab Chip. 2020;20(23):4420-32.
- 114. Rosette KA, Lander SM, VanOpstall C, Looyenga BD. Three-dimensional coculture provides an improved in vitro model for papillary renal cell carcinoma. Am J Physiol Renal Physiol. 2021;321(1):F33-f46.
- 115. Wu D, Berg J, Arlt B, Röhrs V, Al-Zeer MA, Deubzer HE, et al. Bioprinted Cancer Model of Neuroblastoma in a Renal Microenvironment as an Efficiently Applicable Drug Testing Platform. Int J Mol Sci. 2021;23(1).
- 116. Ketcham CM, Crawford JM. The impact of review articles. Lab Invest. 2007;87(12):1174-85.
- 117. Moch H, Amin MB, Berney DM, Compérat EM, Gill AJ, Hartmann A, et al. The 2022 World Health Organization Classification of Tumours of the Urinary System and Male Genital Organs-Part A: Renal, Penile, and Testicular Tumours. Eur Urol. 2022;82(5):458-68.
- 118. Massari F, Ciccarese C, Santoni M, Brunelli M, Piva F, Modena A, et al. Metabolic alterations in renal cell carcinoma. Cancer Treat Rev. 2015;41(9):767-76.
- 119. Kim WY, Kaelin WG. Role of VHL gene mutation in human cancer. J Clin Oncol. 2004;22(24):4991-5004.
- 120. Comprehensive molecular characterization of clear cell renal cell carcinoma. Nature. 2013;499(7456):43-9.

- 121. Linehan WM, Spellman PT, Ricketts CJ, Creighton CJ, Fei SS, Davis C, et al. Comprehensive Molecular Characterization of Papillary Renal-Cell Carcinoma. N Engl J Med. 2016;374(2):135-45.
- 122. Ricketts CJ, Killian JK, Vocke CD, Wang Y, Merino MJ, Meltzer PS, et al. Kidney tumors associated with germline mutations of FH and SDHB show a CpG island methylator phenotype (CIMP). PLoS One. 2022;17(12):e0278108.
- 123. Adam J, Hatipoglu E, O'Flaherty L, Ternette N, Sahgal N, Lockstone H, et al. Renal cyst formation in Fh1-deficient mice is independent of the Hif/Phd pathway: roles for fumarate in KEAP1 succination and Nrf2 signaling. Cancer Cell. 2011;20(4):524-37.
- 124. Crooks DR, Maio N, Lang M, Ricketts CJ, Vocke CD, Gurram S, et al. Mitochondrial DNA alterations underlie an irreversible shift to aerobic glycolysis in fumarate hydratase-deficient renal cancer. Sci Signal. 2021;14(664).
- 125. Krencz I, Vetlényi E, Dankó T, Petővári G, Moldvai D, Sztankovics D, et al. Metabolic Adaptation as Potential Target in Papillary Renal Cell Carcinomas Based on Their In Situ Metabolic Characteristics. Int J Mol Sci. 2022;23(18).
- 126. Moldvai D, Sztankovics D, Dankó T, Vetlényi E, Petővári G, Márk Á, et al. Tumorigenic role of tacrolimus through mTORC1/C2 activation in post-transplant renal cell carcinomas. British Journal of Cancer. 2024;130(7):1119-30.
- 127. Zeppellini A, Patelli G, Ferla F, Pedrani M, Pierri S, Calvanese G, et al. Renal cell carcinoma in kidney transplant recipients receiving immunosuppression: A 55-year retrospective single-center study. Journal of Clinical Oncology. 2025;43(5\_suppl):599-.
- 128. Einollahi B, Nemati E, Rostami Z, Teimoori M, Ghadian AR. Electrolytes Disturbance and Cyclosporine Blood Levels among Kidney Transplant Recipients. Int J Organ Transplant Med. 2012;3(4):166-75.
- 129. Bamgbola O. Metabolic consequences of modern immunosuppressive agents in solid organ transplantation. Ther Adv Endocrinol Metab. 2016;7(3):110-27.
- 130. Ghosh AP, Sudarshan S. Genetics of renal cancer: focus on MTOR. Aging (Albany NY). 2016;8(3):421-2.
- 131. Miricescu D, Balan DG, Tulin A, Stiru O, Vacaroiu IA, Mihai DA, et al. PI3K/AKT/mTOR signalling pathway involvement in renal cell carcinoma pathogenesis (Review). Exp Ther Med. 2021;21(5):540.

- 132. Pal SK, Ali SM, Yakirevich E, Geynisman DM, Karam JA, Elvin JA, et al. Characterization of Clinical Cases of Advanced Papillary Renal Cell Carcinoma via Comprehensive Genomic Profiling. Eur Urol. 2018;73(1):71-8.
- 133. Chen F, Zhang Y, Şenbabaoğlu Y, Ciriello G, Yang L, Reznik E, et al. Multilevel Genomics-Based Taxonomy of Renal Cell Carcinoma. Cell Reports. 2016;14(10):2476-89.
- 134. Pal SK, Quinn DI. Differentiating mTOR inhibitors in renal cell carcinoma. Cancer Treat Rev. 2013;39(7):709-19.
- 135. Bedke J, Gauler T, Grünwald V, Hegele A, Herrmann E, Hinz S, et al. Systemic therapy in metastatic renal cell carcinoma. World J Urol. 2017;35(2):179-88.
- 136. Hudes G, Carducci M, Tomczak P, Dutcher J, Figlin R, Kapoor A, et al. Temsirolimus, interferon alfa, or both for advanced renal-cell carcinoma. N Engl J Med. 2007;356(22):2271-81.
- 137. Park I, Lee SH, Lee JL. A Multicenter Phase II Trial of Axitinib in Patients With Recurrent or Metastatic Non-clear-cell Renal Cell Carcinoma Who Had Failed Prior Treatment With Temsirolimus. Clin Genitourin Cancer. 2018;16(5):e997-e1002.
- 138. Kong D, Duan J, Chen S, Wang Z, Ren J, Lu J, et al. Transplant oncology and anti-cancer immunosuppressants. Front Immunol. 2024;15:1520083.
- 139. Wolfe RA, Ashby VB, Milford EL, Ojo AO, Ettenger RE, Agodoa LY, et al. Comparison of mortality in all patients on dialysis, patients on dialysis awaiting transplantation, and recipients of a first cadaveric transplant. N Engl J Med. 1999;341(23):1725-30.
- 140. Végső G, Tóth A, Toronyi É, Perner F, Máthé Z. Changes in Tumor Characteristics in Kidney Transplanted Patients Over the Last 40 Years. Transplant Proc. 2015;47(7):2198-200.
- 141. Cheung CY, Tang SCW. An update on cancer after kidney transplantation. Nephrol Dial Transplant. 2019;34(6):914-20.
- 142. Karami S, Yanik EL, Moore LE, Pfeiffer RM, Copeland G, Gonsalves L, et al. Risk of Renal Cell Carcinoma Among Kidney Transplant Recipients in the United States. Am J Transplant. 2016;16(12):3479-89.

- 143. Vajdic CM, McDonald SP, McCredie MR, van Leeuwen MT, Stewart JH, Law M, et al. Cancer incidence before and after kidney transplantation. Jama. 2006;296(23):2823-31.
- 144. Adami J, Gäbel H, Lindelöf B, Ekström K, Rydh B, Glimelius B, et al. Cancer risk following organ transplantation: a nationwide cohort study in Sweden. Br J Cancer. 2003;89(7):1221-7.
- 145. Kasiske BL, Snyder JJ, Gilbertson DT, Wang C. Cancer after kidney transplantation in the United States. Am J Transplant. 2004;4(6):905-13.
- 146. Villeneuve PJ, Schaubel DE, Fenton SS, Shepherd FA, Jiang Y, Mao Y. Cancer incidence among Canadian kidney transplant recipients. Am J Transplant. 2007;7(4):941-8.
- 147. Collett D, Mumford L, Banner NR, Neuberger J, Watson C. Comparison of the incidence of malignancy in recipients of different types of organ: a UK Registry audit. Am J Transplant. 2010;10(8):1889-96.
- 148. Fuhrmann JD, Valkova K, von Moos S, Wüthrich RP, Müller TF, Schachtner T. Cancer among kidney transplant recipients >20 years after transplantation: post-transplant lymphoproliferative disorder remains the most common cancer type in the ultra long-term. Clin Kidney J. 2022;15(6):1152-9.
- 149. Friman TK, Jäämaa-Holmberg S, Åberg F, Helanterä I, Halme M, Pentikäinen MO, et al. Cancer risk and mortality after solid organ transplantation: A population-based 30-year cohort study in Finland. Int J Cancer. 2022;150(11):1779-91.
- 150. Howlader N, Ries LA, Mariotto AB, Reichman ME, Ruhl J, Cronin KA. Improved estimates of cancer-specific survival rates from population-based data. J Natl Cancer Inst. 2010;102(20):1584-98.
- 151. D'Arcy ME, Coghill AE, Lynch CF, Koch LA, Li J, Pawlish KS, et al. Survival after a cancer diagnosis among solid organ transplant recipients in the United States. Cancer. 2019;125(6):933-42.
- 152. Arellano F, Krupp P. Malignancies in rheumatoid arthritis patients treated with cyclosporin A. Br J Rheumatol. 1993;32 Suppl 1:72-5.
- 153. Cockburn IT, Krupp P. The risk of neoplasms in patients treated with cyclosporine A. J Autoimmun. 1989;2(5):723-31.

- 154. Dantal J, Hourmant M, Cantarovich D, Giral M, Blancho G, Dreno B, et al. Effect of long-term immunosuppression in kidney-graft recipients on cancer incidence: randomised comparison of two cyclosporin regimens. Lancet. 1998;351(9103):623-8.
- 155. Herman M, Weinstein T, Korzets A, Chagnac A, Ori Y, Zevin D, et al. Effect of cyclosporin A on DNA repair and cancer incidence in kidney transplant recipients. J Lab Clin Med. 2001;137(1):14-20.
- 156. Paul CF, Ho VC, McGeown C, Christophers E, Schmidtmann B, Guillaume JC, et al. Risk of malignancies in psoriasis patients treated with cyclosporine: a 5 y cohort study. J Invest Dermatol. 2003;120(2):211-6.
- 157. Marcil I, Stern RS. Squamous-cell cancer of the skin in patients given PUVA and ciclosporin: nested cohort crossover study. Lancet. 2001;358(9287):1042-5.
- 158. Langeland T, Engh V. Topical use of tacrolimus and squamous cell carcinoma on the penis. Br J Dermatol. 2005;152(1):183-5.
- 159. Becker JC, Houben R, Vetter CS, Bröcker EB. The carcinogenic potential of tacrolimus ointment beyond immune suppression: a hypothesis creating case report. BMC Cancer. 2006;6:7.
- 160. Castellsague J, Kuiper JG, Pottegård A, Anveden Berglind I, Dedman D, Gutierrez L, et al. A cohort study on the risk of lymphoma and skin cancer in users of topical tacrolimus, pimecrolimus, and corticosteroids (Joint European Longitudinal Lymphoma and Skin Cancer Evaluation JOELLE study). Clin Epidemiol. 2018;10:299-310.
- 161. Wang L, Ma K, Yao Y, Yu L, Wu J, Zhao Q, et al. Carcinogenicity risk associated with tacrolimus use in kidney transplant recipients: a systematic review and meta-analysis. Transl Androl Urol. 2022;11(3):358-66.
- 162. Wimmer CD, Angele MK, Schwarz B, Pratschke S, Rentsch M, Khandoga A, et al. Impact of cyclosporine versus tacrolimus on the incidence of de novo malignancy following liver transplantation: a single center experience with 609 patients. Transpl Int. 2013;26(10):999-1006.
- 163. Trushkin RN, Isaev TK, Medvedev PE, Shcheglov NE, Variasin VV, Lysenko MA, et al. Renal cell carcinoma in a transplanted kidney: a retrospective evaluation. BMC Nephrol. 2024;25(1):237.

- 164. Devasenapathy N, Chu A, Wong M, Srivastava A, Ceccacci R, Lin C, et al. Cancer risk with topical calcineurin inhibitors, pimecrolimus and tacrolimus, for atopic dermatitis: a systematic review and meta-analysis. Lancet Child Adolesc Health. 2023;7(1):13-25.
- 165. Asgari MM, Tsai AL, Avalos L, Sokil M, Quesenberry CP, Jr. Association Between Topical Calcineurin Inhibitor Use and Keratinocyte Carcinoma Risk Among Adults With Atopic Dermatitis. JAMA Dermatol. 2020;156(10):1066-73.
- 166. Arana A, Pottegård A, Kuiper JG, Booth H, Reutfors J, Calingaert B, et al. Long-Term Risk of Skin Cancer and Lymphoma in Users of Topical Tacrolimus and Pimecrolimus: Final Results from the Extension of the Cohort Study Protopic Joint European Longitudinal Lymphoma and Skin Cancer Evaluation (JOELLE). Clin Epidemiol. 2021;13:1141-53.
- 167. Undre NA, Moloney FJ, Ahmadi S, Stevenson P, Murphy GM. Skin and systemic pharmacokinetics of tacrolimus following topical application of tacrolimus ointment in adults with moderate to severe atopic dermatitis. Br J Dermatol. 2009;160(3):665-9.
- 168. Jahr H, van der Windt AE, Timur UT, Baart EB, Lian WS, Rolauffs B, et al. Physosmotic Induction of Chondrogenic Maturation Is TGF-β Dependent and Enhanced by Calcineurin Inhibitor FK506. Int J Mol Sci. 2022;23(9).
- 169. Satake M, Sakuraba H, Hiraga H, Yoshida S, Akemoto Y, Ota S, et al. Tacrolimus Up-regulates Expression of TGFβ Receptor Type II via ERK, Providing Protection Against Intestinal Epithelial Injury. In Vivo. 2022;36(4):1684-93.
- 170. Datta D, Contreras AG, Basu A, Dormond O, Flynn E, Briscoe DM, et al. Calcineurin inhibitors activate the proto-oncogene Ras and promote protumorigenic signals in renal cancer cells. Cancer Res. 2009;69(23):8902-9.
- 171. Sørensen HT, Mellemkjaer L, Nielsen GL, Baron JA, Olsen JH, Karagas MR. Skin cancers and non-hodgkin lymphoma among users of systemic glucocorticoids: a population-based cohort study. J Natl Cancer Inst. 2004;96(9):709-11.
- 172. Trattner A, Hodak E, David M, Sandbank M. The appearance of Kaposi sarcoma during corticosteroid therapy. Cancer. 1993;72(5):1779-83.
- 173. Engberg H, Wehberg S, Bistrup C, Heaf J, Sørensen SS, Thiesson HC, et al. Cancer risk and mortality after kidney transplantation: a population-based study on

- differences between Danish centres using standard immunosuppression with and without glucocorticoids. Nephrol Dial Transplant. 2016;31(12):2149-56.
- 174. Piette C, Deprez M, Roger T, Noël A, Foidart JM, Munaut C. The dexamethasone-induced inhibition of proliferation, migration, and invasion in glioma cell lines is antagonized by macrophage migration inhibitory factor (MIF) and can be enhanced by specific MIF inhibitors. J Biol Chem. 2009;284(47):32483-92.
- 175. Huynh TP, Barwe SP, Lee SJ, McSpadden R, Franco OE, Hayward SW, et al. Glucocorticoids suppress renal cell carcinoma progression by enhancing Na,K-ATPase beta-1 subunit expression. PLoS One. 2015;10(4):e0122442.
- 176. McGeown MG, Douglas JF, Middleton D. One thousand renal transplants at Belfast City Hospital: post-graft neoplasia 1968-1999, comparing azathioprine only with cyclosporin-based regimes in a single centre. Clin Transpl. 2000:193-202.
- 177. Pasternak B, Svanström H, Schmiegelow K, Jess T, Hviid A. Use of azathioprine and the risk of cancer in inflammatory bowel disease. Am J Epidemiol. 2013;177(11):1296-305.
- 178. Zheng KYC, Guo CG, Wong IOL, Chen L, Chung HY, Cheung KS, et al. Risk of malignancies in patients with inflammatory bowel disease who used thiopurines as compared with other indications: a territory-wide study. Therap Adv Gastroenterol. 2020;13:1756284820967275.
- 179. Jiyad Z, Olsen CM, Burke MT, Isbel NM, Green AC. Azathioprine and Risk of Skin Cancer in Organ Transplant Recipients: Systematic Review and Meta-Analysis. Am J Transplant. 2016;16(12):3490-503.
- 180. Armstrong RG, West J, Card TR. Risk of cancer in inflammatory bowel disease treated with azathioprine: a UK population-based case-control study. Am J Gastroenterol. 2010;105(7):1604-9.
- 181. Zhang Z, Wang M, Xu L, Jiang B, Jin T, Shi T, et al. Cancer occurrence following azathioprine treatment in myasthenia gravis patients: A systematic review and meta-analysis. J Clin Neurosci. 2021;88:70-4.
- 182. Robson R, Cecka JM, Opelz G, Budde M, Sacks S. Prospective registry-based observational cohort study of the long-term risk of malignancies in renal transplant patients treated with mycophenolate mofetil. Am J Transplant. 2005;5(12):2954-60.

- 183. Hirunsatitpron P, Hanprasertpong N, Noppakun K, Pruksakorn D, Teekachunhatean S, Koonrungsesomboon N. Mycophenolic acid and cancer risk in solid organ transplant recipients: Systematic review and meta-analysis. Br J Clin Pharmacol. 2022;88(2):476-89.
- 184. Vos M, Plasmeijer EI, van Bemmel BC, van der Bij W, Klaver NS, Erasmus ME, et al. Azathioprine to mycophenolate mofetil transition and risk of squamous cell carcinoma after lung transplantation. J Heart Lung Transplant. 2018;37(7):853-9.
- 185. Eberhard OK, Kliem V, Brunkhorst R. Five cases of Kaposi's sarcoma in kidney graft recipients: possible influence of the immunosuppressive therapy. Transplantation. 1999;67(1):180-4.
- 186. Campbell SB, Walker R, Tai SS, Jiang Q, Russ GR. Randomized controlled trial of sirolimus for renal transplant recipients at high risk for nonmelanoma skin cancer. Am J Transplant. 2012;12(5):1146-56.
- 187. Campistol JM, Eris J, Oberbauer R, Friend P, Hutchison B, Morales JM, et al. Sirolimus therapy after early cyclosporine withdrawal reduces the risk for cancer in adult renal transplantation. J Am Soc Nephrol. 2006;17(2):581-9.
- 188. Yanik EL, Gustafson SK, Kasiske BL, Israni AK, Snyder JJ, Hess GP, et al. Sirolimus use and cancer incidence among US kidney transplant recipients. Am J Transplant. 2015;15(1):129-36.
- 189. Opelz G, Unterrainer C, Süsal C, Döhler B. Immunosuppression with mammalian target of rapamycin inhibitor and incidence of post-transplant cancer in kidney transplant recipients. Nephrol Dial Transplant. 2016;31(8):1360-7.
- 190. Effect of sirolimus on malignancy and survival after kidney transplantation: systematic review and meta-analysis of individual patient data. BMJ: British Medical Journal. 2014;349:g7543.
- 191. Xie X, Jiang Y, Lai X, Xiang S, Shou Z, Chen J. mTOR inhibitor versus mycophenolic acid as the primary immunosuppression regime combined with calcineurin inhibitor for kidney transplant recipients: a meta-analysis. BMC Nephrol. 2015;16:91.
- 192. Lopez-Soler RI, Chen P, Nair L, Ata A, Patel S, Conti DJ. Sirolimus use improves cancer-free survival following transplantation: A single center 12-year analysis. Transplantation Reports. 2020;5(2):100040.

- 193. Naik MG, Arns W, Budde K, Diekmann F, Eitner F, Gwinner W, et al. Sirolimus in renal transplant recipients with malignancies in Germany. Clin Kidney J. 2021;14(9):2047-58.
- 194. Infante B, Coviello N, Troise D, Gravina M, Bux V, Castellano G, et al. Rapamycin Inhibitors for Eye Squamous Cell Carcinoma after Renal Transplantation: A Case Report. Kidney Blood Press Res. 2021;46(1):121-5.
- 195. Kampaktsis PN, Doulamis IP, Asleh R, Makri E, Kalamaras I, Papastergiopoulos C, et al. Characteristics, Predictors, and Outcomes of Early mTOR Inhibitor Use After Heart Transplantation: Insights From the UNOS Database. J Am Heart Assoc. 2022;11(17):e025507.
- 196. Budde K, Becker T, Arns W, Sommerer C, Reinke P, Eisenberger U, et al. Everolimus-based, calcineurin-inhibitor-free regimen in recipients of de-novo kidney transplants: an open-label, randomised, controlled trial. Lancet. 2011;377(9768):837-47.
- 197. Lebranchu Y, Thierry A, Toupance O, Westeel PF, Etienne I, Thervet E, et al. Efficacy on renal function of early conversion from cyclosporine to sirolimus 3 months after renal transplantation: concept study. Am J Transplant. 2009;9(5):1115-23.
- 198. Khalid H, Fareed MM, Dandekar T, Shityakov S. Calcineurin and mTOR inhibitors in kidney transplantation: integrative metamodeling on transplant survival and kidney function. Int Urol Nephrol. 2024;56(4):1403-14.
- 199. Laczkó-Rigó R, Bakos É, Jójárt R, Tömböly C, Mernyák E, Özvegy-Laczka C. Selective antiproliferative effect of C-2 halogenated 13α-estrones on cells expressing Organic anion-transporting polypeptide 2B1 (OATP2B1). Toxicol Appl Pharmacol. 2021;429:115704.
- 200. Han SS, Kim DH, Lee SM, Han NY, Oh JM, Ha J, et al. Pharmacokinetics of tacrolimus according to body composition in recipients of kidney transplants. Kidney Research and Clinical Practice. 2012;31(3):157-62.
- 201. Saunders RN, Metcalfe MS, Nicholson ML. Rapamycin in transplantation: a review of the evidence. Kidney Int. 2001;59(1):3-16.
- 202. Krencz I, Sebestyén A, Fábián K, Márk Á, Moldvay J, Khoor A, et al. Expression of mTORC1/2-related proteins in primary and brain metastatic lung adenocarcinoma. Human Pathology. 2017;62:66-73.

- 203. Petővári G, Moldvai D, Raffay R, Dankó T, Sztankovics D, Reszegi A, et al. Mimicking breast cancer tissue—3D bioprinted models in accurate drug sensitivity tests. VIEW.n/a(n/a (in press)):20250092.
- 204. Đokić S, Gazić B, Grčar Kuzmanov B, Blazina J, Miceska S, Čugura T, et al. Clinical and Analytical Validation of Two Methods for Ki-67 Scoring in Formalin Fixed and Paraffin Embedded Tissue Sections of Early Breast Cancer. Cancers (Basel). 2024;16(7).
- 205. Follo C, Barbone D, Richards WG, Bueno R, Broaddus VC. Autophagy initiation correlates with the autophagic flux in 3D models of mesothelioma and with patient outcome. Autophagy. 2016;12(7):1180-94.
- 206. Baghy K, Ladányi A, Reszegi A, Kovalszky I. Insights into the Tumor Microenvironment-Components, Functions and Therapeutics. Int J Mol Sci. 2023;24(24).
- 207. Li J, Zhou BP. Activation of  $\beta$ -catenin and Akt pathways by Twist are critical for the maintenance of EMT associated cancer stem cell-like characters. BMC Cancer. 2011;11:49.
- 208. Liu J, Xiao Q, Xiao J, Niu C, Li Y, Zhang X, et al. Wnt/β-catenin signalling: function, biological mechanisms, and therapeutic opportunities. Signal Transduct Target Ther. 2022;7(1):3.
- 209. Barzegar Behrooz A, Talaie Z, Jusheghani F, Łos MJ, Klonisch T, Ghavami S. Wnt and PI3K/Akt/mTOR Survival Pathways as Therapeutic Targets in Glioblastoma. Int J Mol Sci. 2022;23(3).
- 210. Park YL, Kim HP, Cho YW, Min DW, Cheon SK, Lim YJ, et al. Activation of WNT/β-catenin signaling results in resistance to a dual PI3K/mTOR inhibitor in colorectal cancer cells harboring PIK3CA mutations. Int J Cancer. 2019;144(2):389-401.
- 211. Hynes RO, Destree AT, Perkins ME, Wagner DD. Cell surface fibronectin and oncogenic transformation. Journal of Supramolecular Structure. 1979;11(1):95-104.
- 212. Lin TC, Yang CH, Cheng LH, Chang WT, Lin YR, Cheng HC. Fibronectin in Cancer: Friend or Foe. Cells. 2019;9(1).
- 213. Debnath P, Huirem RS, Bhowmick A, Ghosh A, Ghosh D, Dutta P, et al. Epithelial mesenchymal transition induced nuclear localization of the extracellular matrix protein Fibronectin. Biochimie. 2024;219:142-5.

- 214. Adkins F, Akcakanat A, Chen H, Do K-A, Gonzalez-Angulo AM, Mills G, et al. Epithelial-mesenchymal transition confers resistance to rapamycin. Journal of the American College of Surgeons. 2011;213(3, Supplement):S144.
- 215. Dudás J, Ramadori G, Knittel T, Neubauer K, Raddatz D, Egedy K, et al. Effect of heparin and liver heparan sulphate on interaction of HepG2-derived transcription factors and their cis-acting elements: altered potential of hepatocellular carcinoma heparan sulphate. Biochem J. 2000;350 Pt 1(Pt 1):245-51.
- 216. Szatmári T, Ötvös R, Hjerpe A, Dobra K. Syndecan-1 in Cancer: Implications for Cell Signaling, Differentiation, and Prognostication. Dis Markers. 2015;2015:796052.
- 217. Nguyen TL, Grizzle WE, Zhang K, Hameed O, Siegal GP, Wei S. Syndecan-1 overexpression is associated with nonluminal subtypes and poor prognosis in advanced breast cancer. Am J Clin Pathol. 2013;140(4):468-74.
- 218. Kind S, Jaretzke A, Büscheck F, Möller K, Dum D, Höflmayer D, et al. A shift from membranous and stromal syndecan-1 (CD138) expression to cytoplasmic CD138 expression is associated with poor prognosis in breast cancer. Mol Carcinog. 2019;58(12):2306-15.
- 219. Burbach BJ, Friedl A, Mundhenke C, Rapraeger AC. Syndecan-1 accumulates in lysosomes of poorly differentiated breast carcinoma cells. Matrix Biol. 2003;22(2):163-77.
- 220. Abdelrahman KS, Hassan HA, Abdel-Aziz SA, Marzouk AA, Narumi A, Konno H, et al. JNK signaling as a target for anticancer therapy. Pharmacol Rep. 2021;73(2):405-34.
- 221. Deng Y, Adam V, Nepovimova E, Heger Z, Valko M, Wu Q, et al. c-Jun N-terminal kinase signaling in cellular senescence. Arch Toxicol. 2023;97(8):2089-109.
- 222. Phukhum P, Phetcharaburanin J, Chaleekarn K, Kittirat Y, Kulthawatsiri T, Namwat N, et al. The impact of hypoxia and oxidative stress on proteo-metabolomic alterations of 3D cholangiocarcinoma models. Sci Rep. 2023;13(1):3072.
- 223. Fujimoto Y, Morita TY, Ohashi A, Haeno H, Hakozaki Y, Fujii M, et al. Combination treatment with a PI3K/Akt/mTOR pathway inhibitor overcomes resistance to anti-HER2 therapy in PIK3CA-mutant HER2-positive breast cancer cells. Sci Rep. 2020;10(1):21762.

- 224. Rhodes N, Heerding DA, Duckett DR, Eberwein DJ, Knick VB, Lansing TJ, et al. Characterization of an Akt kinase inhibitor with potent pharmacodynamic and antitumor activity. Cancer Res. 2008;68(7):2366-74.
- 225. Okuzumi T, Fiedler D, Zhang C, Gray DC, Aizenstein B, Hoffman R, et al. Inhibitor hijacking of Akt activation. Nat Chem Biol. 2009;5(7):484-93.
- 226. Lin K, Lin J, Wu WI, Ballard J, Lee BB, Gloor SL, et al. An ATP-site on-off switch that restricts phosphatase accessibility of Akt. Sci Signal. 2012;5(223):ra37.
- 227. Riedl A, Schlederer M, Pudelko K, Stadler M, Walter S, Unterleuthner D, et al. Comparison of cancer cells in 2D vs 3D culture reveals differences in AKT-mTOR-S6K signaling and drug responses. J Cell Sci. 2017;130(1):203-18.
- 228. Dankó T, Petővári G, Raffay R, Sztankovics D, Moldvai D, Vetlényi E, et al. Characterisation of 3D Bioprinted Human Breast Cancer Model for In Vitro Drug and Metabolic Targeting. Int J Mol Sci. 2022;23(13).
- 229. Weigelt B, Lo AT, Park CC, Gray JW, Bissell MJ. HER2 signaling pathway activation and response of breast cancer cells to HER2-targeting agents is dependent strongly on the 3D microenvironment. Breast Cancer Res Treat. 2010;122(1):35-43.
- 230. Frtús A, Smolková B, Uzhytchak M, Lunova M, Jirsa M, Hof M, et al. Hepatic Tumor Cell Morphology Plasticity under Physical Constraints in 3D Cultures Driven by YAP-mTOR Axis. Pharmaceuticals (Basel). 2020;13(12).
- 231. Taurin S, Alzahrani R, Aloraibi S, Ashi L, Alharmi R, Hassani N. Patient-derived tumor organoids: A preclinical platform for personalized cancer therapy. Transl Oncol. 2025;51:102226.
- 232. Liu Y, Wu W, Cai C, Zhang H, Shen H, Han Y. Patient-derived xenograft models in cancer therapy: technologies and applications. Signal Transduct Target Ther. 2023;8(1):160.
- 233. Panizo S, Martínez-Arias L, Alonso-Montes C, Cannata P, Martín-Carro B, Fernández-Martín JL, et al. Fibrosis in Chronic Kidney Disease: Pathogenesis and Consequences. Int J Mol Sci. 2021;22(1).
- 234. Anders HJ, Vielhauer V, Schlöndorff D. Chemokines and chemokine receptors are involved in the resolution or progression of renal disease. Kidney Int. 2003;63(2):401-15.

- 235. To WS, Midwood KS. Plasma and cellular fibronectin: distinct and independent functions during tissue repair. Fibrogenesis & Tissue Repair. 2011;4(1):21.
- 236. Higgins SP, Tang Y, Higgins CE, Mian B, Zhang W, Czekay RP, et al. TGF-β1/p53 signaling in renal fibrogenesis. Cell Signal. 2018;43:1-10.
- 237. Cernaro V, Lacquaniti A, Donato V, Fazio MR, Buemi A, Buemi M. Fibrosis, regeneration and cancer: what is the link? Nephrol Dial Transplant. 2012;27(1):21-7.
- 238. Zhao H, Wu L, Yan G, Chen Y, Zhou M, Wu Y, et al. Inflammation and tumor progression: signaling pathways and targeted intervention. Signal Transduct Target Ther. 2021;6(1):263.
- 239. Chandra Jena B, Sarkar S, Rout L, Mandal M. The transformation of cancer-associated fibroblasts: Current perspectives on the role of TGF-β in CAF mediated tumor progression and therapeutic resistance. Cancer Lett. 2021;520:222-32.
- 240. Peng D, Fu M, Wang M, Wei Y, Wei X. Targeting TGF-β signal transduction for fibrosis and cancer therapy. Mol Cancer. 2022;21(1):104.
- 241. Basu A, Banerjee P, Contreras AG, Flynn E, Pal S. Calcineurin inhibitor-induced and Ras-mediated overexpression of VEGF in renal cancer cells involves mTOR through the regulation of PRAS40. PLoS One. 2011;6(8):e23919.
- 242. Rodriguez-Rodriguez AE, Donate-Correa J, Rovira J, Cuesto G, Luis-Ravelo D, Fernandes MX, et al. Inhibition of the mTOR pathway: A new mechanism of  $\beta$  cell toxicity induced by tacrolimus. Am J Transplant. 2019;19(12):3240-9.
- 243. Asleh R, Clavell AL, Pereira NL, Smith B, Briasoulis A, Alnsasra H, et al. Incidence of Malignancies in Patients Treated With Sirolimus Following Heart Transplantation. J Am Coll Cardiol. 2019;73(21):2676-88.
- 244. Bollano E, Andreassen AK, Eiskjaer H, Gustafsson F, Rådegran G, Gude E, et al. Long-term follow-up of the randomized, prospective Scandinavian heart transplant everolimus de novo study with early calcineurin inhibitors avoidance (SCHEDULE) trial. The Journal of Heart and Lung Transplantation. 2024;43(12):1948-59.
- 245. Wen SY, Li CH, Zhang YL, Bian YH, Ma L, Ge QL, et al. Rictor is an independent prognostic factor for endometrial carcinoma. Int J Clin Exp Pathol. 2014;7(5):2068-78.

- 246. Cao RZ, Min L, Liu S, Tian RY, Jiang HY, Liu J, et al. Rictor Activates Cav 1 Through the Akt Signaling Pathway to Inhibit the Apoptosis of Gastric Cancer Cells. Front Oncol. 2021;11:641453.
- 247. Sticz T, Molnár A, Márk Á, Hajdu M, Nagy N, Végső G, et al. mTOR activity and its prognostic significance in human colorectal carcinoma depending on C1 and C2 complex-related protein expression. J Clin Pathol. 2017;70(5):410-6.
- 248. Krencz I, Sebestyen A, Papay J, Lou Y, Lutz GF, Majewicz TL, et al. Correlation between immunohistochemistry and RICTOR fluorescence in situ hybridization amplification in small cell lung carcinoma. Hum Pathol. 2019;93:74-80.
- 249. Shigematsu T, Tajima S, Fu R, Zhang M, Itoyama Y, Tsuchimoto A, et al. The mTOR inhibitor everolimus attenuates tacrolimus-induced renal interstitial fibrosis in rats. Life Sci. 2022;288:120150.

# 9. Bibliography of the candidate's publications

#### Publications related to the thesis

1st author publications (the basis of the dissertation)

**Moldvai D**, Raffay R, Petővári G, Dankó T, Sztankovics D, Krencz I, Vetlényi E, Sebestyén, A. 3D bionyomtatott szöveti és tumormodellek a daganatkutatásban. GYÓGYSZERÉSZET 2022 66(6), 295–302. (**IF: 0**)

**Moldvai D**, Sztankovics D, Dankó T, Szalai F, Miyaura R, Petővári G, Krencz I, Gelencsér R, Sebestyén A. 3D szöveti szerkezet hatása a gyógyszerérzékenységre – 3D bionyomtatott "szövetmodellek" a daganatkutatásban [Effects of 3D tissue structure on drug sensitivity - 3D bioprinted tissue mimetic structures in cancer research]. Magy Onkol. 2023 Sep 28;67(3):237-246. Hungarian. Epub 2023 Sep 5. PMID: 37768119. (**IF: 0**)

Sztankovics D\*, **Moldvai D**\*, Petővári G, Gelencsér R, Krencz I, Raffay R, Dankó T, Sebestyén A. 3D bioprinting and the revolution in experimental cancer model systems-A review of developing new models and experiences with in vitro 3D bioprinted breast cancer tissue-mimetic structures. Pathol Oncol Res. 2023 Feb 9;29:1610996. doi: 10.3389/pore.2023.1610996. PMID: 36843955; PMCID: PMC9946983. **(IF: 2.3)** \*shared first author

**Moldvai D**, Sztankovics D, Dankó T, Vetlényi E, Petővári G, Márk Á, Patonai A, Végső G, Piros L, Hosszú Á, Pápay J, Krencz I, Sebestyén A. Tumorigenic role of tacrolimus through mTORC1/C2 activation in post-transplant renal cell carcinomas. Br J Cancer. 2024 Apr;130(7):1119-1130. doi: 10.1038/s41416-024-02597-8. Epub 2024 Feb 10. PMID: 38341510; PMCID: PMC10991560. **(IF: 6.8)** 

Petővári G\*, **Moldvai D**\*, Raffay R, Dankó T, Sztankovics D, Reszegi A, Miyaura R, Gelencsér R, Rókusz A, Tolnai-Kriston Cs, Vilimi Zs, Kállai-Szabó N, Visnovitz T,

Sebestyén A. VIEW. 2025, 20250092. doi: 10.1002/VIW.20250092 (IF: 8.4) \*shared first author

# Other related publications

Sebestyén A, Dankó T, Sztankovics D, **Moldvai D**, Raffay R, Cervi C, Krencz I, Zsiros V, Jeney A, Petővári G. The role of metabolic ecosystem in cancer progression - metabolic plasticity and mTOR hyperactivity in tumor tissues. Cancer Metastasis Rev. 2021 Dec;40(4):989-1033. doi: 10.1007/s10555-021-10006-2. Epub 2022 Jan 14. PMID: 35029792; PMCID: PMC8825419. (**IF: 9.237**)

Krencz I, Vetlényi E, Dankó T, Petővári G, **Moldvai D**, Sztankovics D, Raffay R, Mészáros K, Sebestyén E, Végső G, Pápay J, Sebestyén A. Metabolic Adaptation as Potential Target in Papillary Renal Cell Carcinomas Based on Their In Situ Metabolic Characteristics. Int J Mol Sci. 2022 Sep 13;23(18):10587. doi: 10.3390/ijms231810587. PMID: 36142502; PMCID: PMC9503093. (**IF: 5.6**)

Dankó T, Petővári G, Raffay R, Sztankovics D, **Moldvai D**, Vetlényi E, Krencz I, Rókusz A, Sipos K, Visnovitz T, Pápay J, Sebestyén A. Characterisation of 3D Bioprinted Human Breast Cancer Model for In Vitro Drug and Metabolic Targeting. Int J Mol Sci. 2022 Jul 4;23(13):7444. doi: 10.3390/ijms23137444. PMID: 35806452; PMCID: PMC9267600. **(IF: 5.6)** 

#### **Publications not related to the thesis**

Sztankovics D, Szalai F, **Moldvai D**, Dankó T, Scheich B, Pápay J, Sebestyén A, Krencz I. Comparison of molecular subtype composition between independent sets of primary and brain metastatic small cell lung carcinoma and matched samples. Lung Cancer. 2025 Jan;199:108071. doi: 10.1016/j.lungcan.2024.108071. Epub 2024 Dec 22. PMID: 39721126. **(IF: 4.4)** 

Sztankovics D, Szalai F, **Moldvai D**, Dankó T, Nagy N, Pápay J, Khoór A, Krencz I, Sebestyén A. Increased mTOR activity and RICTOR copy number in small cell lung carcinoma progression. Eur J Cell Biol. 2024 Dec;103(4):151468. doi: 10.1016/j.ejcb.2024.151468. Epub 2024 Nov 19. PMID: 39571513. (**IF: 4.3**)

Krencz I, Sztankovics D, Sebestyén A, Pápay J, Dankó T, **Moldvai D**, Lutz E, Khoor A. RICTOR amplification is associated with Rictor membrane staining and does not correlate with PD-L1 expression in lung squamous cell carcinoma. Pathol Oncol Res. 2024 Apr 19;30:1611593. doi: 10.3389/pore.2024.1611593. PMID: 38706776; PMCID: PMC11066283. (**IF: 2.3**)

Benkő BM, Tóth G, **Moldvai D**, Kádár S, Szabó E, Szabó ZI, Kraszni M, Szente L, Fiser B, Sebestyén A, Zelkó R, Sebe I. Cyclodextrin encapsulation enabling the anticancer repositioning of disulfiram: Preparation, analytical and in vitro biological characterization of the inclusion complexes. Int J Pharm. 2024 May 25;657:124187. doi: 10.1016/j.ijpharm.2024.124187. Epub 2024 May 1. PMID: 38697585. **(IF: 6.4)** 

Sztankovics D, **Moldvai D**, Petővári G, Dankó T, Szalai F, Miyaura R, Varga V, Nagy N, Papp G, Pápay J, Krencz I, Sebestyén A. mTOR hyperactivity and RICTOR amplification as targets for personalized treatments in malignancies. Pathol Oncol Res. 2024 Mar 7;30:1611643. doi: 10.3389/pore.2024.1611643. PMID: 38515456; PMCID: PMC10954904. **(IF: 2.3)** 

Szalai F, Sztankovics D, Krencz I, **Moldvai D**, Pápay J, Sebestyén A, Khoor A. Rictor-A Mediator of Progression and Metastasis in Lung Cancer. Cancers (Basel). 2024 Jan 26;16(3):543. doi: 10.3390/cancers16030543. PMID: 38339294; PMCID: PMC10854599. (**IF: 4.4**)

Sztankovics D, Krencz I, **Moldvai D**, Dankó T, Nagy Á, Nagy N, Bedics G, Rókusz A, Papp G, Tőkés AM, Pápay J, Sápi Z, Dezső K, Bödör C, Sebestyén A. Novel RICTOR amplification harbouring entities: FISH validation of RICTOR amplification in tumour tissue after next-generation sequencing. Sci Rep. 2023 Nov 10;13(1):19610. doi: 10.1038/s41598-023-46927-x. PMID: 37949943; PMCID: PMC10638425. (**IF: 3.8**)

Szalai F, Krencz I, **Moldvai D**, Petővári G, Dankó T, Nagy N, Papp G, Pápay J, Sebestyén A, Sztankovics D. Az mTOR-hiperaktivitás és a RICTORamplifikáció jelentősége, és az ezzel összefüggő célzott terápiás lehetőségek rosszindulatú daganatokban [he importance of mTOR hyperactivity and RICTOR amplification, and the associated targeted therapy

possibilities in malignant tumours]. Magy Onkol. 2023 Sep 28;67(3):165-180. Hungarian. Epub 2023 Sep 13. PMID: 37768116. (IF: 0)

Mohás A, Krencz I, Váradi Z, Arató G, Felkai L, Kiss DJ, **Moldvai D**, Sebestyén A, Csóka M. In Situ Analysis of mTORC1/C2 and Metabolism-Related Proteins in Pediatric Osteosarcoma. Pathol Oncol Res. 2022 Mar 22;28:1610231. doi: 10.3389/pore.2022.1610231. PMID: 35392503; PMCID: PMC8980219. **(IF: 2.3)** 

Dankó T, Petővári G, Sztankovics D, **Moldvai D**, Raffay R, Lőrincz P, Visnovitz T, Zsiros V, Barna G, Márk Á, Krencz I, Sebestyén A. Rapamycin Plus Doxycycline Combination Affects Growth Arrest and Selective Autophagy-Dependent Cell Death in Breast Cancer Cells. Int J Mol Sci. 2021 Jul 27;22(15):8019. doi: 10.3390/ijms22158019. PMID: 34360785; PMCID: PMC8347279. (**IF: 6.208**)

### 10. Acknowledgements

They say science is about asking the right questions. I began this journey with only one: *Why you?* I still don't have the answer – but this is what grew from that question.

I would like to express my heartfelt gratitude to everyone who supported and helped me in any way during my PhD work.

First and foremost, I am deeply grateful to Professor Dr. András Matolcsy, Head of the Department of Pathology and Experimental Cancer Research at Semmelweis University, for giving me the opportunity to conduct my research at this esteemed institute.

I would like to extend my sincerest thanks to my supervisor, Dr. Anna Sebestyén, for allowing me to carry out both my undergraduate thesis and PhD research within her research group, and for her patient guidance and support over the years. Thank you for your trust, for the invaluable professional and personal encouragement, and for always being there to help me navigate any challenges I encountered along the way, whether they were practical problems, personal struggles, or emotional difficulties, always responding with empathy and kindness.

I am also grateful to the former and current PhD students and colleagues of the Tumor Biology Laboratory for creating a friendly and motivating atmosphere. My special thanks go to Dr. Ildikó Krencz, Dr. Gábor Petővári, Dr. Zoltán Hujber, Dr. Enikő Vetlényi, and Dr. Titanilla Dankó, from whom I learned numerous techniques as an undergraduate student. I also wish to thank Dr. Dániel Sztankovics, Regina Raffay, Dr. Viktória Varga, Dr. Miyaura Risa, and Dr. Fatime Szalai for their support, advice, assistance with experiments, and for helping me through difficult times – whether with insightful words, a sweet treat, or simply coming with me for a coffee when I needed it most. I am grateful to our enthusiastic undergraduate students, Rebeka Gelencsér, Nóra Förhécz, and Bálint Csikós, for their energetic help in daily tasks and experiments.

I am indebted to Dr. Gábor Barna, Dr. Gábor Szalóki, Dr. Csilla Tolnai-Kriston, and Dr. Ágnes Márk for their assistance with flow cytometry measurements; to Dr. Zsófia Vilimi and Dr. Nikolett Kállai-Szabó of the Faculty of Pharmacy for their help with analyzing

the gels we used in 3D bioprinting; and to Dr. Kornélia Baghy for her valuable guidance in interpreting adhesion markers.

I wish to thank the staff of the Biopsy Laboratories for their technical support in section preparation, especially Csilla Kurucz, Anna Tamási and Ferencné Kárpáti for their dedicated assistance.

My sincere thanks go to the staff of the Animal Facility at the Department of Pathology and Experimental Cancer Research – András Sztodola, Natália Sztodola – as well as Dr. Ádám Hosszú, for their invaluable help with the *in vivo* experiments and in establishing the ischemic kidney model.

I am grateful to all the employees of the Department of Pathology and Experimental Cancer Research, who were always willing to help me with my questions, administrative issues, or other day-to-day tasks. I would like to thank Cecília Laczik for her assistance with the administrative matters related to my PhD studies.

Since the moment I first set foot here as a second-year university student, many people have come and gone, and it would be impossible to name everyone individually; nevertheless, I am deeply thankful to everyone who, in any way, contributed to this work.

I am deeply grateful to my family, and especially to my husband, Patrik Nagy, who patiently endured the many evenings I spent absorbed in my work, even when I seemed to disappear completely, and who, in those moments, took a huge weight off my shoulders – something for which I am endlessly thankful. I also wish to thank my special friends, who never held it against me that I was often unavailable, and who, despite everything, always asked me how I was when we met again.

To my parents: You didn't live to see the pages of this dissertation, but you live in the margins, between the lines, in the reasons behind every word.

In memory of my parents, whose lives ended before this chapter began.

May this work honor your fight.